



NRC-CNRC

Water Distribution Systems
**Climate Change Risks and
Opportunities**

Author(s): Ehsan Roshani, Yehuda Kleiner, Andrew Colombo, Elad Salomons

Report No.: CRBCPI-Y5-19

Report Date: 10 January 2022

Contract No.: A1-009962

Agreement Date: 29 November 2016



National Research
Council Canada

Conseil national de
recherches Canada

Canada 

© (2022) Her Majesty the Queen in Right of Canada,
as represented by the National Research Council Canada.

PDF: Cat. No. NR24-99/2022E-PDF
ISBN 978-0-660-41386-0

Également disponible en français

Water Distribution Systems

Climate Change Risks and Opportunities

Author and project manager: _____

Ehsan Roshani Ph.D., P.Eng. PMP
Sustainable Resilient Infrastructures and Communities
NRC Construction Research Centre

Author: Yehuda Kleiner, Ph.D., P.Eng,

Author: Andrew Colombo, Ph.D., P.Eng,

Author: Elad Salomons, M.Sc.

Approved

Marianne Armstrong, M.Sc., P.Eng.
Initiative Leader, Climate Resilient Built Environment (CRBE)
NRC Construction Research Centre

Report No: CRBCPI-Y5-19
Report Date: 06 January 2022
Contract No: A1-009962
Agreement date: 29 November 2016
Program: Climate Resilient Buildings and Core Public Infrastructure

120 pages

Copy no. 1 of 1

This report may not be reproduced in whole or in part without the written consent of the National Research Council Canada and the Client.

(This page is intentionally left blank)

Table of Contents

Table of Contents.....	5
List of Figures	8
List of Tables	11
Executive Summary	12
1 Introduction	15
1.1 Background	15
1.2 Water Distribution System Risk and Opportunity Project.....	16
1.3 Climate Variables and their expected range in Canada.....	17
1.3.1 Temperature	17
1.3.2 Precipitation.....	19
1.3.3 Summary and commentary.....	20
2 Impacts on water consumption rate and hydraulic capacity.....	21
2.1 Recommended approach to quantify climate change impacts on demand	23
2.2 Case study and demonstration	24
2.2.1 Data preparation	25
2.2.2 Nonlinear model summer data	26
2.2.3 Linear model summer data	29
2.2.4 Linear model non-summer data	31
3 Climate change impacts on water main capacity.....	33
3.1 Suggested Methodology to Evaluate the Impact of Climate change on WDS Capacity	33
3.2 Case studies	36
3.3 Results and analysis	37
3.4 Conclusions	38
3.5 Recommendations.....	40
4 Impact of climate change on Water Main Breaks	42
4.1 Suggested Methodology to Evaluate the Impact of Climate Change on WDS Watermain Breaks	44
4.1.1 Non Homogeneous Poisson Process based model	46
4.1.2 Covariates of the NHPP model	48

4.1.3	Zero-inflated Poisson (ZIP) process.....	50
4.1.4	Model training and validation	51
4.1.5	I-WARP Model.....	52
4.2	Case Study	54
4.2.1	Data preparation	54
4.2.2	Analysis of historical breakage patterns.....	55
4.2.3	Risk Analysis and Simulation Assumptions.....	56
4.2.4	Case Study simulation and Results	57
4.3	Recommendations.....	59
5	Impact on Energy Consumption	60
5.1	Suggested Methodology to Evaluate the Impact of Climate Change on Energy Consumption in WDS.....	61
5.2	Demonstration Case studies.....	62
5.3	Concluding comments	64
6	Impacts on Chlorine Residuals.....	66
6.1	Correlation between air and water temperature	68
6.2	Integrating water temperature in chlorine decay modeling in WDSs.....	74
6.2.1	Modeling Chlorine decay in the drinking water distribution system.....	75
6.2.2	Bulk Flow Reactions	76
6.2.3	Bulk reaction rate coefficient changes with temperature	77
6.2.4	Summary for the bulk decay coefficient	82
6.2.5	Wall Reactions.....	82
6.2.6	Wall reaction rate coefficient change with temperature	84
6.2.7	Summary for the wall decay coefficient.....	86
6.2.8	Modeling temperature in the drinking water distribution system	86
6.2.9	Temperature modelling in pipes.....	87
6.2.10	Temperature modelling in tanks.....	89
6.2.11	Summary of temperature modelling in WDN	91
6.3	Conceptual model development for modeling temperature and chlorine decay	92
6.3.1	Temperature modelling.....	92
6.3.2	Chlorine decay modelling.....	94
6.3.3	Proof of Concept.....	94

6.3.4	Temperature model in a long pipe	94
6.3.5	Temperature and Chlorine model in a small network	95
6.3.6	Network 1 water distribution network	100
6.4	Conclusions	107
7	Summary and Conclusions	109
	Acknowledgments	112
	References	113
	Appendix A -	119
A.1	Limitations and issues with EPANET-MSX	119

List of Figures

Figure 1. Observed changes ($^{\circ}\text{C}$) in annual temperature between 1948 and 2016 (Bush, 2019)	17
Figure 2. Future projections for selected temperature indices (extremes) (Bush, 2019)	19
Figure 3. Projected precipitation changes for summer season (Bush, 2019)	20
Figure 4 City's total daily water production	24
Figure 5 City's mean daily temperature	25
Figure 6 City's daily precipitation	25
Figure 7 Demand variations during summer and non-summer months	26
Figure 8. Normalise summer data	27
Figure 9. Nonlinear model results	28
Figure 10, Goodness of fit of the nonlinear model	28
Figure 11. Goodness of fit for nonlinear model applied to summer data without extreme values.	29
Figure 12. Goodness of fit of linear model with non-normalised summer data	30
Figure 13. Climate and demand data (non-normalised) during non-summer months	31
Figure 14. Goodness of fit linear model of non-summer (raw) data.	31
Figure 15. Global Average Surface Temperature Change (Relative to 1986-2005) (Pachauri & Meyer, 2015)	34
Figure 16. Histogram of the demand distributions for one node with the base demand of 28.2 lps.	35
Figure 17. HydraCAL and Its New Add-ins for Evaluating Demand Growth	36
Figure 18. The Selected WDSs. Red Links Indicate the Impacted Pipes for RCP8.5.	39
Figure 19 Network Resiliency Tool in HydraCAL	46
Figure 20 Break Modeling Tool in HydraCAL	47
Figure 21 Case study network with categorized water mains based their diameter in HydraCAL.	53
Figure 22 Historical and predicted annual freezing index for the case study	57
Figure 23 Total number of breaks for PVC cohort under three scenarios (i.e., Status Quo, RCP 2.6, and RCP 8.5)	58
Figure 24 Number of people disconnected from the system for the Cohort 4 under three scenarios (i.e., Status Quo, RCP 2.6, and RCP 8.5)	58
Figure 25 Electricity Daily Price Pattern in Ontario	63
Figure 26 Network 1 energy consumption and cost increase ("Base" = year of analysis)	63
Figure 27 Network 3 energy consumption and cost increase ("Base" = year of analysis)	64
Figure 28 Daily concentration of Hypochlorite in Network 3 water distribution systems correlated with air temperature from 2011 to 2021	66
Figure 29 Hourly air and water temperature variation during September in Logger 1.	68
Figure 30 Hourly air and water temperature variation during February in Logger 1.	68
Figure 31 Logger locations and distribution across Network 1 Case Study.	70

Figure 32 Daily minimum, mean, and maximum temperature in Network 1, and water temperature inside watermains in Logger 1 to 4 (gaps in logger data due to malfunction or battery power depletion).....	71
Figure 33 Daily minimum, mean, and maximum temperature in Network 1, and water temperature inside watermains in Logger 5 to 8 (gaps in logger data due to malfunction or battery power depletion).....	72
Figure 34 Daily minimum, mean, and maximum temperature in Network 1, and water temperature inside watermains in Logger 9 to 12 (gaps in logger data due to malfunction or battery power depletion).....	73
Figure 35: Relationship between bulk decay coefficient and water temperature for different TOC levels using (Ki����, Lu, & L����, 1998) and (Koechling, 1998).....	78
Figure 36: bulk decay coefficient as a function of temperature (Nagatani, et al., 2006)	79
Figure 37: Relationship between bulk decay coefficient and water temperature using (Nagatani, et al., 2006) and (Koechling, 1998)	80
Figure 38: bulk decay coefficient as a function of temperature (Powell, Hallam, West, Forster, & Simms, 2000).....	81
Figure 39: Relationship between bulk decay coefficient and water temperature using (Powell, Hallam, West, Forster, & Simms, 2000) and (Koechling, 1998)	81
Figure 40: Viscosity of Water as a function of Temperature (https://wiki.anton-paar.com/en/water/)	85
Figure 41: Diffusion coefficient of chlorine in water, Kramers et al. (1959)	85
Figure 42: seasonal frost effects on soil temperatures (Goodrich 1982)	87
Figure 43: heat capacity of water change with temperature.....	91
Figure 44: Kinematic Viscosity change with temperature	93
Figure 45: Prandtl number change by temperature	93
Figure 46: simple network for temperature modelling.....	94
Figure 47: temperature change at nodes over time for the single pipe example	95
Figure 48: EPANET NET1 example network.....	96
Figure 49: temperature simulation for Net1	97
Figure 50: Chlorine simulation for Net1	98
Figure 51: Chlorine simulation using EPANET	98
Figure 52: Chlorine concentration at node 21 for different pipe Lambda values	99
Figure 53: Temperature at node 11 for different source temperatures.....	99
Figure 54: Temperature profiles at logger's locations	100
Figure 55: Zone 4 connectivity schema	101
Figure 56: PS 2 pumping station outflow	101
Figure 57: PS 2 pumping station outflow	102
Figure 58: PS 5 pumping station outflow	102
Figure 59: PS 1 pumping station outflow 1	102
Figure 60: PS 1 pumping station outflow 2	103
Figure 61: PS 4 pumping station outflow 1	103
Figure 62: PS 4 pumping station outflow 2	103
Figure 63: Res 3 inflow	104

Figure 64: Res 2 Reservoir inflow	104
Figure 65: Res 2 Reservoir level	104
Figure 66: Res1 Reservoir level	105
Figure 67: Res 3 level	105
Figure 68: Daily Ground Temperature, NRC(°C)	106
Figure 69: Average Chlorine levels at demand junction.....	107

List of Tables

Table 1. Observed changes in annual and seasonal mean temperature between 1948 and 2016 for six regions and for all Canadian land area (Bush, 2019)	18
Table 2. Projected change in annual mean surface air temperature for six regions and for all Canadian land area, relative to 1986–2005 (Bush, 2019).....	18
Table 3. Observed changes in normalized annual and seasonal precipitation between 1948 and 2012 for six regions and for all Canadian land area (Bush, 2019)	19
Table 4. Case Studies Characteristics	37
Table 5. Results, Affected Watermain Lengths.....	40
Table 6 Case Study Watermain Material, Length, and Installation Year	54
Table 7 Case Study Watermain Diameter Distribution.....	54
Table 8. Details of case-study cohorts	55
Table 9 Estimated covariate values by I-WARP for final variables considered in each pipe group.	55
Table 10: Results of first-order bulk decay tests (Boulos, Vasconcelos, Rossman, Clark, & Grayman, 1997)	76
Table 11: calculation of θ by (Koechling, 1998).....	77
Table 12: depth of penetration of diurnal and annual temperature cycles (Florides & Kalogirou, 2001)	86
Table 13: Empirical correlations for the average Nusselt number (Çengel, 1998)	88
Table 14: change of Prandtl number with temperature	89
Table 15: typical values of heat transfer–related parameters (Mirjam Blokker & Pieterse-Quirijns, Modeling temperature in the drinking water distribution system, 2013)	90
Table 16: data for temperature modelling proof of concept	95

Executive Summary

As part of a broad initiative to develop decision support tools for the design and rehabilitation of core public infrastructure to ensure adequate performance under existing climate and future climate change, the National Research Council of Canada (NRC) and Infrastructure Canada (INFC), in partnership with collaborators and stakeholders, undertook a study to examine risks and potential opportunities emerging from changes in precipitation, temperature and freeze/thaw cycles on water distribution system resilience and performance. Specifically, the project addressed the following: 1) the impacts of temperature and precipitation changes on water consumption and the ensuing implications for hydraulic capacity, 2) the impacts of temperature and precipitation changes on energy consumption in water distribution system operation, 3) the impacts of changes in temperature, precipitation and freeze/thaw cycles on water main breaks, and 4) the impacts of temperature changes on water quality (through tracking of chlorine residuals). This work is envisaged to serve as a first step toward the development of a set of tools for water utility companies to evaluate their system vulnerabilities to changing climate.

Section 1 addresses the broad questions of climate change impacts in Canada, focusing on temperature and precipitation, likely the most significant factors likely to impact water distribution system operation and planning: . The section outlines some recent studies, in particular from ECCC, observing changes in mean temperature and precipitation across Canada. Both the observed and projected increases in mean temperature in Canada are about twice the corresponding increases in the global mean temperature, regardless of emission scenario. Annual and seasonal mean temperatures across Canada have increased, with the greatest warming occurring in winter. Between 1948 and 2016, the best estimate of mean annual temperature increase is 1.7°C for Canada as a whole and 2.3°C for northern Canada. Overall, precipitation is expected to increase throughout Canada; however, summertime precipitation is expected to decrease 10-20%, especially in southern Canada.

Sections 2 and 3 consider how the climate trends described in Section 1 are likely to influence water consumption (Section 2) and the consequent impact on the hydraulic capacity of water mains (Section 3). Consulting a variety of studies for New York, Serbia, Calgary, British Columbia and Toronto, existing water demand was shown to increase with every one degree °C above a temperature threshold (reported in the range 15-25 C), with the exact number depending on location. Municipal water demand in winter exhibited essentially no correlation with temperature for the Northern hemisphere locations in the studies. Section 2 offers a case study of a Canadian city for which temperature, precipitation and water production data in the period 2011-2020 were examined and correlated. Both linear and non-linear models were fit to the summer and non-summer demand. Non-summer demand was shown to be little influenced by climate, while summer demand revealed some influence, exhibiting magnitudes commensurate with relationships reported in the literature.

Section 3 proposes a methodology for evaluating climate change impact on water distribution system capacity, incorporating IPCC temperature scenarios, a utility's own water consumption

records and historical weather data, and employing Monte Carlo simulation with thread-based parallel processing (for testing different scenarios efficiently). Three case studies using this method are described. The studies (using data from actual Canadian utilities) considered what fraction of pipes in a network were significantly impacted by imposing extra water demands (resulting from climate change) with reference to two key network design criteria: headloss and water velocity in a pipe. The studies revealed that the headloss criteria (resulting in sub-standard service water pressure) is often the one which is violated due to the extra demand imposed by climate change, while the velocity criteria is generally still satisfied. Therefore, with reference to the headloss criteria, a larger fraction of “impacted” pipes would be identified. Also, pipes grouped into the mid-range diameter of 400-900 mm were more likely to exhibit a greater percentage of headloss criterion violation than smaller distribution pipes and large transmission mains.

Section 4 addresses the issue of pipe failure and how climate change may impact the frequency of pipe breaks in a system. It has been observed by a significant body of research that in cold countries, like Canada, pipe breakage frequency increases as the temperatures drop. Frost loading and dry weather soil shrinkage imposing loads on buried pipes were named the likely culprits. Studies examining pipe breaks have generally worked on developing straightforward correlations between pipe breaks and freezing degree days. More recently, data mining techniques have been applied to pipe break analysis. These have incorporated a variety of parameters including weather data to predict breakage. A non-homogeneous Poisson process (NHPP) is demonstrated as a way to consider predicted future climate in the estimation of pipe breaks under a changed climate. Essentially, a relationship between climatic factors and pipe breakage rate is established based on historic network break data (multiple models are available in the literature, of which NHPP is but one). This relationship is subsequently used to estimate future pipe breakage rates with forecasted climate scenarios. A risk-based approach that focuses on intangible damages (number of people either cut-off from the network or experience pressure reduction due to a pipe break) is presented. The approach is demonstrated with a case-study and results reinforced the general understanding that, in cold locations, higher mean temperatures will result in lower rates of water main breaks due to the diminished impact of frost penetration.

Section 5 addresses how climate change-induced alterations in water demand translate into new patterns of energy consumption. Because most municipal water systems rely on pumping to bring water to consumers, electricity consumed to run pumps is a good indicator of the energy used to provide water. Traditionally, studies examining energy use in water distribution systems focused on maximizing pump efficiency and optimizing pump schedules – mostly to save on utilities’ energy bills. Increasingly, focus has broadened to include a more holistic view of energy use in WDS, now including multi-objective optimization strategies for design and operation that include cost minimization, as well as energy and greenhouse gas reduction goals, even incorporating concepts as embodied energy and manufacturing of infrastructure components. A simple approach for evaluating potential climate change impacts on WDS energy use is presented. It employs the projection of future demand increase, the translation of

this increase into an appropriate diurnal demand pattern, and then the application of extended period simulations (EPSs) using software. Many utilities already have coded representations of their networks in either the public domain EPANET software, or other commercially available hydraulic modelling packages, facilitating the application of this approach. Two real networks serve as a case study for demonstrating the approach. For both systems, the extra water demand arising from climate change led to an essentially linear increase in energy use to run pumps (increased frictional losses are non-linear but represent a smaller total portion of the energy burden). The case studies demonstrate that nodal pressures will reduce as a result of greater headlosses resulting from larger flows. This projection will help in understanding when and where the distribution network will require reinforcement to maintain the required service pressure. .

Municipal water distribution systems must not only supply water in necessary quantities and at adequate pressures, but such water must also be safe for drinking. Section 6 considers how climate change might impact water quality in these systems. As the term “water quality” is not a quantitative term, disinfectant (chlorine) residuals are considered as surrogate and this section is therefore focused on how warmer air and water temperatures could impact their concentration in the water. The water temperature in a distribution network is largely governed by source water temperature (which, depending on the source, is in turn influenced to varying degrees by air temperature) and temperature of the soil surrounding the pipes (which is also influenced by air temperature). A literature scan reflected a complete absence of a software tool capable of considering any thermal effects on the water in a distribution system. Consequently, a water quality model was developed, which is capable of accounting for water temperature variations in the distribution network that result from ambient temperature variations in the air and in the soil. This model was realised as an add-in module in EPANET software..

The network of a participating utility was instrumented with various sensors and two years of data were collected, including air temperature, water temperatures in 12 locations across the network as well as pressure data. Water temperature in the winter was found to be fairly constant (as expected), while in the summer it was observed to follow the seasonal variation of air temperature, however at a lag of a few weeks and with a lesser amplitude.

The model was then applied to a case study network (a zone from a participating utility’s system). As expected, higher chlorine concentrations are observed with lower source water and ground temperatures. For this particular case study, residual chlorine levels at 5°C were about 4-5% higher than those at 25°C, suggesting that disinfectant boosting protocols may need to adjust for climate change.

Section 7 summarizes the overall report and offers observations derived from the different sections and case studies, along with some suggestions for future research.

1 Introduction

1.1 Background

Canada's buildings, bridges, roads, water and wastewater systems may be at risk due to the effects of climate change and extreme weather. There are limitations in current approaches to design and rehabilitation of Core Public Infrastructure (CPI) that are based on past climatic loads and not on expected future climatic loads, which may lead to early failure of CPI, long service disruption, high rehabilitation and replacement costs, and considerable negative socio-economic impact. The consequences of failure of existing and new CPI, including, buildings, bridges, roads, water and wastewater systems and post disaster facilities can be quite significant and could include fatalities, injuries and illnesses, increased costs to infrastructure owners, and unforeseen costs to the infrastructure users, to insurers, and to the municipal, provincial/territorial and federal governments.

The owners and managers of Canadian core public infrastructure (CPI) are looking for cost-effective approaches to build resilient new CPI and rehabilitate existing CPI to ensure their satisfactory performance under climate change and extreme weather events. CPI owners and Canadian industry face two major technical barriers that are hampering their response to climate change, namely, (a) growing risk of failure of existing CPI under effects of climate change and extreme weather events; and (b) lack of innovative approaches and technologies for the construction of resilient new CPI.

The National Research Council of Canada (NRC) and Infrastructure Canada (INFC), in partnership with collaborators and stakeholders are tasked to develop decision support tools, including codes, guides and models for the design of resilient new CPI and rehabilitation of existing CPI to ensure adequate capacity against existing and future climate change and extreme weather events. NRC and collaborators will integrate advances in risk assessment and management, resilient design of CPI, new climatic loads, green technologies, material science, structural engineering, life cycle assessment (LCA), and life cycle cost analysis (LCCA) to deliver and deploy decision support tools and technologies, including: (a) codes, standards, design/user guides, specifications, evaluations, maintenance guides, risk analysis of assets, and evidence-based solutions, (b) decision support tools for risk-based design of climate-resilient new CPI; and, (c) guidelines and decision support tools for the climate-resilient rehabilitation of existing CPI. These decision support tools will help to improve the manner with which infrastructure owners manage their invaluable assets.

Within this effort, water/wastewater systems management has been identified as one of the most significant areas likely to be impacted by climate change through changes in temperature, precipitation and freeze/thaw cycles. In particular, water supply systems could, under some circumstances, see potential increase in risk while other circumstances could give rise to potential opportunities. The project endeavours to quantify these risks and opportunities in various water distribution systems (WDSs) across the nation and develop a set of tools (e.g.,

models, guidelines, procedures) for water utilities to assess their assets under a changing climate and ensure that the risks and opportunities are properly accounted for and addressed.

1.2 Water Distribution System Risk and Opportunity Project

The project at hand has been defined to answer the following questions:

- 1- What are the impacts of temperature and precipitation changes on water consumption rate and the consequent implication to the hydraulic capacity of distribution systems?
- 2- What are the impacts of temperature and precipitation changes on energy consumption in WDS?
- 3- What are the impacts of changes in temperature, precipitation and freeze/thaw cycles on water main breaks? And finally,
- 4- What are the impacts of temperature changes on water quality (i.e., chlorine residuals) in water distributions?

The impact of increasing temperatures on water distribution system loads is evaluated through literature review of water consumption rates and climatic covariates. The consequent implications on asset capacity (e.g., increasing energy requirements, water main capacity reduction) are studied through extended simulations and extensive hydraulic modeling. Asset deterioration (manifested through water main failure frequency) are investigated after updating pipe failure datasets collected in previous projects. Extensive field work was undertaken to record water temperatures across a moderately large system. These data were used to also investigate the impact of changing freezing index on water main breaks. Finally, the temperatures collected in the previous stage are combined with hydraulic modeling and simulations to develop/calibrate a water quality/temperature model, which is used to evaluate climate change's potential impacts on WDS water quality.

This work is part of a broader effort undertaken by the National Research Council of Canada (NRC) to investigate and adapt Climate Resilient Building and Core Public Infrastructures (CRB-CPI) to climate change. This work is envisaged to serve as a first step toward the development of a set of tools for water utility companies to evaluate their system vulnerabilities to changing climate.

The next section (Section 1.3) provides a brief overview on climate variables and their expected forecasted range in Canada. Section 2 investigates how changing climate is likely to change water demand, and Section 3 investigates how these new demands are likely to affect water distribution network capacity. Climate change potential impact on water main breaks is discussed in Section 4, followed by an investigation of the likely impact of all these changes on energy consumption in Section 5. Likely impact of climate change on water quality in the distribution system is discussed in Section 6. Summary and conclusions are provided in Section 7.

1.3 Climate Variables and their expected range in Canada

Temperature and precipitation are the two key climatic parameters that are expected to affect water distribution systems. Higher temperature has been correlated with higher demand and lower precipitation is also correlated with higher irrigation demands (M.L. Parry, 2007). The following sections summarize the key outcomes of Environment and Climate Change Canada's report (Bush, 2019) on the current and expected trends in these two key climatic factors with minimum changes to the original text. In the following sections we only focus on the aspects of the temperature and precipitation that are affecting water distribution systems the most. These includes a) average and extreme temperature, and b) summer precipitation which effects the water consumption for irrigation purposes.

1.3.1 Temperature

It is virtually certain that Canada's climate has warmed and that it will warm further in the future. Both the observed and projected increases in mean temperature in Canada are about twice the corresponding increases in the global mean temperature, regardless of emission scenario. Annual and seasonal mean temperatures across Canada have increased, with the greatest warming occurring in winter. Between 1948 and 2016, the best estimate of mean annual temperature increase is 1.7°C for Canada as a whole and 2.3°C for northern Canada (Figure 1 and Table 1). Annual and seasonal mean temperature is projected to increase everywhere, with much larger changes in northern Canada in winter. Averaged over the country, warming projected in a low emission scenario is about 2°C higher than the 1986–2005 reference period, remaining relatively steady after 2050, whereas in a high emission scenario, temperature increases will continue, reaching more than 6°C by the late 21st century.

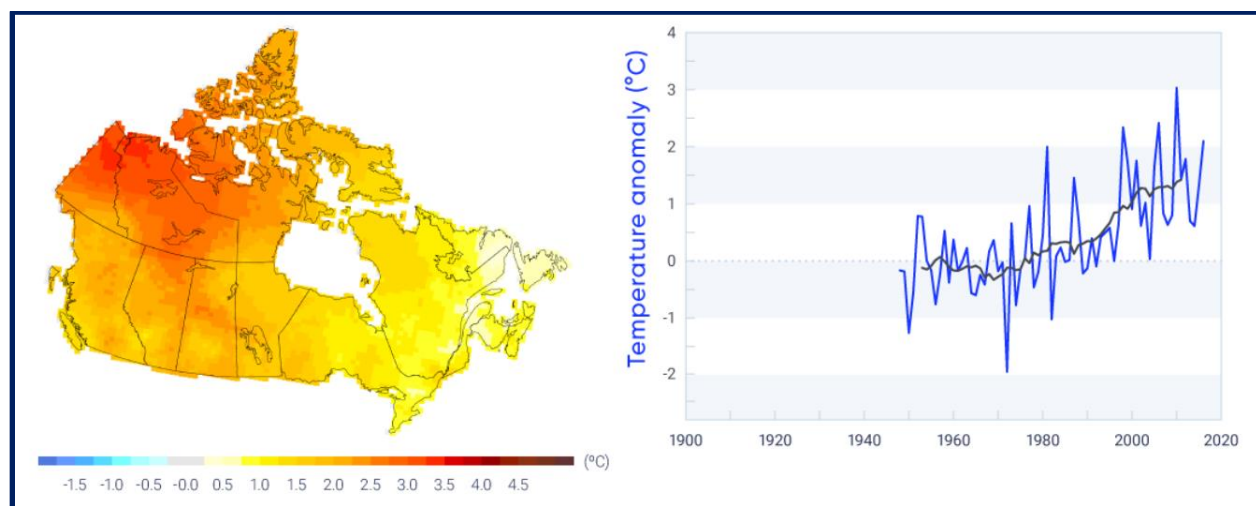


Figure 1. Observed changes (°C) in annual temperature between 1948 and 2016 (Bush, 2019)

Table 1. Observed changes in annual and seasonal mean temperature between 1948 and 2016 for six regions and for all Canadian land area (Bush, 2019)

REGION	CHANGE IN TEMPERATURE, °C				
	Annual	Winter	Spring	Summer	Autumn
British Columbia	1.9	3.7	1.9	1.4	0.7
Prairies	1.9	3.1	2.0	1.8	1.1
Ontario	1.3	2.0	1.5	1.1	1.0
Quebec	1.1	1.4	0.7	1.5	1.5
Atlantic	0.7	0.5	0.8	1.3	1.1
Northern Canada	2.3	4.3	2.0	1.6	2.3
Canada	1.7	3.3	1.7	1.5	1.7

Future warming will be accompanied by a longer growing season, fewer heating degree days, and more cooling degree days. Extreme temperature changes, both in observations and future projections, are consistent with warming. For example, (Colombo, Etkin, & Karney, 1999) employed ARIMA time series analysis to historical temperature data from nine sites across Canada and showed how small changes in descriptive climate parameters (e.g., mean daily maximum temperature or variance) could result in a greater frequency of protracted heat waves. Extreme warm temperatures have become hotter, while extreme cold temperatures have become less cold. Such changes are projected to continue in the future, with the magnitude of change proportional to the magnitude of mean temperature change (Table 2 and Figure 2).

Table 2. Projected change in annual mean surface air temperature for six regions and for all Canadian land area, relative to 1986–2005 (Bush, 2019)

REGION ^a	SCENARIO; PERIOD; MEDIAN TEMPERATURE (25TH, 75TH PERCENTILE), °C			
	RCP2.6		RCP8.5	
	2031–2050	2081–2100	2031–2050	2081–2100
British Columbia	1.3 (0.8, 1.9)	1.6 (1.1, 2.1)	1.9 (1.4, 2.5)	5.2 (4.3, 6.2)
Prairies	1.5 (1.1, 2.1)	1.9 (1.2, 2.2)	2.3 (1.7, 3.0)	6.5 (5.2, 7.0)
Ontario	1.5 (1.1, 2.1)	1.7 (1.0, 2.1)	2.3 (1.7, 2.9)	6.3 (5.3, 6.9)
Quebec	1.5 (1.0, 2.1)	1.7 (1.0, 2.2)	2.3 (1.7, 2.9)	6.3 (5.3, 6.9)
Atlantic	1.3 (0.9, 1.8)	1.5 (0.9, 2.0)	1.9 (1.5, 2.4)	5.2 (4.5, 6.1)
North	1.8 (1.2, 2.5)	2.1 (1.3, 2.5)	2.7 (2.0, 3.5)	7.8 (6.2, 8.4)
Canada	1.5 (1.0, 2.1)	1.8 (1.1, 2.5)	2.3 (1.7, 2.9)	6.3 (5.6, 7.7)

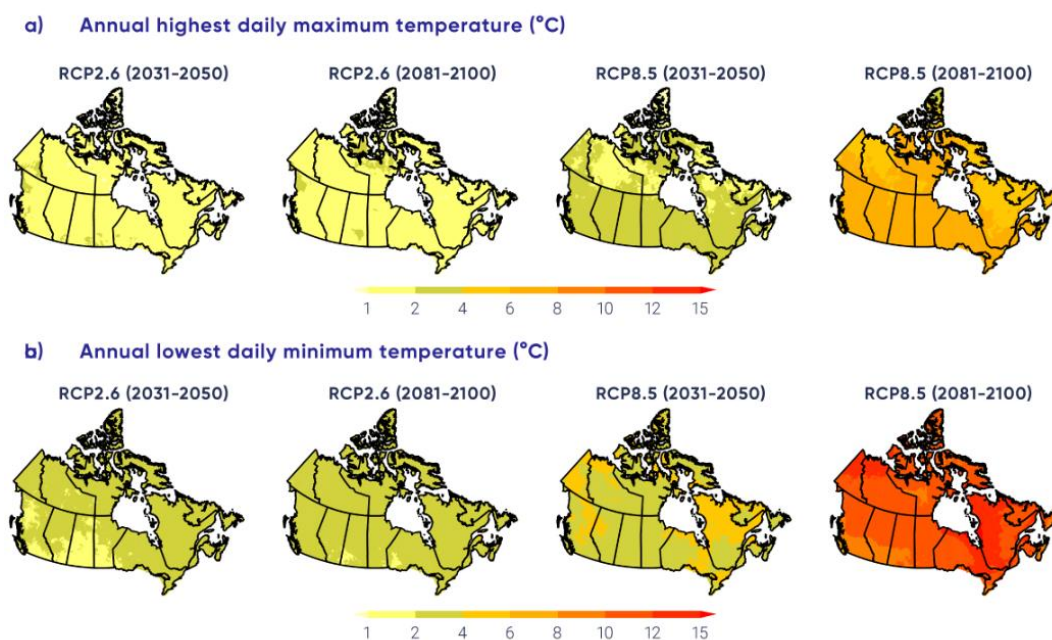


Figure 2. Future projections for selected temperature indices (extremes) (Bush, 2019)

1.3.2 Precipitation

There is medium confidence that annual mean precipitation has increased (Table 3), on average, in Canada, with larger percentage increases in northern Canada. Annual and winter precipitation is projected to increase everywhere in Canada over the 21st century, with larger percentage changes in northern Canada. Summer precipitation is projected to decrease over southern Canada (Figure 3) under a high emission scenario toward the end of the 21st century, but only small changes are projected under a low emission scenario. For Canada as a whole, observational evidence of changes in extreme precipitation amounts, accumulated over periods of a day or less, is lacking. However, in the future, daily extreme precipitation is projected to increase (high confidence).

Table 3. Observed changes in normalized annual and seasonal precipitation between 1948 and 2012 for six regions and for all Canadian land area (Bush, 2019)

REGION	CHANGE IN PRECIPITATION, %				
	Annual	Winter	Spring	Summer	Autumn
British Columbia	5.0	-9.0	18.2	7.9	11.5
Prairies	7.0	-5.9	13.6	8.4	5.8
Ontario	9.7	5.2	12.5	8.6	17.8
Quebec	10.5	5.3	20.9	6.6	20.0
Atlantic	11.3	5.1	5.7	11.2	18.2
Northern Canada	32.5	54.0	42.2	18.1	32.1
Canada	18.3	20.1	25.3	12.7	19.0

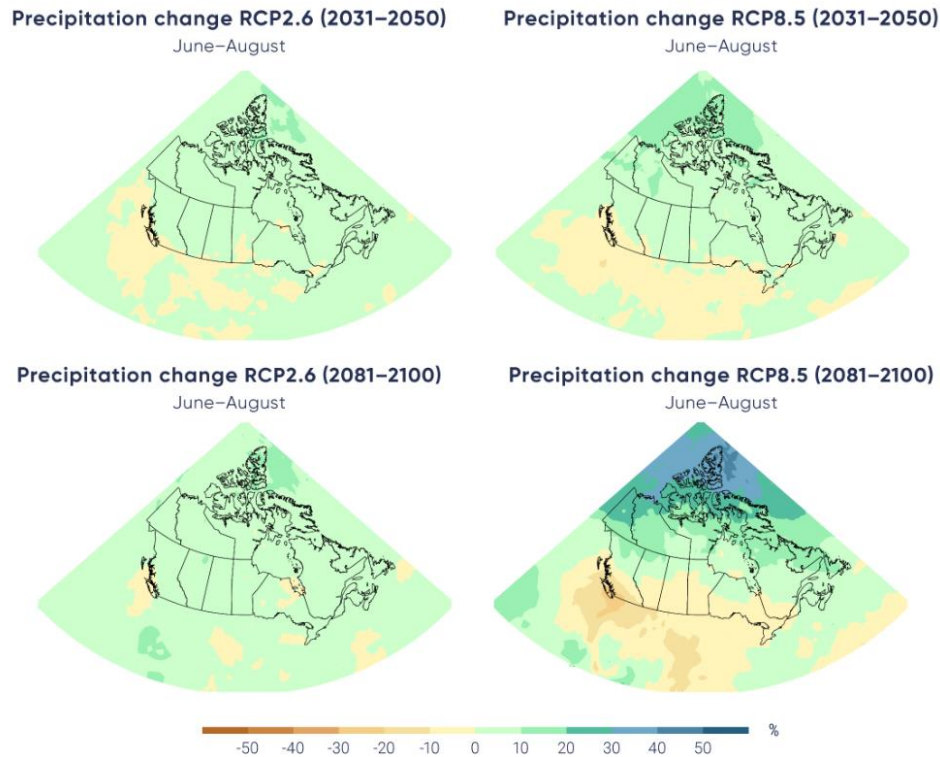


Figure 3. Projected precipitation changes for summer season (Bush, 2019)

1.3.3 Summary and commentary

Climate forecasts by Environment and Climate Change Canada (ECCC) predicts that average temperature could rise by 6°C by the end of this century. Although precipitation in winter might increase as a result of this temperature rise, ECCC predicts that summer precipitation for southern Canada will decrease between 10 to 20 percent (Figure 3). This is where most Canadian live and when precipitation is needed the most specially to irrigate lawns. Next section will examine the impact of this rising temperature and decreasing precipitation on water consumption rates.

2 Impacts on water consumption rate and hydraulic capacity

Forecasting water consumption in urban environments is important for appropriate planning and sustainable development. A variety of factors influences these forecasts. Most early works in this area focused on socio-economic factors. However, since the late 1990s researchers started to account for climate variables in their estimates. The change of such variables may result in increasing water consumption in areas where observed trends indicate that the general temperature is rising and/or precipitation is decreasing. Literature in this area is scant and the estimated range of impact varies significantly. (Mote, et al., 1999) studied the impacts of climate variability and change in the US's Pacific Northwest. They described an econometric model developed by the City of Portland's Bureau of Water Works to aid in estimating near and long-term water demands. The model established the relationship between the total water demand and selected economic and demographic variables (e.g., price, income, employment, and population growth) in combination with variables representing weather and the normal cycle of demand. The impact of a particular weather in their model is estimated by applying the "weather effect" of a specific year (i.e., temperature and rainfall observations) to the demand forecasted based on economic and population variables along with average weather for the 1940 to 1998 period. Their 2050 forecast used regional projection of employment and population for that year and they tailored their estimates to reflect the influence of a particular weather year (1991 in their work) by applying the observed weather pattern from the 1991 to the projection. They showed that climate change could increase Portland's daily demand between 5% to 8% and their peak day demand between 5% and 10%. They indicated that the increase in the average peak season demand (i.e., summer) would affect the Bureau's ability to meet water supply needs over the entire summer season. They also indicated that increase in the peak day demand, on the other hand, more directly affected their transfer capabilities.

Climate Change and Demand for Water (CCDeW) project in 2003 used various models including statistical analysis for domestic demand, expert judgement combined with statistical models for industrial and commercial demands, dynamic simulation and optimization and agent-based social simulation to estimate the demand growth. Four high resolution regional climate change scenarios from low to high global emissions were also considered. The relationship between degree days (above 10 °C) and frequency of water use was also considered for the domestic demand estimates. The assumed behavioral link is that with warmer weather people perspire more, leading to an increased frequency of washing. A soil moisture deficit model was used to estimate garden watering. The authors estimated the increase of 1.8% to 3.7% in UK's average annual domestic demand by 2050. These increases are over the socio-economic growth (Downing, et al., 2003).

The short term response of daily municipal water demand to rainfall and air temperature variations were studied for nine cities in USA by (Maidment & Miaou, 1986). These cities were located in Florida, Pennsylvania and Texas. The authors showed that the response of water use to temperature and rainfall in Texas and Florida are very similar while Pennsylvania [closer to Canadian climate] is more sensitive to air temperature and less to rainfall. They also pointed out

that city size has little impact on the response. Rainfall more than 0.13 cm/day decreases the seasonal water by a proportion of yesterday's water use by 38% for the Texas cities, 42% for the Florida cities, and 7% for the Pennsylvania cities (with colder climate). They showed that water use will increase by air temperature beyond 21 °C.

A statistical analysis of water use in New York City showed that above 25°C, daily per capita water use increases by 11 litres/1°C (roughly 2% of current daily per capita use) (Protopapas, Katchamart, & Platonova, 2000). The authors used daily water use data for New York City from 1982 to 1991 and found that during winter months, weather has little effect on water use. However in summer periods, precipitation causes a decrease of 5% of yesterday's demand.

Neale et al (2007) examined the water sufficiency by studying various scenarios of future residential water demand while integrating population growth, climate change, housing type and demand side management in three cities (i.e., Town of Oliver, City of Penticton, and City of Kelowna) in the Okanagan Basin of British Columbia (Neale, Carmichael, & Cohen, 2007). The future water demand scenarios were calculated annually for the period from 2001 to 2069. They estimated that per-capita water use will increase by 3 to 10% from 2001 to 2020s and from 7 to 19% in 2050s due to the changing climate. They also noted that when combined with population growth, and the current preferences of housing (i.e., single house) the impact of climate change was magnified. This could increase water use by 4 to 21% in the 2020s and 18 to 86% in the 2050s with smaller communities (i.e., Oliver) at the lower end of this range.

(Praskievicz & Chang, 2009) studied the effects of weather variables (i.e., temperatures, daylight length, precipitation, wind speed, relative humidity, and cloud cover) on the seasonal water used in Seoul, South Korea. They used daily and monthly data from 2002 to 2007 and applied Pearson, Kendall, and Spearman tests to study the correlation's significance. Their result indicated that temperature and precipitation have significant positive and negative correlation with per capita water use in most time scales. They also showed that consumption in July increases up to 4 liters per person with a one degree increase in max temperature.

(Dimkić, 2020) estimated the temperature correlation with water production in water supply systems for two largest cities in Serbia (i.e., Belgrade and Nis) in the warmer half of the year (May to October). They divided these months to three 2-month periods. His estimates indicate that July and August (Average daily Temperature 25°C for Belgrade and 23°C for Nis) have the highest increase in water production daily average per degree of centigrade change in the temperature. He showed that water production in Belgrade and Nis increase by 0.8% and 1% per degree of temperature change.

In a similar study (Akuoko-Asibey, Nkemdirim, & Draper, 2013) correlated the average maximum weekly temperature and weekly water consumption of the city of Calgary. They showed that weekly total water consumption seems to be fairly steady when the average maximum weekly temperature is below 15°C. They indicated that one degree increase in temperature could cause an average increase in the total weekly consumption by 4.2% above 15°C. For the City of Toronto, (Sadiq & Karney, 2004) also found a comparable threshold (at around 15-20 °C) to exist for daily maximum temperature and water demand. The study

revealed that a 1°C increase in summer maximum daily temperature would result in a 2% increase in average daily summer demand and 1.8% increase in peak day demand.

Analysis of the observed daily drinking water consumption for the period 2011-2016 in the City of Montreal indicated that average daily consumption would increase by 3% above 12°C (Rasifaghihi, Li, & Haghighat, 2020). The authors used Bayesian statistics methods and split their data in two clusters (i.e., base and seasonal water use). They also showed that the base water use is independent of climate.

The per capita water consumption rate in Chapman, British Columbia was found to be significantly correlated to ambient temperature, where an average rise in summer temperatures of 1°C caused a consumption increase of 34 liter per capita per day (Staats, 2018). That was. (Akuoko-Asibey, Nkemdirim, & Draper, 2013) similarly estimated an increase of 40 LPCD for each 1°C rise, over 15 °C in the city of Calgary. If true, such increases in water demand may impose higher stress on water distribution networks and their components.

2.1 Recommended approach to quantify climate change impacts on demand

The range of available approaches to study the impact of temperature and precipitation on municipal demand could include very detailed approaches with sophisticated statistical analysis to simple correlation studies. However, most sophisticated analysis requires access to expertise that may not be available, especially in smaller municipalities or it may be costly. In the case study presented in the next sections, we investigate this impact using both complex nonlinear models as well as more simple linear ones. We show that a relatively simple linear regression (easily applicable in Excel using the straightforward “Linest” function) can capture the essence of this impact without the complexity of more involved models. This may provide municipal planners with a relatively accurate and simple means to account for the impacts of climate change on their water distribution system demands.

Most municipalities record their water production volumes on a daily bases. These data combined with mean daily temperature and precipitation records (both accessible from <http://climate.weather.gc.ca/>) are enough to estimate the climate-driven increase or decrease in the municipal water demand.

A few notes of caution are warranted here:

- Although in this text we refer to “water demand”, in reality available data is in fact “water production” (and not “demand”). This is important because non-revenue water (AKA water losses) could also have variability which, if not accounted for (e.g., through leak-detection campaigns, changes in undetected leaks, etc.), could introduce extra “noise” into the demand data.
- Variations in water demand are driven by several factors. Among these are temperature and precipitation; however, these are not the only ones and often these are not even the most significant. Issues like the aforementioned non-revenue water (including leakage,

theft, disastrous pipe breaks, pipe flushing, etc.), malfunctions or problems in the treatment plants, educational campaigns on water usage reduction, odd/even irrigation policy, a wave of fires, etc., are also potentially important contributors to demand fluctuations.

- In the case study presented below, total demand was not normalized to per capita demand. This however, this could be easily done with average yearly population data.
- One could attempt to predict the contribution of climate change on future water demand by applying regression models to predicted climate data (found for example, in Section 1.3 in this report or, more precisely, using Pacific Climate Impacts Consortium (PCIC) downscaled forecasts that are available at <https://www.pacificclimate.org/data>). However, one should remember that climate is not the only driver of variations in water demand. Moreover, there is no way of knowing whether trends discerned from 10 years of data would persist decades into the future.
- Some of the demand patterns described in the case study are characteristic to cold-climate municipalities, where summer demand pattern is significantly different than non-summer. The approach described in the case study is flexible enough to accommodate all types of climate conditions but some specifics (e.g., the exact irrigation season) would have to be modified to the specific location of the municipality on the analysis is performed.

2.2 Case study and demonstration

A relatively large city generously shared their daily production data with us for the years 2011 to 2020 (Figure 4). Daily temperature (Figure 5) and precipitation data (Figure 6) were downloaded from <http://climate.weather.gc.ca/>.

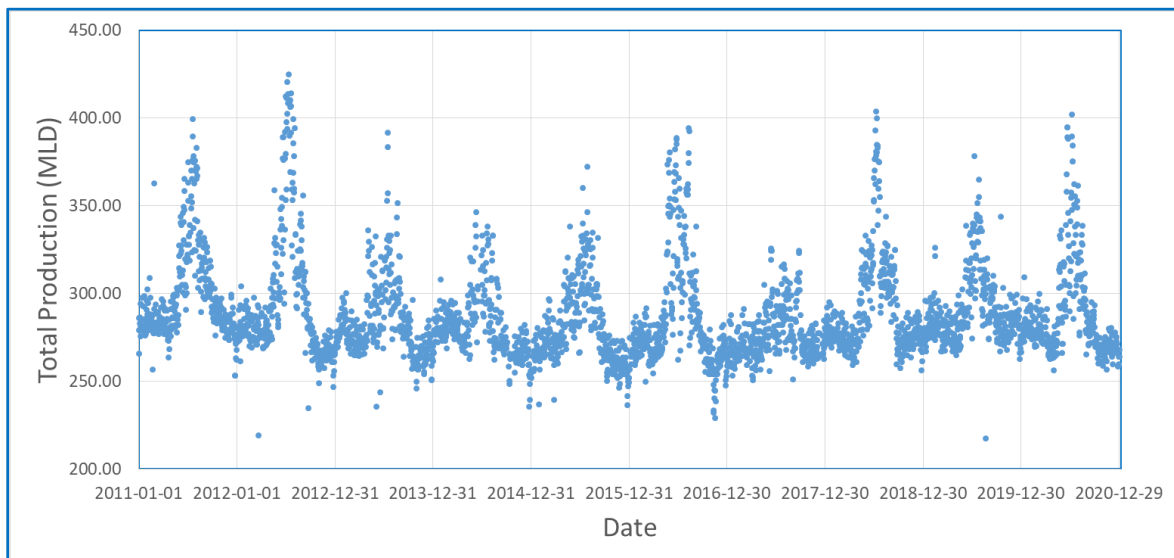


Figure 4 City's total daily water production

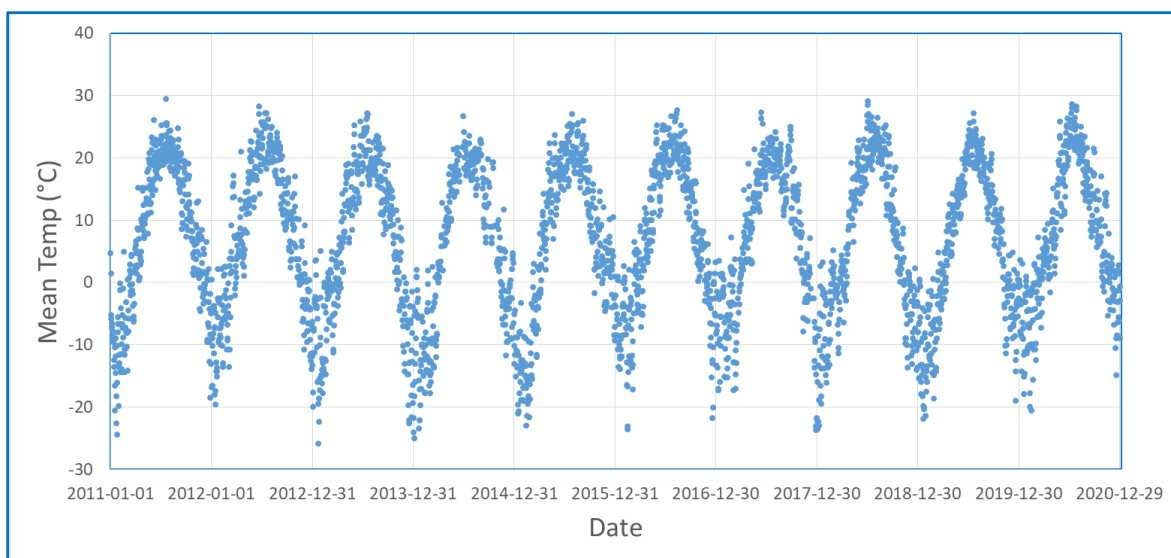


Figure 5 City's mean daily temperature

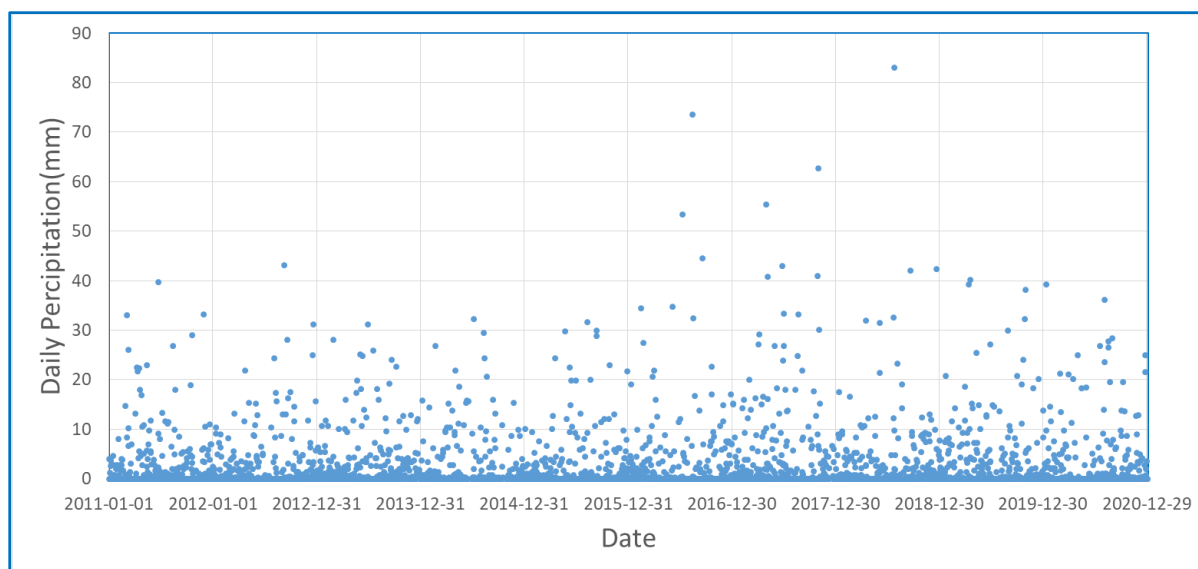


Figure 6 City's daily precipitation

2.2.1 Data preparation

To avoid relying on a single weather station dataset, especially since precipitation is an extremely localised phenomenon, three weather stations in the Case study area were found to have the required data for the entire analysis time period. Due to their location with respect to City's populated areas (and therefore by extension the proportions of total demand), the stations were assigned weights of 30%, 55% and 10% (respectively) in computing the weighted average of mean daily temperature and total daily precipitation in the City area.

Initial examination of the demand data (Figure 4) discloses a rather constant demand during the colder seasons and fluctuating demand during the summer months. This observation was corroborated by plotting the demand frequency in summer versus non-summer months (Figure 18). This observation corroborates the assumption that a significant portion of demand fluctuations in the City are attributed mainly to summer activities such as irrigation and swimming pools.

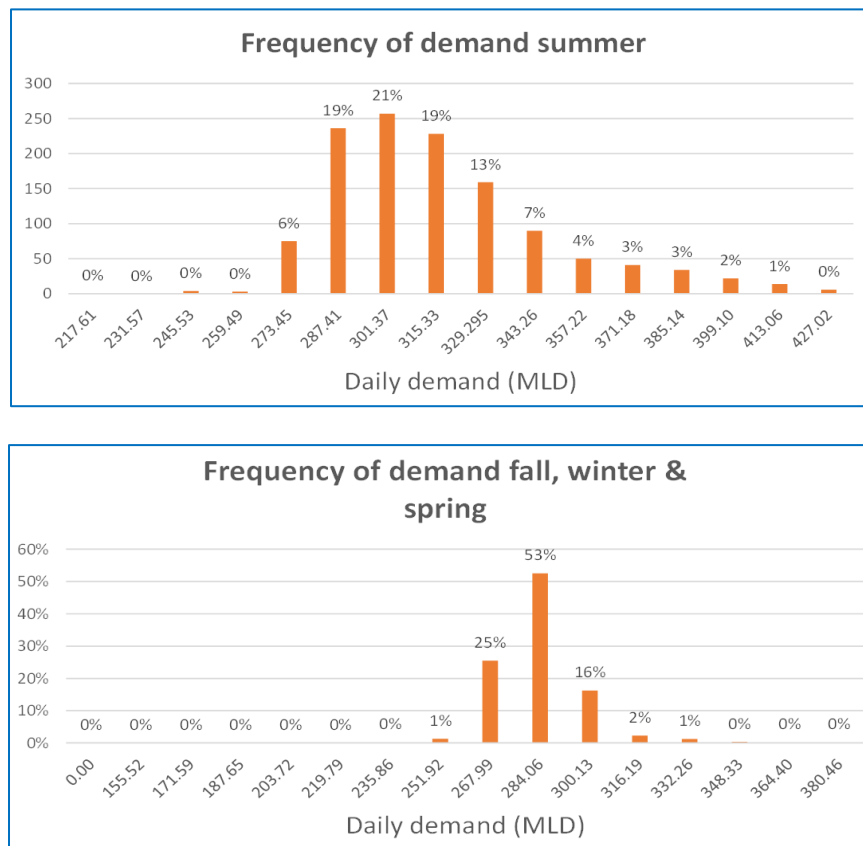


Figure 7 Demand variations during summer and non-summer months.

Consequently, the dataset was partitioned into summer months (June, July, August and September – total of 1220 daily records) and non-summer months (January through May and October through December – a total of 2432 records). All subsequent analyses were performed separately on these two datasets.

2.2.2 Nonlinear model summer data

Since nonlinear models can be sensitive to data that have many zeros and that may have significant scale discrepancies (such as ambient temperatures in °C, precipitation in mm and water demand in MLD) the summer data were normalised using the equation

$$x_i = t_{min} + t_i / (t_{max} - t_{min})$$

where x_i is the normalised value of data point i , t_i is the raw value of data point i , t_{max} and t_{min} are the maximum and minimum t values (respectively) in the dataset. It is worth noting that Z-score normalisation was found to be inappropriate due to the large number of zeroes (and consequent significant skewness) in the precipitation data. The normalised data are illustrated in Figure 8.

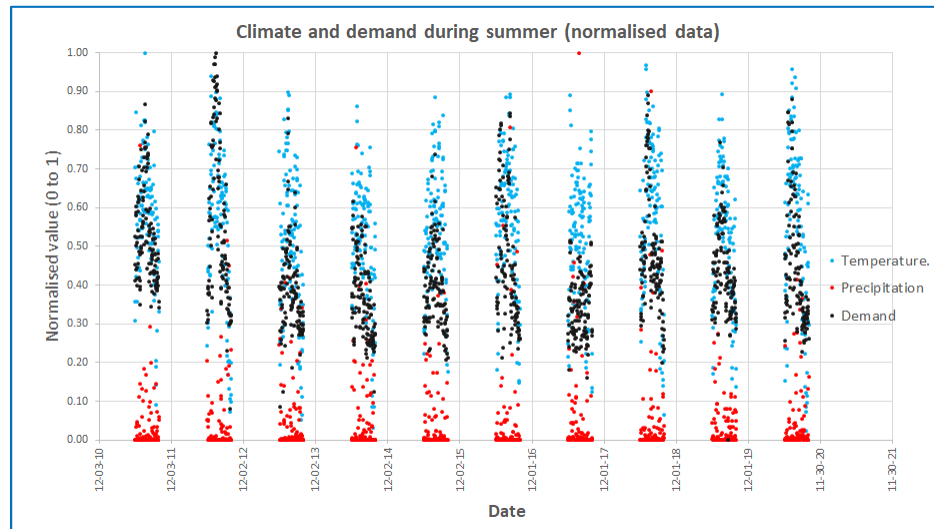


Figure 8. Normalise summer data

A nonlinear model was fit into the (normalised) data of the form:

$$\hat{D} = C + \alpha T^{\beta} + \delta P^{\epsilon}$$

Where \hat{D} is the estimated (normalised) demand, T is the normalised (observed) mean temperature, P is the normalised (observed) daily precipitation and α , β , δ , and ϵ are regression coefficients. The regression results are presented in Figure 9.

The following is noted:

1. The coefficient of determination was $R^2 = 0.491$. However, while R^2 is a meaningful statistic for linear regression it is generally not appropriate for nonlinear regression. Instead, a standard error $SE = 0.108$ was obtained.
2. The statistical significance of the pairs α , β and δ , ϵ as well as of constant C was tested. P-values of nearly zero were obtained for all, indicating high statistical significance.
3. An additional covariate comprising the product of T and P was also examined, to explore possible interaction between the two covariates, but was found to increase the standard error, therefore deemed un-necessary.
4. A positive α confirms intuitive understanding that demand increases with higher temperatures.
5. A negative δ confirms intuitive understanding that demand decreases with higher precipitation.

6. The magnitude of the regression coefficients do not tell us much beyond trends because they are associated with normalised data.

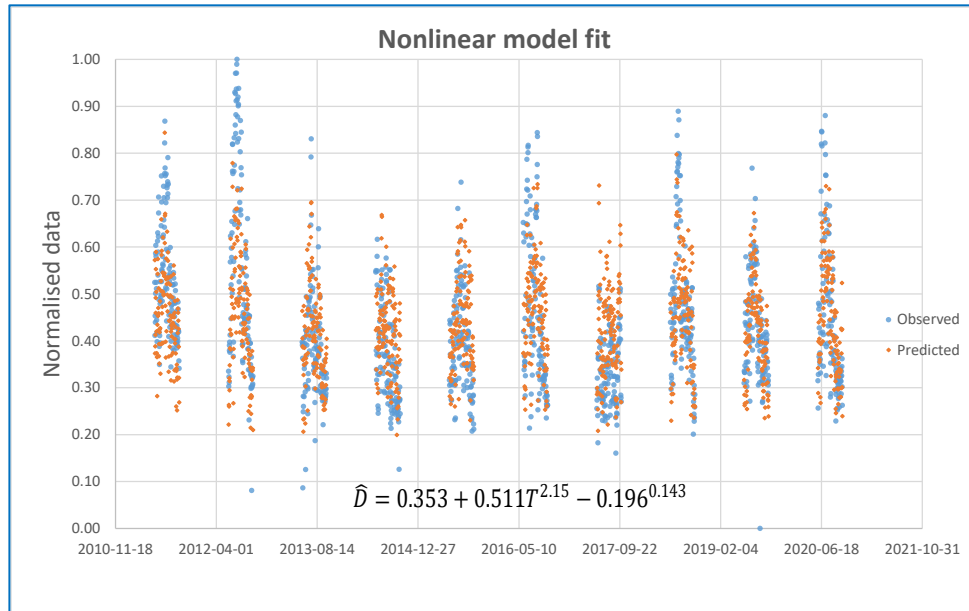


Figure 9. Nonlinear model results

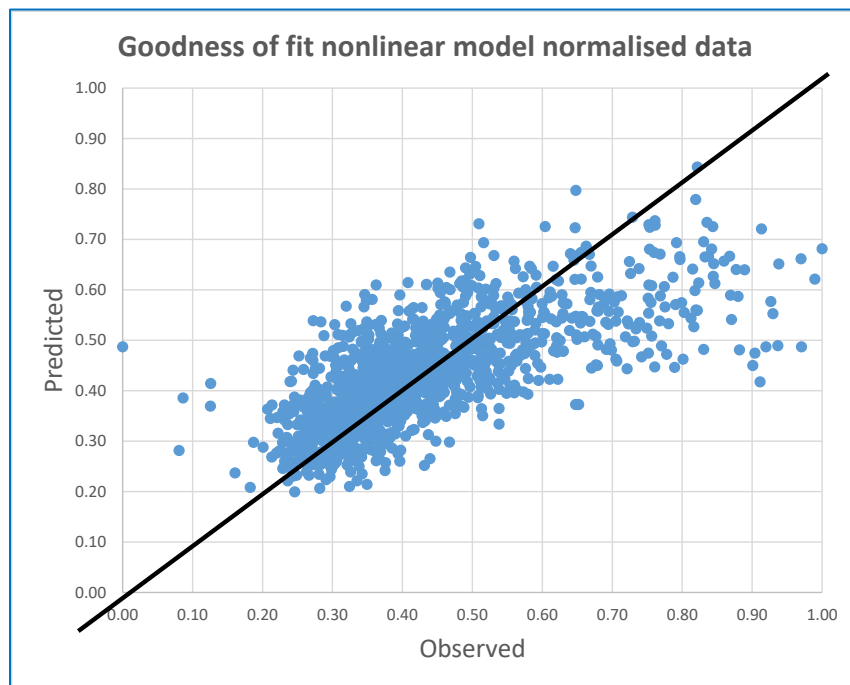


Figure 10, Goodness of fit of the nonlinear model

Figure 10 provides a "Goodness of fit" chart, where the diagonal line is the line of equality - data points on the line are perfect fit, above the line are overestimates and below the line are underestimates. This chart shows that the nonlinear model tends to overestimate very small demand values and underestimate very high demand values.

To explore this phenomenon the frequency of the demand values were examined (Figure 7 – top) and it became apparent that the extreme values of the summer demand data comprise only about 10% of the total dataset. A subset of the data, comprising only records of daily demand between 260 and 375 MLD, was extracted (a total of 1095 records). The same nonlinear model was fit into this data subset and the results are presented in Figure 11. The standard error was reduced to 0.077 (compared to 0.108), which may indicate that extreme demand values are driven by factors other than climate.

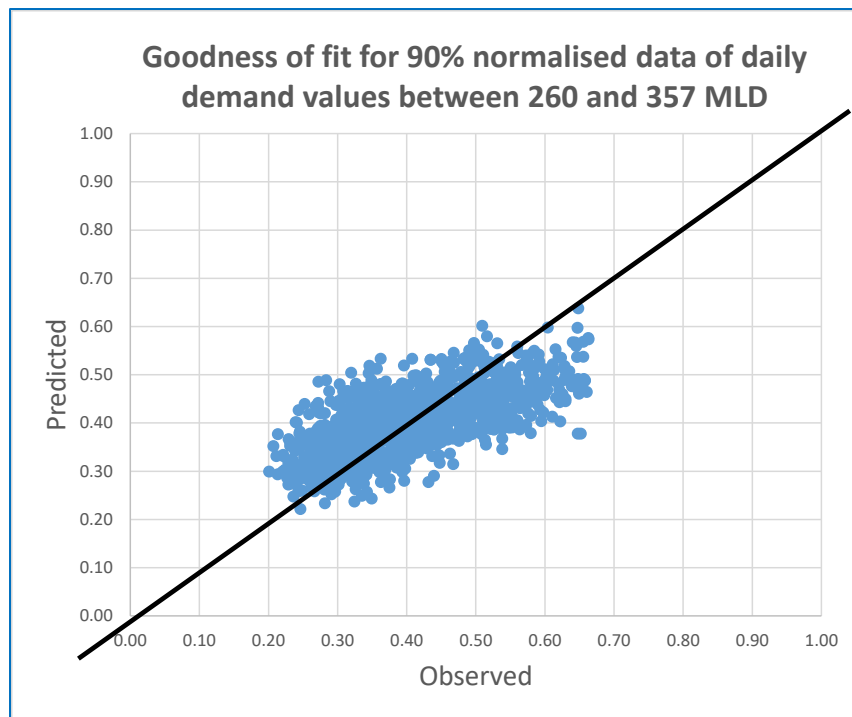


Figure 11. Goodness of fit for nonlinear model applied to summer data without extreme values.

2.2.3 Linear model summer data

To obtain a sense of the parametric impact of climate variables on summer water demand, a linear model was applied to the non-normalised summer data. The coefficient of determination was $R^2 = 0.404$ and the standard error was $SE = 24.5$ MLD. The model was statistically significant (P-value approaching zero).

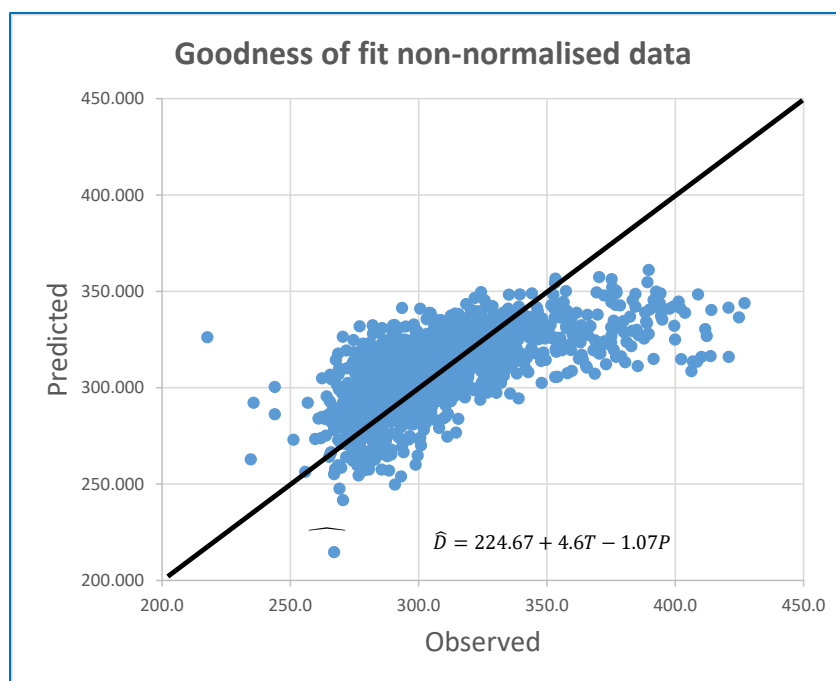


Figure 12. Goodness of fit of linear model with non-normalised summer data

The following is noted:

1. Results indicate that an increase of 1°C is associated with about 4.6 MLD (~1.5%) increase in water demand in the summer.
2. Similarly, an increase of 1 mm of rain is associated with about 1.1 MLD (~0.35%) reduction in water demand.
3. The coefficient of determination of 0.4 means that these climate covariates are able to explain only about 40% of the variation in water demand, meaning that other factors (e.g., population variations, policy factors such as restrictions or water conservation education, also interruptions due to failures) may be additional contributors to demand variation. This is similar to the results of the nonlinear model.
4. The same analysis applied to non-normalised data without extremes (i.e., 90%) of all the summer data, yielded regression results with a substantially smaller standard error (16.87 MLD) but a somewhat lower R^2 (0.384). This implies (same as in the nonlinear model) that factors other than climate may be more influential on extreme deviations of water demand.
5. Caution is warranted when trying to apply regression results to predicted future (especially far future) water demand. There is no way of knowing whether trends discerned based on 10 years of data would persist decades into the future, especially if drastic increases in temperature/precipitation predicted by some models do materialise. It is quite possible that significant increases in future demand might drive behavioural changes (e.g., drastic reduction in irrigated landscape), which in turn would affect the current demand trends.

2.2.4 Linear model non-summer data

Figure 13 charts temperature, precipitation and water demand values during the non-summer period. It is visually apparent that little correlation exists between climate and demand, as demand appears to have relatively little variation (as is also discerned from Figure 7 bottom), except perhaps some peaks in late May.

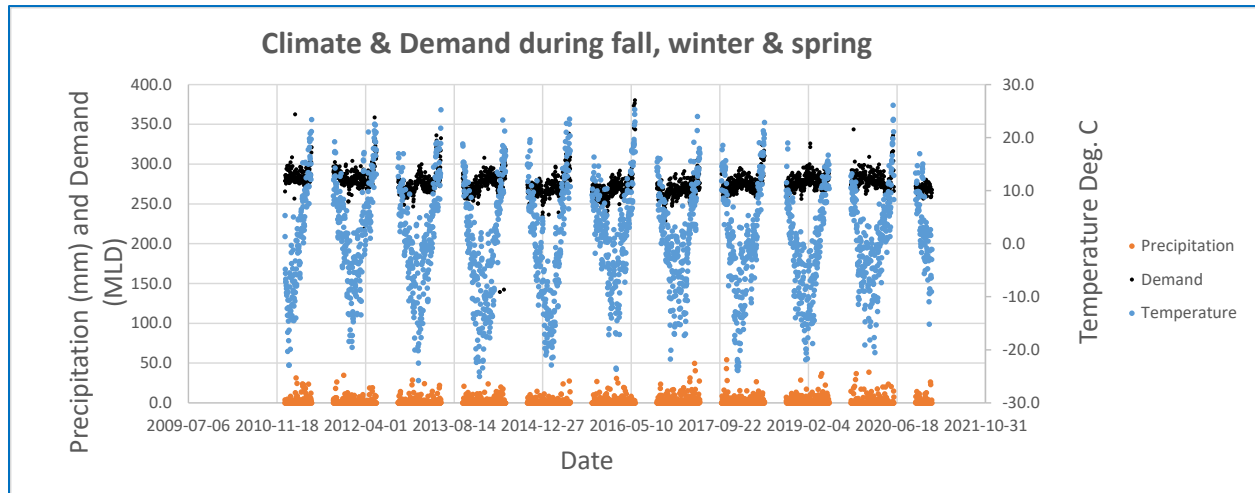


Figure 13. Climate and demand data (non-normalised) during non-summer months.

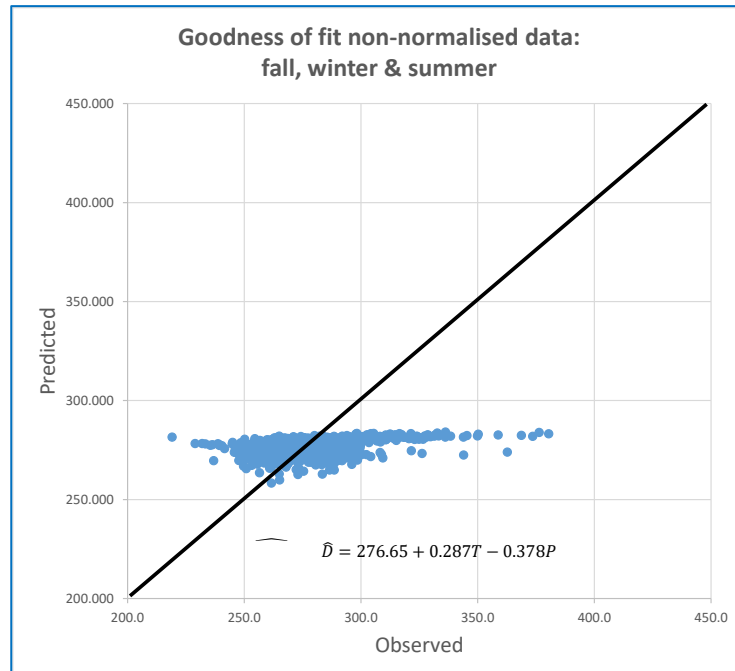


Figure 14. Goodness of fit linear model of non-summer (raw) data.

A linear model was fit to the non-normalised (raw) non-summer data. Figure 14 illustrates the results. The coefficient of determination was $R^2 = 0.046$ the standard error $SE = 14.38$ MLD and

P-value near zero, indicating statistical significance. It is to be noted that the relatively low values of the regression coefficients indicated low impact of climate factors on water demand. Moreover, the very low coefficient of determination implies that climate covariates are able to explain only 4.5% of the variation in demand, which means that this (very low) variation in non-summer months is driven mainly by factors other than climate.

3 Climate change impacts on water main capacity

While a direct mechanism by which changes in climate impact the hydraulic capacity of water mains was not apparent, a search for such a study in the literature was performed, revealing few – if any – publications have contemplated a direct impact of climate on water pipe capacity. . Most of the work addressed the impact of climate change on network capacity albeit indirectly through anticipated increased demand rather than directly on physical hydraulic capacity of the pipes. For example, Basupi & Kapelan (2015) investigated the impact of uncertain future demand and how it would be applied in the optimal design of new water distributions systems. Roshani & Filion (2013) investigated the impact of various climate change mitigation scenarios on design, expansion and rehabilitation of distribution systems and on water distribution rehabilitation planning (Roshani & Filion, 2014).

While properly designed water distribution systems generally include some redundancy in hydraulic capacity to account for population growth, fire flows and unforeseen contingencies, few if any, have considered the extra capacity that would be required to address loads caused by climate change. According to the IPCC 5th edition report (Pachauri & Meyer, 2015) global average temperatures could rise between 2 and 6 °C by 2100. Assuming a base maximum day demand (MDD) of 500 LPCD, such a temperature increase could result in a corresponding demand increase ranging from 14% to 45% in cities such as Chapman, British Colombia (Staats, 2018), Calgary (Akuoko-Asibey, Nkemdirim, & Draper, 2013), or the Case study in Section 2.2.

In the next section, a simple approach is proposed with the goal of determining how well water mains in distribution systems are suited to handle these extra loads. To achieve this, future demand growth scenarios were generated using various Representative Concentration Pathways (RCPs) suggested by the Intergovernmental Panel on Climate Change (IPCC) (Pachauri & Meyer, 2015). These scenarios were then applied to three real, moderately large North American WDSs and the hydraulic capacity of each was evaluated under various demand scenarios that were generated using Monte Carlo Simulations (MCS) while considering climate impacts.

3.1 Suggested Methodology to Evaluate the Impact of Climate change on WDS Capacity

Most large cities in Canada, are managing their water distributions system's growth based on their master plans, which are often updated every 5 years and establish a 25 to 50 years planning horizon. Based on the IPCC report (Pachauri & Meyer, 2015) this planning span is long enough for most climate change impacts on temperature or precipitation to materialize. The range of global temperature rise predicted by IPCC report (Pachauri & Meyer, 2015) is shown in Figure 15 based on various scenarios.

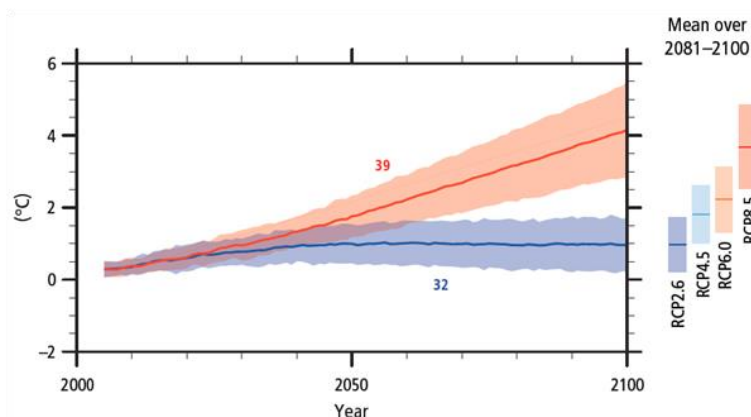


Figure 15. Global Average Surface Temperature Change (Relative to 1986-2005) (Pachauri & Meyer, 2015)

As can be seen, a wide range of temperature rise from 0.7°C (corresponding to RCP2.6) to 3°C (corresponding to RCP8.5) is expected in the next 50 years¹. However, as noted in the previous section, caution should be exercised in extrapolating demand to forecasts over periods that are much longer than the period upon which demand increase is based. Moreover, some of the climate models forecast significant changes in climate, plausibly leading to significant behavioural changes that, in turn, may affect significant changes on current demand patterns. Consequently, it is recommended that planning horizon for system capacity be limited to 25-30 years. This translates into a significant increase in the per capita demand (i.e., from 3% to 18%, assuming a 34 LPCD increase for each degree rise (Staats, 2018) and MDD equal to 560 LPCD). Additionally, the uncertainties associated with various RCP scenarios and distribution of the load across the network make it difficult to choose a single scenario, estimate its impact on the demands, and compare its results with the status quo (i.e., deterministic approach). Monte Carlo simulation can be used to account for these uncertainties, but the approach requires a large number of computationally expensive hydraulic simulations. The thread based parallel processing technique has been deployed to address this issue and achieve reasonable computational duration. The steps of the proposed methodology are:

- 1- Simulate the system with baseline (i.e., year of analysis) demand and record all water mains velocity and headloss.
- 2- Estimate average demand increase expected as a result of higher temperature in the target year. Compute corresponding nodal demand.
- 3- For every demand node in the system, assign a demand normal probability distribution with a mean value (obtained in step 2) and a standard deviation. The Monte Carlo simulation will draw a random demand from this distribution (99.8% of the sampling demand will be in the range of mean demand \pm 3 standard deviations).

¹ We used global climatic models here to first simplify the calculation and to preserve the anonymity of the case studies. However, a more proper way is to rely on the downscaled regional climatic models or use the information provided in Table 2 to estimate the range of future mean temperature change.

- 4- If possible, divide the simulations between available cores to speed up computations.
- 5- Run all hydraulic simulations and collect results.
- 6- Calculate the aggregated results (i.e., average velocity and headloss and their standard deviations) for each water main.
- 7- Compare the aggregates with the baseline values and quantify the impacted on water mains.

Note: various water utilities may design their WDS based on different demand scenarios, such as Average Day Demand (ADD), Maximum Day Demand, (MDD) or Peak Hour Demand (PHD). The proposed approach does not restrict the design scenario but all steps must be applied consistently with the preferred demand scenario.

The IPCC report introduces roughly 300 scenarios among which RCP2.6 with a stringent mitigation scenario keeps the temperature rise below two degrees by the end of the century, while the two intermediate scenarios (i.e., RCP4.5, and RCP6.0) limit the temperature to 3 degrees, and one with very high GHG emissions (i.e., RCP8.5) raises the temperature by 5 degree (Pachauri & Meyer, 2015). As mentioned previously most WDSs master plans are developed for the next 50 years therefore, the temperature raise resulted by the aforementioned RCPs should be limited to 2060s. Based on the four selected RCPs, three raising temperatures (i.e., 1 °C for RCP2.6, 2 °C for RCP4.5-6.0, and 3 °C for RCP8.5), have been selected as representative of 2060s temperature. Then the rise in temperature could be translated to a rise in water demand.

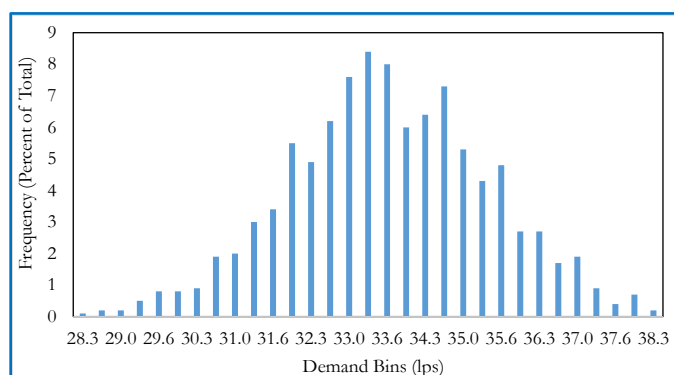


Figure 16. Histogram of the demand distributions for one node with the base demand of 28.2 lps.

In step 3, the normal distribution generates demand multipliers for each demand node, creating a discretized distribution from which the Monte Carlo process samples in each simulation. .. Figure 16 illustrates this discretized distribution, with of the demand for a node which had a base demand of 28.3 lps while its demand increase due to climate change was estimated to be 17%. As can be seen, the generated demands deriving from a Gaussian distribution are averaged on 33.3 lps, which is 17% more than the original base demand. Each node in a system has its own set of demands generated in the Monte Carlo simulation process. This allows for accounting of potential uneven distribution of future demands due to uneven development in the system.

If possible, a thread pool programming approach whereby each generated Monte Carlo scenario is then sent to an available core to simulate, can be used in the fourth step. Depending on the number of cores utilized for this purpose, the overall simulation time could be significantly reduced. On each core the WDS is simulated to estimate its hydraulic variables using EPANET2 (Rossman L. , 2000). The result of each simulation is then sent back to the master thread to aggregate. The master thread calculates the average and standard deviation of the desired variables (i.e., velocity and headloss) add them to the GIS layer representing the pipes.

The proposed model was programmed as an add-in to HydraCAL (Roshani, HydraCAL User's Manual, 2014). HydraCAL uses parallel processing to expedite lengthy simulations. It also uses a simple but powerful GIS environment which allows for various statistical and spatial analyses. Figure 17 shows HydraCAL with the newly added demand growth simulator.

3.2 Case studies

To evaluate the impact of demand growth due to rising temperature caused by changing climate, three real world and large WDSs in Canada (Table 4) with numerous pressure zones and sources are selected. These networks are anonymized due to security reasons and are shown in Figure 18. The maximum day demand scenario is selected for evaluation. The demands are estimated based on population growth and land use by the consulting firms who developed the master plans for these systems. Note that some of these networks account for demand reduction due to the implementation of various water conservation policies.

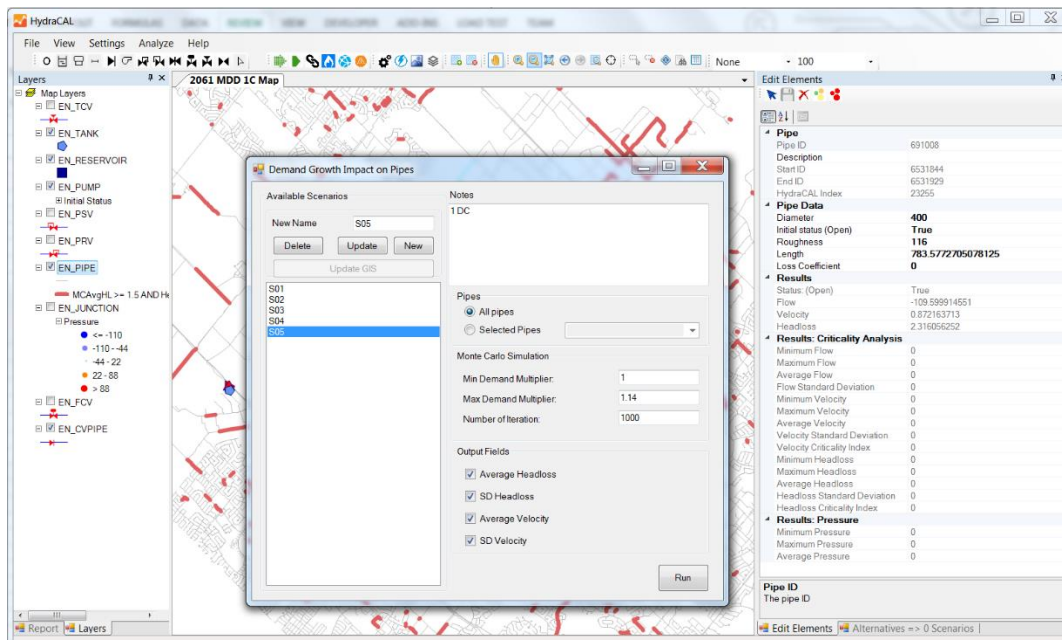


Figure 17. HydraCAL and Its New Add-ins for Evaluating Demand Growth.

The impacts of these policies have already been considered in the estimated future loads. Since no studies were done for the relationship between temperature increase and demand for these

particular WDSs, a rate of 34 LPCD per one degree of temperature increase (Staats, 2018) was utilized for all three case studies and the future demands were adjusted accordingly. A more appropriate technique would have used the methodology suggested in Section 2.1. The system components are also representative of the future plans. For instance, if a water main or a pump station is supposed to be in service or decommissioned by a certain year before the planning horizon, it is already represented in the model as such.

In each WDS 1,000 randomly generated demand scenarios (based on Gaussian distribution) were simulated on a laptop computer with 8 cores. On average, each simulation took approximately 3 minute to finish, a practical result considering the large size of each system.

Table 4. Case Studies Characteristics

Number	Serving Population	Total Pipe Length (km)	Planning Year	Model Status
1	1,400,000	4,100	2061	Detailed Model
2	2,700,000	2,876	2060	Some Pressure Zones are Detailed and Some are Skeletonized
3	1,300,000	2,950	2061	Detailed Model

3.3 Results and analysis

The simulation results for all of scenarios generated with Monte Carlo simulation were aggregated and then compared with the baseline simulation (i.e., MDD without the impact of climate change) for each case study. Since during design of each watermain two hydraulic criteria (i.e., headloss and velocity) are satisfied to be below certain limits, both parameters are used to identify affected water mains as follows:

- 1) All water mains with the baseline headloss below 1.5 m/km and the average MCS headloss above the 1.5 m/km.
- 2) All water mains with the baseline velocity below 1.5 m/s and the average MCS headloss above 1.5 m/s.

A summary of the results is shown in

Table 5, and the distribution of the affected pipes based on their headloss criteria could be found in Figure 18. Overall, the impact of climate driven demand increase seems to be moderately small in the selected case studies. For instance, at most only 3.9% of the water mains are impacted in Case Study 1 under RCP8.5, which has the highest demand increase. Although this is a small percentage, it includes approximately 160 km (of 4100 km) of water mains in Cast Study 1. This amount would be expensive for the utility to rehabilitate. These extra demands could push more water mains to operate while exceeding headloss criteria, even while the velocity constraint remains satisfied. This pattern can be seen for all three cases, in all watermain diameter categories, and under all RCPs. This occurs because most utilities,

including those in the selected case studies, prefer to design their water mains under a conservatively lower velocity criteria (i.e., 1 m/s) rather than what is allowed in their guidelines (i.e., 1.5 m/s). Consequently, most of the pipes have extra capacity to compensate for the higher demands. Additionally, and as expected, more severe RCPs (i.e., higher temperature) would lead to a higher percentage of water mains exceeding their design criteria in all of the categories.

It is worth noting that Case Study 1 seems to have a higher number of affected water mains that are distributed across the entire system (Figure 18) in comparison with other systems. This mainly arises because this WDS is located in a city, which has the highest rate of intensification amongst the case studies. Thus, most of the water mains are expected to operate near their capacity and adding the extra water demand imposed by climate change pushes them over their limit.

Table 5 categorizes water mains based on their diameter into four groups. A) below 150 mm which supplies most subdivisions; B) between 150 mm and 400 mm which is the subdivision level distribution; C) between 400 mm and 900 which are mainly distribution trunks; and finally, D) above 900 mm which are the main transmission lines. Barring the transmission lines (i.e., above 900 mm), almost in all of the case studies, the percent of affected pipes increases with larger diameter. This is mainly due to the fact that transmission level mains are generally designed conservatively and thus have a greater inherent capacity to accommodate the extra flow.

3.4 Conclusions

Monte Carlo simulation is combined with parallel processing to evaluate the impacts of climate driven demands on the capacity of water mains in three large real world water distribution systems. The results indicate that the headloss criteria is more typically violated than the velocity constraint. Additionally, the extra demand due to climate change affected larger diameter distribution mains more, while it had minimal effects on transmission lines.

The existing work is limited in scope to the impact of extra demands on WDS's watermain capacities under the MDD condition (a more prevalent demand scenario). Future research could focus on studying the impact of rising demands on distribution of pressure, fire flow, and other system components such as pump stations, reservoirs, and energy consumptions, or system/supply redundancies. Other demand scenarios such as Peak Hourly Demand (PHD) could be looked into. Moreover, the case studies in this work were limited to large and well maintained WDSs. Using a more diverse set of WDSs could result in a different set of observations. Finally, the impacts of altered precipitation regime on demands was not studied. This could also be a source of stress on a WDS and should be investigated further.

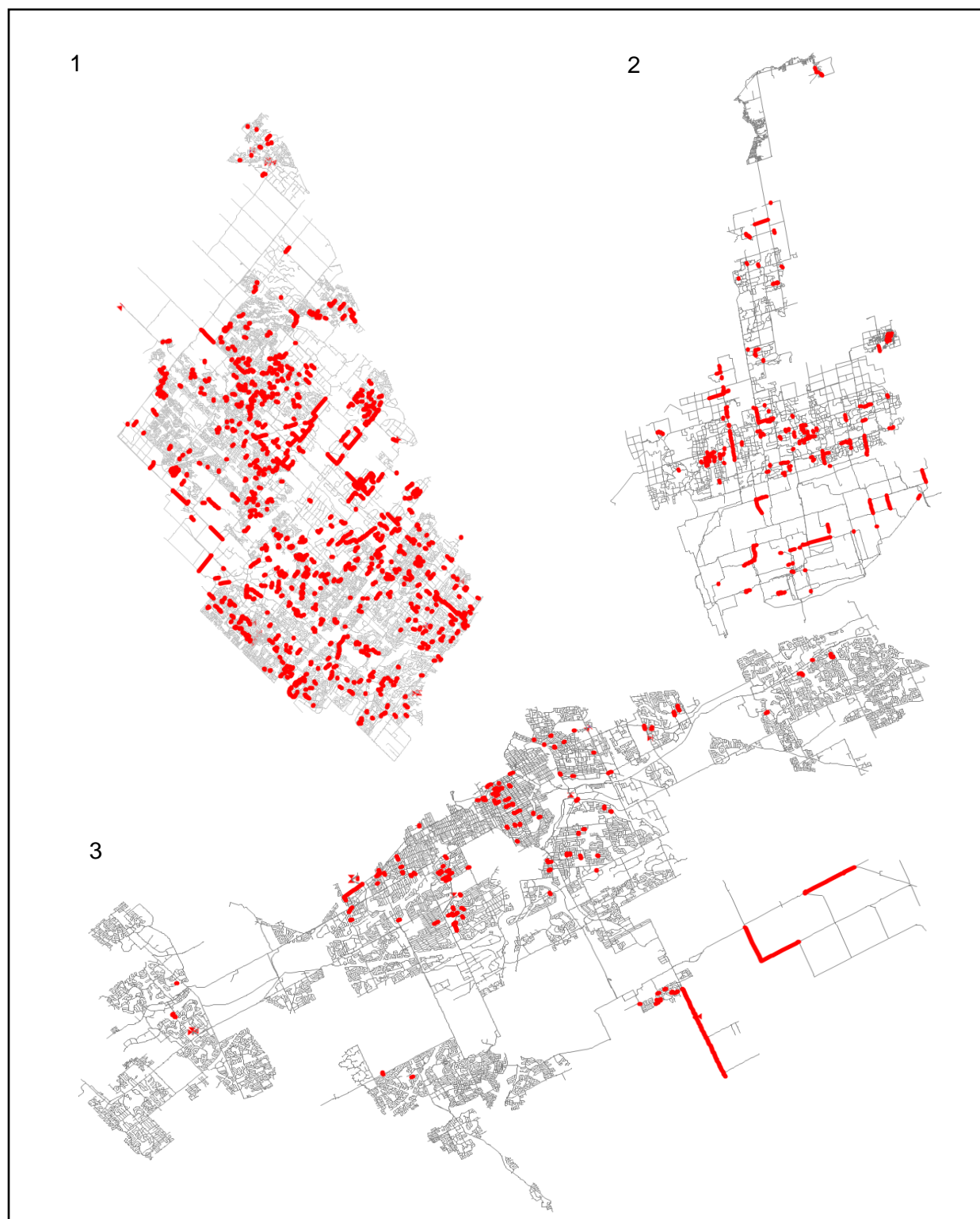


Figure 18. The Selected WDSs. Red Links Indicate the Impacted Pipes for RCP8.5.

Table 5. Results, Affected Watermain Lengths

Case Study	Pipe Diameter (mm)	Total Length in WDS (m)	Affected Pipe Length (m) (% to total) (Headloss)			Affected Pipe Length (m) (% to total) (Velocity)		
			RCP2.6 (1 °C) Increase	RCP4.5 & 6.0 (2 °C) Increase	RCP8.5 (3 °C) Increase	RCP2.6 (1 °C) Increase	RCP4.5 & 6.0 (2 °C) Increase	RCP8.5 (3 °C) Increase
1	D ≤ 150	1,558,401	16,358 (1.0%)	27,354 (1.8%)	39,307 (2.5%)	606 (0.0%)	1,471 (0.1%)	2,520 (0.2%)
	150 < D ≤ 400	2,046,290	32,218 (1.6%)	60,013 (2.9%)	91,755 (4.5%)	10,720 (0.5%)	18,215 (0.9%)	26,700 (1.3%)
	400 < D ≤ 900	348,116	7,684 (2.2%)	12,076 (3.5%)	27,036 (7.8%)	3,853 (1.1%)	7,077 (2.0%)	9,548 (2.7%)
	900 < D	146,841	52 (0.0%)	107 (0.1%)	175 (0.1%)	6 (0.0%)	78 (0.1%)	170 (0.1%)
	Total	4,099,647	56,312 (1.4%)	99,549 (2.4%)	158,272 (3.9%)	15,186 (0.4%)	26,841 (0.7%)	38,937 (0.9%)
2	D ≤ 150	179,861	456 (0.3%)	1,403 (0.8%)	1,916 (1.1%)	(0.0%)	(0.0%)	(0.0%)
	150 < D ≤ 400	1,515,885	12,701 (0.8%)	24,497 (1.6%)	40,775 (2.7%)	291 (0.0%)	1,140 (0.1%)	1,707 (0.1%)
	400 < D ≤ 900	743,735	10,740 (1.4%)	25,830 (3.5%)	43,322 (5.8%)	2,228 (0.3%)	4,830 (0.6%)	7,084 (1.0%)
	900 < D	437,226	3,213 (0.7%)	3,322 (0.8%)	4,884 (1.1%)	222 (0.1%)	1,202 (0.3%)	1,346 (0.3%)
	Total	2,876,707	27,109 (0.9%)	55,053 (1.9%)	90,897 (3.2%)	2,742 (0.1%)	7,173 (0.2%)	10,137 (0.4%)
3	D ≤ 150	895,384	1,924 (0.2%)	3,800 (0.4%)	8,269 (0.9%)	(0.0%)	(0.0%)	(0.0%)
	150 < D ≤ 400	1,818,755	12,608 (0.7%)	13,704 (0.8%)	20,470 (1.1%)	3 (0.0%)	275 (0.0%)	281 (0.0%)
	400 < D ≤ 900	149,557	885 (0.6%)	885 (0.6%)	2,564 (1.7%)	(0.0%)	(0.0%)	(0.0%)
	900 < D	86,256	(0.0%)	(0.0%)	(0.0%)	(0.0%)	720 (0.8%)	720 (0.8%)
	Total	2,949,951	15,418 (0.5%)	18,390 (0.6%)	31,302 (1.1%)	3 (0.0%)	994 (0.0%)	1,001 (0.0%)

3.5 Recommendations

- The case studies provided here revealed that the headloss criteria is often the one which is violated due to the extra demand imposed by climate change, while the velocity criteria is generally still satisfied. Thus, with reference to the headloss criteria, a larger fraction of “impacted” pipes would be identified. The velocity criteria is relevant for water quality (circulation and water age), scouring of pipes, and the severity of hydraulic transients (the natural shock wave that occurs when, for example, a pump or valve is closed). The headloss criteria has implications for energy dissipation through the system

whereby larger headlosses in pipes mean lower downstream pressures, with possible implications for energy use if pumping is boosted to compensate for these lowered delivery pressures. Both criteria are important and it may be illustrative to consider how many pipes are impacted through the lens of both.

- Larger distribution trunks ($400\text{ mm} < D < 900\text{ mm}$) are expected to be more effected by the extra load in comparison with transmission lines or smaller distribution level mains, likely because small distribution mains are typically oversized for fire extinguishing requirements. Therefore, a higher level of investment is required in these mains so that energy (pressure) loss stays at an acceptable level.

4 Impact of climate change on Water Main Breaks

Underground pipes in water distribution systems are designed to withstand various loads and external forces during their lifespan and before they fail. However, climate change may accelerate or decelerate watermain deterioration processes and vary the loads and forces affecting their failure rate. Unfortunately, there is a lack of knowledge on quantifying the relation between climate change and watermain deterioration (UKWIR, 2012).

Most of the literature available in this field includes work examining the impacts of local climate on pipe breaks for instance (Clark, 1970) examined the impact of weather on various expansive soils during the course of a year and determined their swell index and its impact of pipe breaks. (Newport, 1981) analysed circumferential pipe breakage data from various areas of the Severn-Trent Water Authority. He found that increased breakage rates coincided with cumulative degrees-frost (usually referred to as freezing index in North America and expressed as degree-days) in the winter as well as with very dry weather in the summer. The increase in winter breakage rates was attributed to the increase in earth loads due to frost penetration, (i.e., frost loads), and the summer breakage rates were linked to the increase in shear stress exerted on the pipe by soil shrinkage in a dry summer. It was also observed that when two consecutive cold periods occurred, the breakage rates (in terms of breaks per degree-frost) occurring in the first period exceeded those of the second and rationalised that the early frost “purged” the system of its weakest pipes, causing the later frost to encounter a more robust system. Both authors used data from years 1970-1977 to obtain the following linear relationship (correlation coefficient of 0.9) between the number of water main breaks and the cumulative degrees-frost in a given year

$$\text{Total bursts per year} = 2.5(\text{Total degree of frost}) + 500 \quad (1)$$

This equation was derived for the Soar division of the Severn Trent distribution system but the length of water mains was not specified. This linear model suggests that every degree of frost is responsible for an additional 2.5 breaks but, at the same time, only about 50% of the failures may be explained by cold climate, expressed as cumulative degrees-frost. No model to predict watermain breaks during extreme dry weather was given.

(Habibian, 1994) analysed the distribution system of the Washington (DC) Suburban Sanitary Commission and observed an increase in water main breakage rate as the temperatures dropped. Breakage rates were related to the water temperature at the system intake rather than to the ambient air temperature, reasoning that, although their monthly averages are similar, ambient air temperatures display sharp fluctuations while water temperatures are better surrogates for underground pipe environment. The conclusion was that the water temperature drop, rather than the absolute water temperature, had a determining influence on the pipe breakage rate. It was also observed that, in a given winter, similar consecutive temperature drops did not necessarily result in similar breakage rates; however, almost every time the temperature reached a new low, a surge occurred in the number of pipe breaks. The explanation for this phenomenon concurred with (Newport, 1981), namely, that every temperature low “purged” the system of its weakest pipes. Thus, a new low affected the pipes that were a little more robust than those that had broken in the previous cold spell. During the

warm seasons the pipes continue to deteriorate and the process is repeated in the subsequent cold season. It should be noted that (Habibian, 1994) observations were all based on one-year data.

(Lochbaum, 1993) reported on a study conducted by Public Service Electric and Gas Co. which showed that the breakage rates of cast iron gas pipes increased exponentially with the number of degree-days (degree-days were defined as $S_{i,N}[(65^{\circ}\text{F}-T_i)]$ where T_i is the average temperature in $^{\circ}\text{F}$ in day i and N is the set of days in a given month with average temperature below 65°F). (Lochbaum, 1993) did not present a model relating the number of water main breaks to monthly degree-days; however, observations agreed with those of Newport (1981) and others. No information is provided as to the causes of pipe breaks in the warmer seasons. In their review, (Rajani & Kleiner, 2001) referred to a more sophisticated analysis based on the application artificial neural network (ANN) that included temperature, rainfall and pipe operating pressure to predict pipe breakage.

Freezing index, age, and rainfall deficit were used in a multi-variate exponential model to predict pipe breakage based on historical data by (Hu & Hubble, 2007). Fourier analysis utilized by (Kleiner & Rajani, 2002) and combined with historical climate data to forecast climate. They combined their forecast with pipe aging to predict watermain breaks and showed that using Fourier analysis to generate climate-dependent covariates (e.g., freezing index and rain deficit) could be a reasonable approach when more robust and detailed climate forecasts are unavailable.

Additionally, (Kleiner & Rajani, 2010) and (Kleiner & Rajani, 2012) developed a probabilistic model based on the Non Homogeneous Poisson Process (NHPP) to rank individual water mains in terms of their anticipated break frequency. Their model considered both static (e.g., pipe material, diameter, vintage, surrounding soil, etc.) and dynamic (e.g., climate, operations, cathodic protection, etc.) effects influencing pipe deterioration rates. They tested their models on six different datasets and 37 scenarios. Results indicated that a NHPP-based model is superior in its ability to directly consider quantitative and qualitative time-dependent covariates and has the ability to forecast actual number of breaks, which is important to support effective decision making. They also suggested that, in many instances, at least some of the climate covariates emerged as significant (but not always). This may be due to various reasons. For example, water utilities in cold-climate often bury their water mains quite deep (e.g., 2.4 m in Ottawa) where the potential impact of climate-related factors is greatly dissipated. Further, the predominant failure mode in ductile iron pipes is corrosion holes. Climate-related factors are less likely to impact ductile iron pipes with corrosion holes than, say, cast iron mains which are prone to circumferential or longitudinal pipe failures, often exacerbated by soil movement due to expansion/contraction and/or frost penetration.

Furthermore, (Rajani, Kleiner, & Sink, 2012) examined the impact of temperature changes on observed pipe breakage rate for three pipe materials: cast iron, ductile iron and galvanised steel. Several water and air temperature-based covariates were tested in conjunction with a non-homogeneous Poisson pipe break model to assess their impact on water main breaks, using data sets from three different water utilities in the USA and Canada. Temperature-based

covariates, such as average mean air temperature, maximum air temperature increase and decrease, and how fast the air temperature increases and decreases over a specific period of days, were found to be consistently significant. While the availability of water temperature data (which most utilities do not have) can enhance the prediction of water main breaks, they concluded that it appears that air temperature data alone (which most utilities can access) are usually sufficient.

Evolutionary polynomial regression methods used by (Laucelli, Rajani, Kleiner, & Giustolisi, 2014) to relate pipe breaks with weather data. Authors showed the model was able to make good predictions of pipe bursts in the cold season for the upcoming 1 or 2 years.

Finally, (Wols & Van Thienen, 2014) performed a statistical analysis on the effects of weather variables on pipe failure. Their failure prediction model showed temperature and drought were the most influential for pipe failure. In their later work (Wols & Van Thienen, 2016) used the same model to assess the long-term weather variations on pipe failure.

The aforementioned publications focus on the understanding of the impact of temperature and/or precipitation on the structural integrity of buried water mains. None of them attempts to couple this understanding with climate change, which means that even if there was an attempt to forecast climate effects there was an implicit assumption of climate stationarity.

The following section offers a simple technique based on Non Homogenous Poisson Process (NHPP) previously developed by (Kleiner & Rajani, 2010) to evaluate the climate change impacts on failure rate. The methodology is then applied to a real world water distribution system and the impact on watermain breaks were quantified as the number of people losing their access to the network and finally, results are presented.

4.1 Suggested Methodology to Evaluate the Impact of Climate Change on WDS Watermain Breaks

The climate change impacts on watermain breaks is not limited to the number or frequency of the breaks. It entails potential financial and public access aspects as well. Estimating the financial damages of each break is straightforward and directly correlated to the number of breaks. A holistic view of pipe failure must include direct, indirect tangible and intangible damages. Some of these damages can be monetized (cost of repair, replacement, etc.) while others, such as the number of people affected by a pipe failure and/or other social costs are either impossible or at least difficult to monetize. Often utility companies have a good estimation of direct tangible (monetized) cost of pipe failure based on pipe material, diameter and location. However, the quantification of the number of affected people is often challenging and elusive. Thus, the focus here will be on this intangible damage in the examples ahead.

Since pipe break events are uncertain events, it is recommended to treat them in a risk-based framework. Risk is calculated as the product of damages (e.g., financial or number of people

affected) caused by an event (e.g., watermain break) multiplied by the likelihood of that event (i.e., probability of the event happening).

$$\text{Failure Risk} = \text{Failure likelihood} \times \text{failure consequence (damage)} \quad (2)$$

The likelihood of an individual pipe break could be estimated using various break-prediction models. Although the proposed approach is not restricted to any break-prediction model, the ease of use and availability of free computer software that uses the NHPP approach (e.g., I-WARP) makes it an attractive choice. The details of I-WARP's NHPP are provided in Sections 0 to 4.1.5. Models such as I-WARP (detailed in Section 4.1.5) allow examination of the impact of various covariates on the breakage rate of an individual watermain based on observed historical break data. I-WARP considers different covariates, including those that are climate-related. Therefore, subject to some assumptions, users can endeavor to predict future breaks by inputting predicted climatic covariates in addition to "static" covariates such as pipe diameter, material, etc. The user can use the historic network break data to create the break models and then use the predicted climatic variables to forecast the expectation of breaks in individual mains.

After estimating the break expectation for individual water mains, the "Damages" have to be estimated. As noted earlier, estimated direct monetary damages are typically readily available, therefore, the focus here is on non-monetary impact. We defined non-monetary pipe break damage as the number of people affected by each break. We estimated the number of affected people in two ways.

- 1- Number of people who, upon pipe failure, are completely disconnected from the system.
- 2- Number of people who, upon pipe failure, are experiencing significant pressure loss.

The quantification of disconnected consumers involve simulations, whereby a failed pipe is considered to be completely disconnected and all demand nodes that are disconnected as a result are considered to have not been supplied for the duration of the repair. The volume of water not supplied as a result can easily be translated to the number of affected people. It is noted that in the simulation only one pipe break is considered at a time, although there is a low likelihood that two or more may occur simultaneously.

In order to quantify the number of people affected by a significant pressure drop, a pressure loss criterion is defined as a reduction of at least 25% of the pressure without a break or any pressure drop that reduces the absolute pressure head below 28 m (40 psi,) - the minimum acceptable pressure in many jurisdictions. This is achieved by estimating the supply pressure during normal operation at each node and subsequently estimating the residual pressure in each of the same demand nodes once a pipe has failed and is therefore considered closed. Here again, only one pipe break is considered at a time.

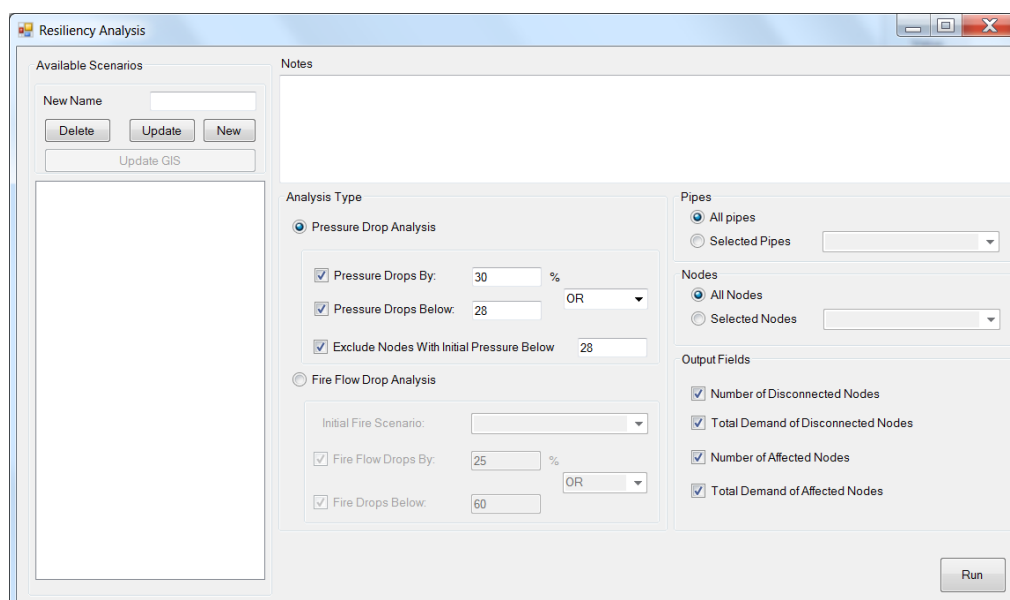


Figure 19 Network Resiliency Tool in HydraCAL.

These calculations require numerous hydraulic simulations (i.e., one simulation per watermain) that could prove time consuming. For this case study, the Network Resiliency Tool in HydraCAL model (previously described at Section 3.1) was used to estimate the number of people affected by each breaks (Figure 20). A new tool was added to HydraCAL that allows for estimating the individual watermain break likelihood based on covariate coefficients estimated for each pipe group using I-WARP (Figure 20).

This toolkit takes the optimized covariate coefficient for each pipe group, the predicted climatic covariates, and then estimates the break expectation for each watermain and converts it to the risk value by multiplying it to the number of people affected by each break. It then creates a spatial map of the affected pipes. The proposed methodology is applied to a real water distribution system, which is explained in more detail in Section 0.

4.1.1 Non Homogeneous Poisson Process based model²

Non-homogeneous Poisson process (NHPP) has been suggested by several researchers to model and forecast water main breaks (e.g., (Constantine & Darroch, 1993) (Constantine, Darroch, & Miller, 1996); (Røstum, 2000); (Jarrett, Hussain, & Van der Touw, 2003); (Economou, Kapelan, & and Bailey, 2008), among others). The approach proposed here is based on the I-WARP tool (Kleiner & Rajani 2010, 2012) and differs from others in that it allows

² The section is carried verbatim from (Kleiner & Rajani, 2012) with authors' permission. Readers that are not interested in the mathematical details could skip this section and continue from Section 4.2

for the consideration of dynamic factors (climate, operations, etc.), while existing NHPP approaches consider only pipe-intrinsic static factors (diameter, length, material, etc.). The proposed NHPP-based model forecast actual breakage rates in individual water mains, rather than just rank their relative rates.

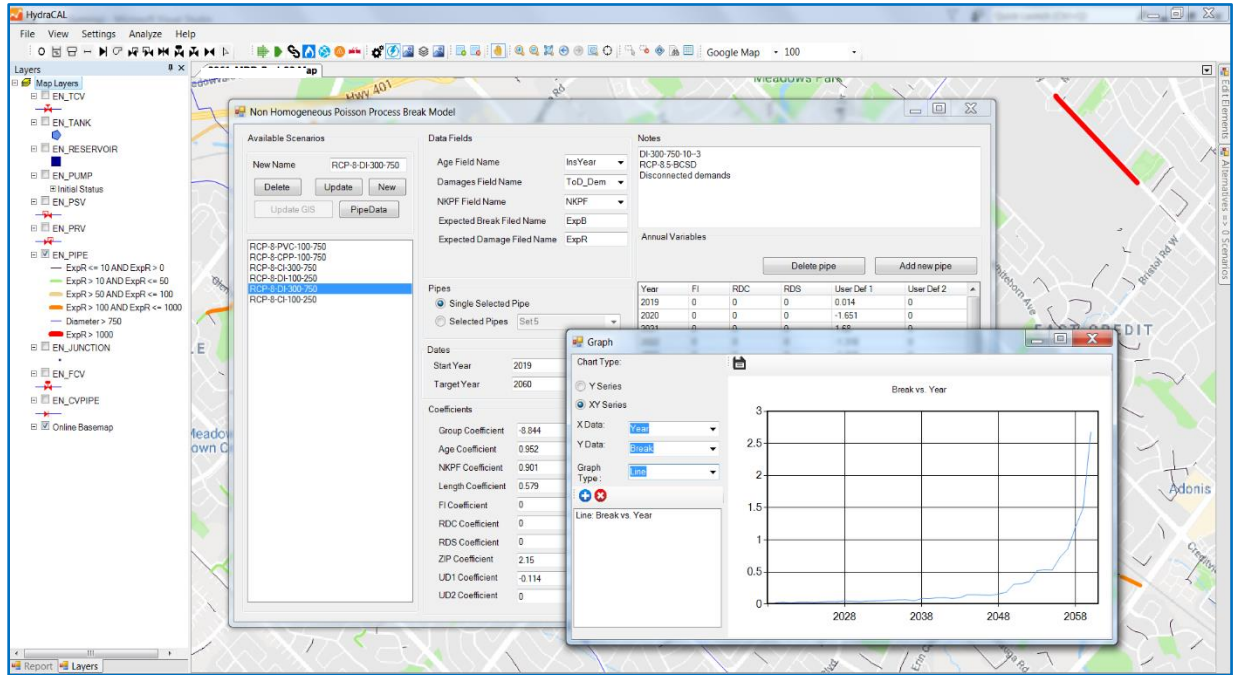


Figure 20 Break Modeling Tool in HydraCAL.

In the proposed model, breaks at year t for an individual pipe i are assumed to be Poisson arrivals with mean intensity (or mean rate of occurrence) $\lambda_{i,t}$. Therefore, the probability of observing $k_{i,t}$ breaks is given by:

$$\Pr(k_{i,t}) = \frac{\lambda_{i,t}^{k_{i,t}} \cdot \exp(-\lambda_{i,t})}{k_{i,t}!} \quad (3)$$

where $\lambda_{i,t} = \exp[\alpha_o + \theta \tau(g_{i,t}) + \underline{\alpha} \underline{z}^i + \underline{\beta} \underline{p}^t + \underline{\gamma} \underline{q}^{i,t}]$

and where α_o is a constant, $\tau(g_{i,t})$ is the age covariate, and θ is its coefficient, $g_{i,t}$ is the age of pipe i at year t , \underline{z}^i is a row vector of pipe-dependent covariates (e.g., length, diameter, etc.) and $\underline{\alpha}$ is a column vector of corresponding coefficients; \underline{p}^t is a row vector of time-dependent covariates (e.g., climate) and $\underline{\beta}$ is a column vector of corresponding coefficients; $\underline{q}^{i,t}$ is a row vector of both pipe-dependent and time-dependent covariates (e.g., number of known previous failure - *NOKPF*, cathodic protection) and $\underline{\gamma}$ is a column vector of corresponding coefficients. In this report, the function $\exp[\theta \tau(g_{i,t})]$ is referred to as the “ageing function” and therefore

coefficient θ is called “ageing coefficient”. Note that if $\tau(g_{i,t}) = g_{i,t}$ then the ageing is exponential, i.e., λ is an exponential function of pipe age, whereas if $\tau(t) = \ln(g_{i,t})$ the ageing function becomes a power function, i.e., λ becomes a power function of pipe age. Year t is taken relative to the first year for which breakage records are available. The likelihood function for (3) is

$$L = \prod_{i=1}^N \prod_{t=1}^T \frac{\lambda_{i,t}^{k_{i,t}} \exp(-\lambda_{i,t})}{k_{i,t}!} \quad (4)$$

Coefficients $\underline{\alpha}, \underline{\beta}, \underline{\gamma}$ are found by maximizing the log-likelihood function (5):

$$LL = \sum_{i=1}^N \sum_{t=1}^T k_{i,t} \cdot \ln(\lambda_{i,t}) - \lambda_{i,t} - \ln(k_{i,t}!) \quad (5)$$

4.1.2 Covariates of the NHPP model

Pipe-dependent covariates. Pipe-dependent covariates can be considered explicitly in the probabilistic model or implicitly by partitioning the data into homogeneous populations with respect to these covariates. For example, if pipe diameter is deemed to impact breakage rate, it can be explicitly considered in the \underline{z}^i vector of covariates (equation (3)) with a corresponding coefficient. Alternatively, the pipe inventory (comprising pipes of diameters, say, 6”, 8” and 12”) can be partitioned (or grouped) into three groups, each comprising only pipes of a certain diameter and each analyzed separately to produce group-specific coefficients. The explicit consideration of a covariate in equation (3) introduces some limitations. For instance, in the example where the pipe inventory consists of three different diameters, if diameter is included in the \underline{z}^i vector and the diameter coefficient is found to be negative, say, $-\alpha_r$, then the implication is that 12” diameter pipes for instance are always expected to have a breakage rate that is smaller than the 6” diameter pipes by a factor of $\exp(2\alpha_r)$. The grouping approach encompasses two advantages: (a) removal of the forced proportionality described above, and (b) obviation of the need to speculate about possible interactions among these covariates. These two advantages outlined above come at the cost of reduced statistical significance due to analysis of smaller pipe populations (groups), as well as the extra pre-processing effort that is needed to form these homogeneous groups.

The model can consider any number of covariates as long as they are supported by available data. Further, covariates can be considered at their physical value (e.g., pipe length, diameter) or configured as categorical covariates (e.g., very long, long, short, large diameter, medium diameter, etc.). Covariates, such as pipe material, soil type, pipe cluster, etc. are inherently categorical and can be considered either as grouping criteria (as described above) or directly in equation (3). To consider a categorical covariate, say, with m categories, m binary (zero/one)

covariates are assigned, one to each category, with corresponding m coefficients, where the sum of these m covariates must equal unity.

Time-dependent covariates. Three climate-related covariates are considered as time-dependent covariates, namely freezing index (FI), cumulative rain deficit (RDc) and snapshot rain deficit (RDs). (Kleiner & Rajani, 2004) provided a detailed introduction and rationale for using these covariates. FI is a surrogate for the severity of a winter, RDc is a surrogate for average annual soil moisture and RDs is a surrogate for locked-in winter soil moisture (appropriate for cold regions, where soil can freeze in the winter). Additional phenomena could be considered in the model if they are deemed to contribute to observed variations in breakage rate, provided these phenomena are supported by available data. Time-dependent covariate data are essentially time series describing these phenomena (one time series per phenomenon) over the observed period. Such phenomena can be represented quantitatively or qualitatively. For example, in a dataset, uncharacteristically elevated breakage rates were observed in a network during two non-contiguous years. A quick inquiry with the utility revealed that the network had experienced pump station failures in those years, which resulted in high breakage rates probably due to transient pressures. A qualitative time series describing this phenomenon was incorporated in the model and the calibration results improved significantly. Other phenomena represented by time-series could include pressure regime changes over time, leak detection campaigns, changes over time of overburden (traffic) intensity, etc.

Note that in general time-dependent covariates such as those related to climate can typically be used to train the model on observed historical breaks but not to forecast (unless one endeavours to forecast climate as well). The rationale for using climate-related covariates is that “true” background ageing rate (in terms of increase in breakage intensity as a function of time) are more likely to emerge if external effects, such as climate, are considered in the training process.

Pipe- and time-dependent covariates. Such covariates include the number of known previous failures ($NOKPF$), a covariate related to hotspot cathodic protection ($HSCP$) and a covariate related to retrofit cathodic protection ($RetroCP$). It should be noted that it may be beneficial to use the $\ln(NOKPF)$ as the covariate in order to ensure stability in the maximum likelihood calculations, especially when discrepancies between breakage rates of individual pipes in the group are substantial.

A hotspot cathodic protection (CP) program is an opportunistic placement of sacrificial anodes, whereby a sacrificial anode is installed every time pipe is exposed for repair. These anodes typically reach full effectiveness some time (typically 1 year) after installation and deplete during operation (typically reaching complete depletion after 15-20 year in the ground), as described in (Kleiner & Rajani, 2004). Consequently, each pipe i has a discernable number of active anodes protecting it in each year t . The covariate $HSCP$ in pipe i at year t is taken as a function of the density of the active anodes along pipe i and is expressed as

$$HSCP_{i,t} = 0.1(1 - \exp(-30q_{i,t-1})) \quad (6)$$

where $q_{i,t}$ is the density of active anodes per meter. Note that HSCP tends asymptotically to 0.1 as the number of active anodes increases. This implies that the efficacy of HSCP protection is maximized at one anode per 10 m of pipe length. The coefficients “0.1” and “30” in equation (6) are chosen so as to assure reasonable values for anode densities found in practice.

Retrofit CP refers to the practice of systematically protecting existing pipes with galvanic cathodic protection. (Kleiner & Rajani, 2004) provided a detailed explanation of how the *RetroCP* covariate was created. The premise is that, once a pipe is retrofitted, the ageing pattern (in terms of growing breakage rate) of a pipe is modified relative to its pre-retrofit ageing. This necessitates the consideration of three distinct phases each that are described by three additional parameters, namely, transition period duration t_{tr} , coefficient θ' to describe ageing during the transition period (which is actually “negative ageing”) and post-retrofit ageing coefficient θ'' . Accordingly, breakage intensity $\lambda_{i,t}$ in equation (3) is modified to include these three phases,

$$\begin{aligned}
 \lambda_{i,t} &= \exp[\underline{\alpha z}^i + \alpha_o + \theta\tau(g_{i,t}) + \underline{\beta p}^t + \underline{\gamma q}^{i,t}] & \text{for } t \leq t_{retrofit} \\
 \lambda_{i,t} &= \exp[\underline{\alpha z}^i + \alpha_o + \theta\tau(g_{i,t_{retrofit}}) + \theta'(g_{i,t} - g_{i,t_{retrofit}}) + \underline{\beta p}^t + \underline{\gamma q}^{i,t}] & \text{for } t_{retrofit} < t \leq t_{retrofit} + t_{tr} \\
 \lambda_{i,t} &= \exp[\underline{\alpha z}^i + \alpha_o + \theta\tau(g_{i,t_{retrofit}}) + \theta'(g_{i,t} - g_{i,t_{retrofit}}) + \theta''\tau(g_{i,t} - (g_{i,t_{retrofit}} + t_{tr})) + \underline{\beta p}^t + \underline{\gamma q}^{i,t}] & \text{for } t > t_{retrofit} + t_{tr}
 \end{aligned} \tag{7}$$

where index $t_{retrofit}$ represents the year in which the pipe was retrofitted with CP, and t_{tr} is the transition time in years. Note that equation (7) implies that retrofit CP impacts only pipe ageing (i.e., only age covariate is modified), and the impact of all other covariates on pre- and post-retrofit breakage intensity remains the same. This may be a reasonable assumption (with the exception of *NOKPF* covariate), however, the model can be easily modified to incorporate an additional, post-retrofit set of covariates/coefficients. Also, in the situation where a specific pipe has been hotspot-protected in years before it is retrofitted at year t , all active hotspot CP anodes starting at year t are assumed to be completely overwhelmed by the high-density of retrofit anodes, with the consequence that the *HSCP* covariate is disregarded after year t .

4.1.3 Zero-inflated Poisson (ZIP) process

In reality, most water mains fail rarely, which means that many (if not most) data points in a typical dataset will have the observed value $k_{i,t} = 0$ (i.e., zero breaks observed for pipe i at year t). It has been observed (e.g., (Lambert, 1992)) that a counting process with many zeros (i.e., many more than what is expected from equation (3)) cannot be adequately represented by a Poisson process. Thus, (Lambert, 1992) proposed a technique referred to as the “zero inflated Poisson” (ZIP) regression, for handling zero inflated count data. In this approach, the counting process at hand is produced simultaneously by two mechanisms, namely a zero generating

process and a Poisson process. (Economou, Kapelan, & Bailey, 2008) used this approach in their model to predict pipe breakage rates, and called the probability of obtaining a zero data point “the natural tendency of the pipe to resist failure”. ZIP process can be incorporated in the proposed model and it has been observed to sometimes (but not always) improve prediction accuracy. The probability of observing $k_{i,t}$ breaks (at year t for an individual pipe i) when zero inflated count is considered becomes,

$$\Pr(k_{i,t}) = \begin{cases} G_{i,t} + (1 - G_{i,t})e^{-\lambda_{i,t}} & \text{for } k_{i,t} = 0 \\ (1 - G_{i,t})\lambda_{i,t}^{k_{i,t}} e^{-\lambda_{i,t}} / k_{i,t}! & \text{for } k_{i,t} > 0 \end{cases} \quad i = 1, 2, K, N ; t = 1, 2, K, T \quad (8)$$

where N is the number of pipes and T is the number of years of available breakage data, $G_{i,t}$ is the parameter of the second mechanism (the first is the Poisson process) that produces $k_{i,t} = 0$ with probability $G_{i,t}$. It is convenient to formulate $G_{i,t}$ in a *Logit* form because its value must lie in the interval $[0, 1]$, i.e., $\text{Logit}(G_{i,t}) = f(\text{some covariates})$ or $G_{i,t} = e^{f(\cdot)} / (1 + e^{f(\cdot)})$.

It is reasonable to assume that $G_{i,t}$ is generally influenced by the same covariates that influence the mean intensity $\lambda_{i,t}$. Therefore we define $G_{i,t}$ as a function of $\lambda_{i,t}$

$$G_{i,t} = \frac{e^{g_0 - \lambda_{i,t}}}{1 + e^{g_0 - \lambda_{i,t}}} \quad (9)$$

where g_0 is the ZIP coefficient. Note that with this formulation $G_{i,t}$ tends to zero as $\lambda_{i,t}$ increases and $G_{i,t}$ tends to unity as $\lambda_{i,t}$ decreases.

4.1.4 Model training and validation

As mentioned earlier, training of the model (or discerning its coefficients) is done by maximizing equation (5) on observed data in the training period. The Lipschitz (-continuous) Global Optimizer (LGO) algorithm (Pintér, 2005) was used in the implementation of the NHPP model but in principle other alternative algorithms can also be used.

Since numerous candidate covariates can be applicable for a specific pipe group, some of the covariates may not always be significant for all datasets. The likelihood ratio (LR) statistic can be used as a criterion to evaluate the significance of candidate covariates (e.g., (Ansell & Phillips, 1994)). A specific covariate is removed or dropped if its contribution to LR does not exceed the required threshold at the desired confidence level (typically 5% or 1%). It should be noted that strictly speaking, it is not sufficient to examine the LR of each covariate at a time, but rather all combinations of the candidate covariates should be tested as well because it is possible that a pair of covariates considered simultaneously in the model is statistically significant, even if each of the covariates on its own is not.

The discerned coefficients of the trained model (for a specific dataset) are used to forecast the number of breaks for the validation period and then compare the observed and forecasted number of breaks. Two criteria need to be examined when evaluating validation results, namely, accuracy of the prediction of number of breaks for every pipe at every year in the validation period (point prediction) and ranking ability. Although it is clear that perfect accuracy in point prediction will result in perfect ranking ability, the two parameters should nonetheless be evaluated independently since in practice, perfect point prediction is unrealistic.

4.1.5 I-WARP Model³

Individual Water mAins Renewal Planner (I-WARP) is a Microsoft Excel-based software that was previously developed at NRC and implements Non Homogeneous Poisson Process model (Kleiner & Rajani, 2010). I-WARP differs from other NHPP-based models in that it can consider static and dynamic influences on water main failure rate, where static influences include factors like pipe diameter, material, vintage, etc. and dynamic influences include climate, cathodic protection, etc.. Covariates can be applied at two levels, namely at group level (for covariates that are presumed to act on all pipes in the group in the same manner) and at pipe level (for covariates that are presumed to act differently on different pipes in the homogeneous group).

I-WARP intentionally does not explicitly consider some static covariates such as pipe diameter, installation vintage, soil type, etc. This is because these static covariates can be considered by grouping cohort of pipes for analysis and analysing one cohort at a time (thereby circumventing the fact that by including them explicitly in the analysis they are considered to act independently on the pipes and any (probable) interactions between them is ignored). The covariates considered by I-WARP are therefore:

- Pipe age (Age) - a time-dependent and pipe-dependent covariate;
- Pipe length (Length) – a static covariate that is pipe-dependent;
- Number of known previous failures (NOKPF) – a time-dependent and pipe-dependent covariate;
- Freezing index (FI) – a dynamic (time-dependent) climate-related covariate that provides a measure of the severity of winter during a specified period;
- Cumulative rain deficit (RDc) a dynamic (time-dependent) climate-related covariate that provides a measure of how dry the soil is a given year (impact on soil shrinkage);
- Snapshot rain deficit (RDs) - a dynamic (time-dependent) climate-related covariate that provides a measure of how dry the soil is at the beginning of a freezing season (impact on frost penetration);
- Hot spot cathodic protection (HS CP) – a time-dependent and pipe-dependent covariate that provides a measure of how much a pipe is protected by hot spot CP anodes;

³ I-WRAP user manual and model could be downloaded from https://www.waterrf.org/system/files/resource/2019-07/3052_0.pdf

- Retrofit cathodic protection (Retrofit CP) – a time-dependent and pipe-dependent covariate that provides an indication whether and when a pipe was retrofitted with CP;
- Clusters (as a categorical covariate) – a static covariate that can possibly serve as a surrogate for geographically related factors for which no direct quantitative data are available.
- Custom covariates. An additional user-defined quantitative or qualitative time-dependent covariate could be considered to account for time dependent parameters such as historical sporadic effects of pump station failures, leak-detection campaigns, etc.

In addition, I-WARP can be (optionally) modified by the so-called ‘zero inflated Poisson’ (ZIP) process, which can account (and compensate) for the fact that often pipe/break datasets contain a lot of zeros (i.e., there are many years in which individual pipes experience zero breaks) – a situation that pure NHPP may not accurately capture. I-WARP provides a forecast of the mean number of breaks anticipated in each pipe at each year of the forecast period.

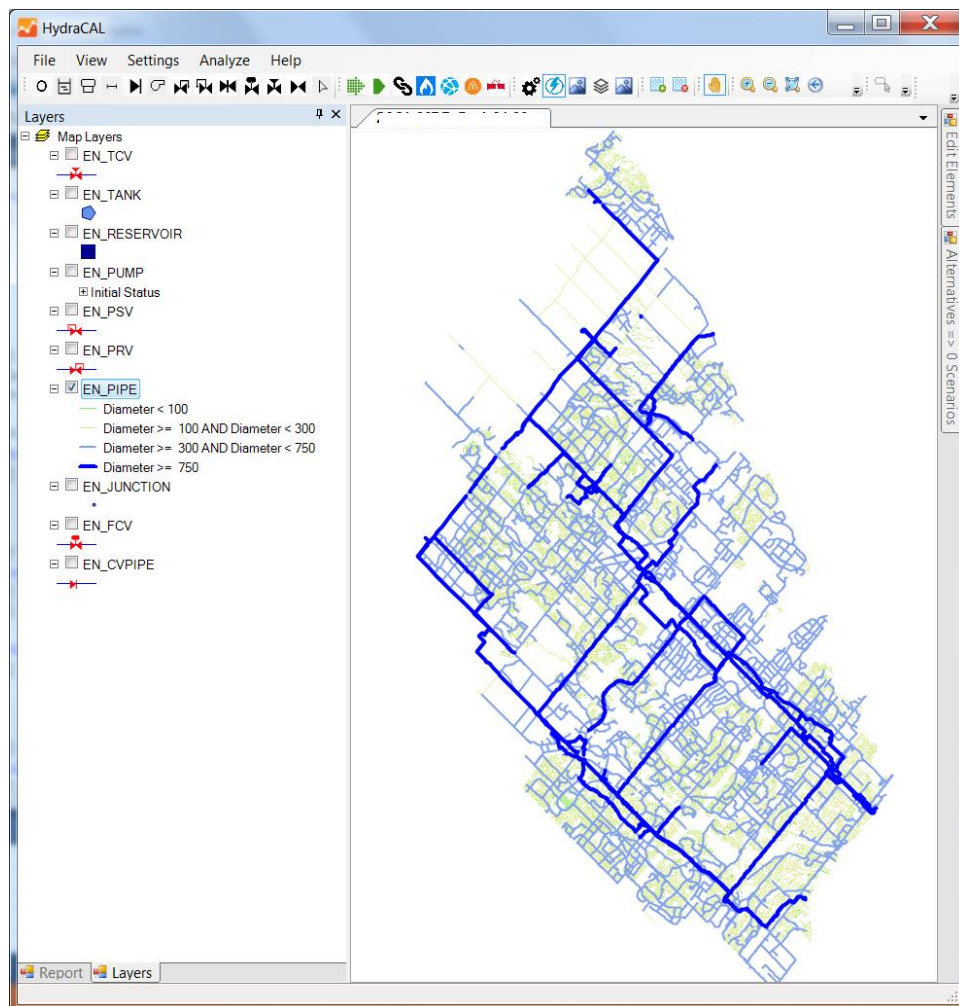


Figure 21 Case study network with categorized water mains based their diameter in HydraCAL.

4.2 Case Study

To evaluate the impact of changing climatic variables on watermain breaks a real world and large WDS in Canada (Figure 21) with numerous pressure zones and supplies is selected.

The WDS anonymized due to security reasons. The pipe material distributions (Table 6) and watermain diameter distribution (Table 7) is summarized below. A total of 3900 break were recorded for the network in the 24 years from 1995 to 2018 (when this study was executed). These records were used to create the break-prediction models for each pipe category.

Table 6 Case Study Watermain Material, Length, and Installation Year

Row Labels	Total Length (km)	Average of Installation Year
CI	221	1969
CPP	560	1984
DI	664	1981
PVC	2884	1999

Table 7 Case Study Watermain Diameter Distribution

Diameter (mm)	Length (km)
Less than 100 mm	158
Between 100 mm and 300 mm	2455
Between 300 mm and 750 mm	2428
Greater than 750 mm	330

4.2.1 Data preparation

The network in our case study encompasses pipes that have been installed as early as 1850 and as late as 2017, as well as pipes with diameter as small as 50 mm and as large as 4,000mm. Soil types and data on other static covariates were not available, as well data about cathodic protection of metallic pipes. Additionally, the database indicated 30 different pipe materials in the network. As indicated earlier, static factors such pipe diameter, pipe material and pipe vintage (or installation year) are very often found to have a significant impact on observed historical breakage rates. In order to consider those in the analysis, I-WARP requires that the entire inventory be grouped into relatively homogeneous cohorts (homogeneous with respect to these static covariates). Additionally, the grouping should balance carefully between

cohorts that are homogeneous enough, yet large enough to provide statistical significance to the analysis.

To demonstrate the use of I-WARP for our objectives, four representative cohorts were prepared from the available data, as described in Table 8:

Table 8. Details of case-study cohorts

Cohort	Material	Diameter (mm)	Vintage	# of pipes	Total length (km)	Total #braks
1	CI	150-200	1900-1975	782	104	686
2	CPP	400-600	1960-1980	547	122	58
3	DI	150-200	1970-1990	1,935	297	1,111
4	PVC	150-200	1970-1995	5,318	792	153

Each of these cohorts was analysed in I-WARP and the results are presented in the next section.

4.2.2 Analysis of historical breakage patterns

The covariate coefficients for all four cohorts were estimated and listed in Table 9.

Table 9 Estimated covariate values by I-WARP for final variables considered in each pipe group.

Covariate coefficients ⁷	Cohort			
	1 (CI)	2 (CPP)	3 (DI)	4 (PVC)
Constant	-3.64	-9.40	-5.315	-6.57
Ageing	-0.132	0.970	0.849	0.563
NOKPF ¹	0.631		0.528	
Length ²	0.758	0.634	0.611	0.505
Freezing index				0.147
Rain Deficit C ³			-0.104	
Rain Deficit S ⁴				
Cluster 1 ⁵	-1.997		-3.11	
Cluster 2	-1.643		-2.204	
ZIP ⁶	0.897	2.847	2.093	4.329

¹ Acronym for number of known previous failures

² Length of the individual pipe.

³ Rain Deficit Cumulative

⁴ Rain Deficit Snapshot

⁵ Clusters were determined visually. Breaks in cohorts 2 and 4 displayed no visual clusters.

⁶ Zero Inflated Poisson.

⁷ All coefficients in the table were found to be statistically significant at 5% level.

The following observations are noteworthy.

1. A positive ageing coefficient means that as the pipes in the cohort age, breakage rate increases (as can be expected). While the ageing coefficients of cohorts 2, 3, 4 are positive, ageing seems to be negative (albeit small) for the cast iron cohort. This is an indication that the surviving cast iron mains are not deteriorating in terms of increase in breakage rate. As some of these pipes are extremely old, it stands to reason that they are buried in a non-corrosive environment (e.g., well-drained sandy soil).
2. While the number of previously known number of failures is a significant covariate in the metallic pipes (cast iron and ductile iron) it does not appear to be so in the concrete and PVC pipes.
3. The Freezing Index covariate (describes in detail in Section 4.1.2) is supposed to be one of the covariates that is capable of capturing the potential impact of climate change (i.e., mean temperature increase or decrease). The analysis results indicate no statistically significant impacts of temperature on pipe breakage for 3 of the 4 cohorts. The positive (albeit small) coefficient obtained for the PVC pipe cohort indicates that as freezing index increases (e.g., mean temperatures drop) pipe breakage rate increases. This is consistent with many other studies that attributed higher breakage rates to very low temperatures in cold countries. The fact that the Freezing Index coefficient is either not significant or relatively (positive and) small in our samples could be attributed to the burial depth of the pipes in our case study network (minimum 6' to avoid frost penetration). At any rate, expected higher mean temperatures in the future will likely only work to reduce pipe breakage rates.
4. Cumulative Rain Deficit measures total annual rain that percolates into the ground. It is statistically significant (albeit small) only in the ductile iron cohort. The positive value indicates that as the deficit increases pipe breakage increases, which is typical for pipes that are buried in clay expansive soils. We have insufficient data to speculate on why this is significant only in DI pipes. At any rate, the small values that appears in the coefficient of only one of 4 cohorts, coupled with the fact that according to ECCC mean precipitation is expected to rise with climate change (because in general warmer air can hold greater amounts of moisture) gives rise to the supposition that climate change is not expected to negatively impact pipe breakage rates.

4.2.3 Risk Analysis and Simulation Assumptions

In light of observation #3 in the list of observations at the end of the previous subsection, we use this subsection to demonstrate how a specific analysis and prediction can be carried out on pipe cohort for which freezing index is deemed significant. For this demonstration we use Cohort 4 (PVC pipes), for which freezing index appear to have a statistically significant impact on the number of breaks.

The coefficients for the various covariates (age, length, NOKPF, etc.), extracted from available historical data (1995-2018), are provided in Table 9. Mean daily temperatures were forecasted for the years 2019 to 2060, using downscaled climatic model (i.e., CanESM2) under RCP 2.6

and RCP 8.5. These forecasted mean daily temperatures were used to compute the estimated freezing index values for the corresponding years. Figure 22 illustrates the historical and predicted FI values. As expected, annual values are quite scattered but linear regression on the future values show a clear downtrend (trend for RCP 8.5 steeper than RCP 2.6, as would be expected for a warming climate).

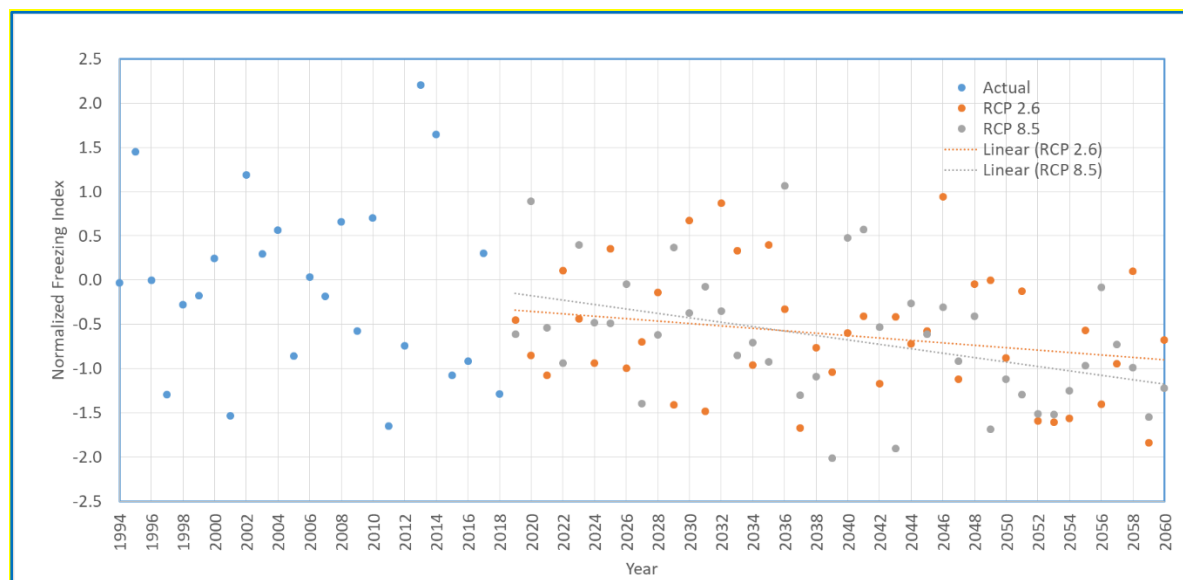


Figure 22 Historical and predicted annual freezing index for the case study.

The municipality owner of the study water distribution network made available to us their water supply system master plan, encompassing water demand predictions as well as planned network-related capital projects extending to the year 2060.. These future demands and progressive changes in network topology (including water main replacements and additions) were considered in the demonstrated simulation presented here. (i.e., water mains scheduled in the master plan for replacement or addition in the years 2018 to 2060, were assumed to undergo the planned action on the planned schedule. It was assumed that each individual pipe could be isolated separately for repair and/or replacement.

4.2.4 Case Study simulation and Results

As noted earlier, coefficient values for covariates were estimated using the non-homogeneous Poisson process through I-WARP (Table 9). These values were entered into the tool created in HydraCAL to predict future individual pipe breaks. Three different scenarios were examined, status quo, RCP 2.6 and RCP 8.5. In the status quo scenario the climate was assumed to be stationary, i.e., mean temperature does not change over the years, which in turn means that the freezing index values used for the years 2019-2060 are constant and equal to the historical mean (because in I-WARP the FI covariate is depicted in Z-scores this constant mean is translated to zero). . In the second and third scenarios forecasted FI values were taken as those illustrated in Figure 22, i.e., under RCP 2.6 and RCP 8.5, respectively.

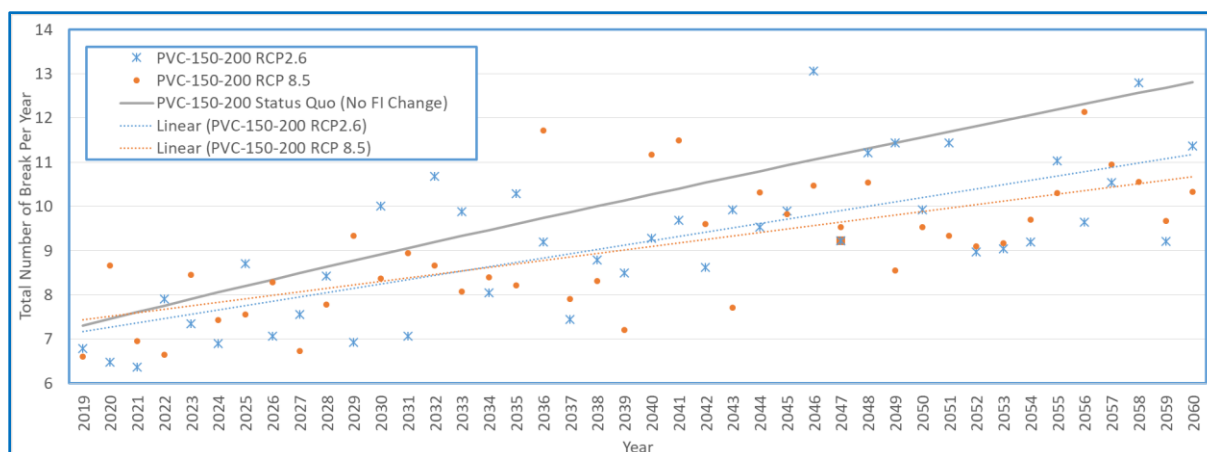


Figure 23 Total number of breaks for PVC cohort under three scenarios (i.e., Status Quo, RCP 2.6, and RCP 8.5)

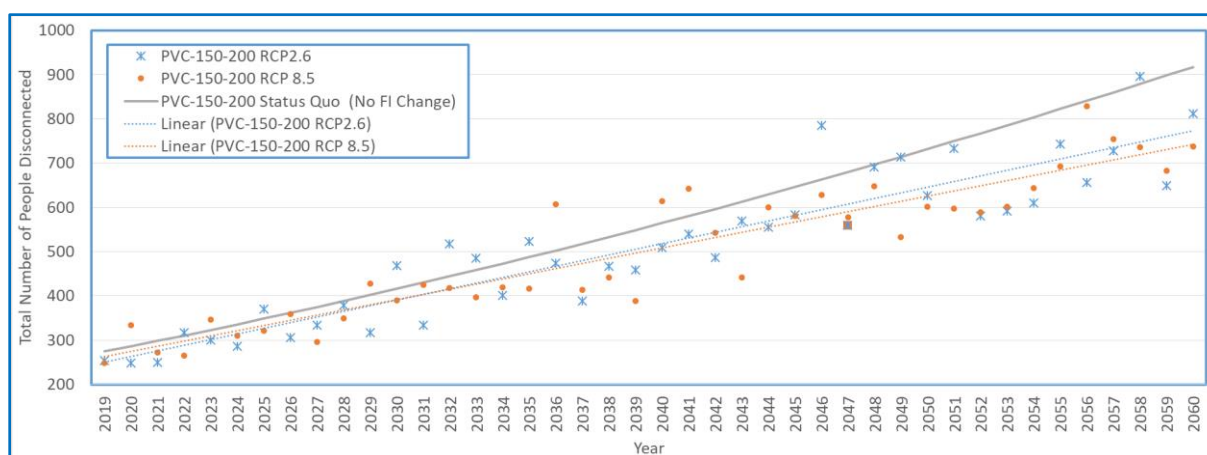


Figure 24 Number of people disconnected from the system for the Cohort 4 under three scenarios (i.e., Status Quo, RCP 2.6, and RCP 8.5)

I-WARP was used to simulate and predict the breaks expected on each pipe in the years 2019 to 2060 and the corresponding number of people disconnected from the system due to breaks occurring in water mains belonging to Cohort 4 (PVC pipes) were estimated. Figure 23 and Figure 24 illustrate the number of PVC pipe breaks and corresponding number of people affected for each of the three aforementioned scenarios. In the status quo scenario the number of breaks increases as a straight line (shown as a continuous gray line in the Figure 23) due to ageing and deterioration (climate influence is considered static, hence no perturbations about the mean). The other two scenarios reflect the expected perturbations about the mean trend. This mean trend is increasing due to pipe ageing and deterioration, albeit this increasing trend slower (smaller slope) than the status quo trend because with warming climate the impact of freezing index is expected to diminish. Also as can be expected, slope associated with the RCP 8.5 scenario is smaller than that associated with the 2.6 scenario because RCP 8.5 corresponds to a faster rate of warming and consequently a faster diminishing influence of freezing index on pipe breakage rate. These results demonstrate quantitatively observation #3 in the previous

section “expected higher mean temperatures in the future will likely only work to reduce pipe breakage rates”.

4.3 Recommendations

- The case study reflects that only PVC pipes appear to be affected by climate change in a statistically significant way. However, this is very likely case-specific and therefore does not reflect a universal truth. At any rate, regardless of pipe material, in a cold country like Canada it can be reasonably expected that increasing future temperatures will act to reduce water main breakage rate as a result of diminishing frost penetration. As for impact due to precipitation, and more specifically due to soil moisture depletion, this is expected to affect only water mains buried in clayey expansive soils. The nature of the impact (i.e., whether it will act to increase or decrease water main breaks) is determined by expected change in precipitation. Since precipitation is a very localised phenomenon it is more difficult to forecast and prediction must be carried out on a case-by case basis.
- In the case-study the scenario with RCP 8.5 resulted in a slightly lower breakage rate compared to RCP 2.6. Both scenarios resulted in breakage rates that were markedly lower than the status quo scenario. It is not clear whether this phenomenon is general or case-specific. .
- The impact of water main break on the water utility customers can manifest in complete disconnection from the network (i.e., no water at all) or lower supply pressure (i.e., reduction in level of service). Clearly, the former is the more significant consequence and as such its prevention should be prioritised.
- There are still several unanswered questions such as. What are other climatic variables possibly affecting break rates? Is it possible to expand the results of this study to similar systems? A more detailed study could be helpful in answering these questions.

5 Impact on Energy Consumption

Human activities and life have always evolved around the nexus of water and energy. Numerous studies in recent years have focused on these key inputs in our lives. The Electric Power Research Institute in the United States estimated that 4% of electricity produced is used in moving and treating water and wastewater, in which 80% is used to move water (EPRI, 2002). It further estimates that 80% of costs associated with water treatment and distribution are for electricity consumption. This portion increases by another 30% if the municipality is supplied from ground water. This is the main reason why many researches have focused on using complicated optimization techniques, such as single or multi objective algorithms, to solve issues such as pump scheduling to deliver water which satisfies volume and pressure constraints while minimizing energy consumption and, in some cases, greenhouse gas emissions.

(Dandy, Roberts, Hewitson, & Chrystie, 2006) developed a multi-objective optimization program that incorporates sustainability objectives of whole-of-life-cycle costs, energy use, greenhouse gas emissions, and resource consumption. The optimization program was applied to a real network in Australia, where the least-cost design was compared with the 'environmentally sustainable' design. The 'sustainable' design was found to have a lower cost, a reduced rate of PVC material and energy use, and lower levels of greenhouse gas emissions. Later, (Dandy, Bogdanowicz, Craven, Maywald, & Liu, 2008) developed a multi-objective optimization program that incorporates the objectives of capital cost and embodied energy of pipes. The multi-objective program was applied to a hypothetical test network to solve both the single-objective and multi-objective problems. In the single-objective problem, the authors found the minimum-cost solution to comprise of PVC-M (modified PVC) pipe with a low unit cost, and the minimum-energy solution to comprise a mixture of PVC-M and PVC-U (unplasticized PVC) pipe with low embodied energy values. The multi-objective analysis indicated a trade-off between the cost and embodied energy objectives.

(Roshani, MacLeod, & Filion, 2012) developed a single-objective optimization framework to assess the effects of proposed Canadian climate mitigation change policies (lowering the discount rate and introducing a carbon tax) on cost, energy use, and GHG emissions in the design and expansion of the Amherstview water distribution network in Amherstview, Ontario, Canada. Their analysis indicated that the proposed discount rate and carbon tax had no significant influence on energy use and GHG emissions in the Amherstview system. This result was attributed to a number of factors that included: 1) adequate installed hydraulic capacity in the Amherstview system, 2) the use of a time-declining GHG emission intensity factor, and 3) the limited scope of the expansion problem.

Other works also could be mentioned (Wu, Simpson, & Maier, Accounting for Greenhouse Gas Emissions in Multiobjective Genetic Algorithm Optimization of Water Distribution Systems, 2010), (Wu, Maier, & Simpson, 2010), (Wu, Simpson, Maier, & Marchi, 2012), and (Wu, Simpson, & Maier, 2012); however, in almost all of them, the focus is on optimizing the energy

consumption, while the specific energy consequences of extra water demand arising from climate change have been largely ignored.

In Section 3 we explored the impact of increased demand on pipe capacity and investigated its impact on headloss in water mains. In this section the focus shifts to pumps, with an investigation into the potential energy use increase and its associated costs. A simple approach to quantify these impacts is described.

5.1 Suggested Methodology to Evaluate the Impact of Climate Change on Energy Consumption in WDS

The estimation of the impact of climate change on the energy consumption in water distribution is conceptually simple and straightforward. It is based on the projection of future demand increase, the translation of this increase into an appropriate diurnal demand pattern and then the application of extended period simulations (EPSs), using software with the capacity to record pump power usage.

Most water purveyors have their distribution system already encoded into a hydraulic model, using publicly available software such as EPANET (Rossman L. , 2000), or proprietary software such as InfoWater, Innovyse, WaterGEMS, or others. All of these software packages are capable of running extended period simulations as well as calculate pumps energy consumption (and even costs).

The following are the detailed steps required for energy demand estimation:

1. Determine or assume the annual demand increase during the period of analysis. An approach to estimate future demands in changing climate is provided in Section 2.1. To account for the significant uncertainty in this projection, a range may be contemplated rather than a point estimate.
2. Determine how future demand increase is expected to affect the currently known diurnal demand pattern in the various demand nodes. The simplest way is to assume that the demand increase will apply uniformly to all nodes throughout the day, thus requiring only that a single multiplication factor be applied to the known pattern for each node. If there is a compelling reason to assume that the forecasted demand increase needs to be applied in a non-uniform manner, the aforementioned software packages have the capacity to accommodate this requirement.
3. Reasonable assumptions have to be made about the sizes of the pumps and pipes in the network. Since the analysis period will typically comprise several decades, some pumps and some pipes will be replaced during this period. The simplest approach is to assume that, even if pumps and pipes are replaced, they will be replaced by an equivalent replacement, in which case the computations for the EPSs will be only minimally affected (i.e., a newer equivalent component will function marginally better than the old one). However, if projected demand increases are significantly larger than current demand in a distribution system that is currently near capacity, some capacity

increase (e.g., larger pipes, more or bigger pumps, etc.) will be required. In such cases it would be reasonable to divide the analysis period into two or more sub-periods, where each sub-period sees a modified network (i.e., some components with higher capacity than the previous sub-period).

4. Run EPS and obtain total power consumption of pumps. In the case of sub-periods due to capacity expansion, each sub-period would have to be simulated on its own and the total energy consumption aggregated after all simulations are complete.
5. The cost of energy can be computed by multiplying the total KWH consumed by the price of KWH. Some jurisdictions have differential energy pricing, where the KWH is more expensive when consumed during peak electricity demand. Some software packages are capable of considering such diurnal price variation.
6. To quantify uncertainty, repeat EPS runs for several projected demand values within the range of uncertainty as stipulated in item 1 above. Note: the absence of weighting the various runs within the range of uncertainty will imply that each of the results within this range is equally likely. Weights could be assigned to various runs to obtain something akin to a probability distribution of results. The most comprehensive way would involve full-fledge Monte Carlo simulation of the system but this would require significantly higher computational resources.

In the next subsection, the proposed approach is explained in detail with the help of two case study network. Networks 1 and 3, used previously in Section 3.2, serve as a case studies for this exercise and shown in Figure 18.

5.2 Demonstration Case studies

Two case studies are presented here to demonstrate the principles articulated in the previous subsection. The following was assumed/applied

1. The analysis period was taken as 40 years.
2. The increase in demand was estimated at 20% for the entire period and the uncertainty range was therefore taken as 0 to 40% increase. Five runs were applied, corresponding to 0%, 10%, 20%, 30%, and 40% increase in the demand. No weighing was applied to these runs.
3. In Network 1, efficiency curves were available for all pumps in the system. However, this information was not available for Network 3 and therefore all pumps in Network 3 were assumed to have 70% efficiency.
4. All pipes and pumps were assumed to be the same (i.e. no increase in physical hydraulic capacity) throughout the analysis period.
5. Diurnal demand pattern was available for Network 1 and for Network 3. Future demand increase was assumed to apply uniformly to all nodes throughout the day (i.e., one multiplication factor).
6. Demand was assumed to increase at a constant rate during the analysis period.
7. Ontario power rates were applied to both case studies, as illustrated in in Figure 25 (average rate 0.14425 \$/KWH).

It is to be noted that projected higher demand due to climate change will impose higher energy consumption due to two effects. Firstly, pumping more water to satisfy increased demand drives an increase in energy consumption that is proportional to the increase in demand. Secondly, higher flow rates in the distribution network create higher pressure losses that necessitate higher pumping pressure to overcome. This second effect is nonlinear in nature.

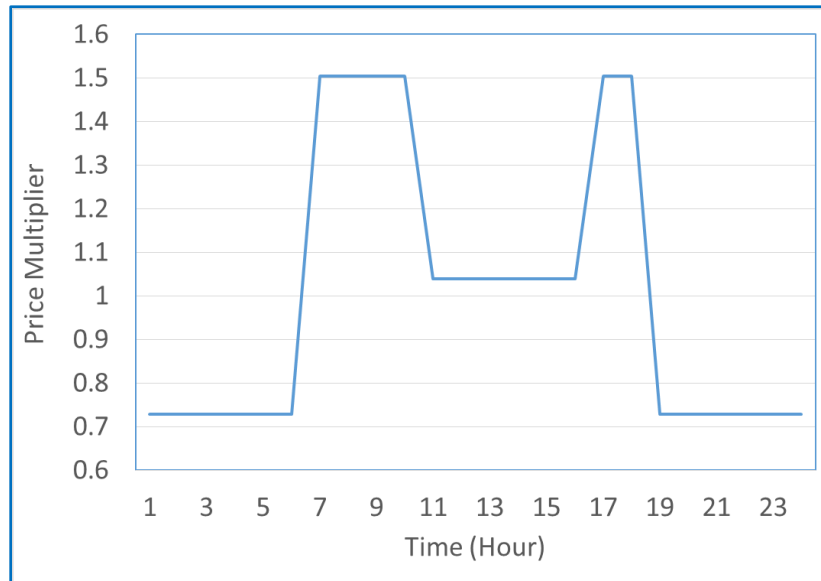


Figure 25 Electricity Daily Price Pattern in Ontario

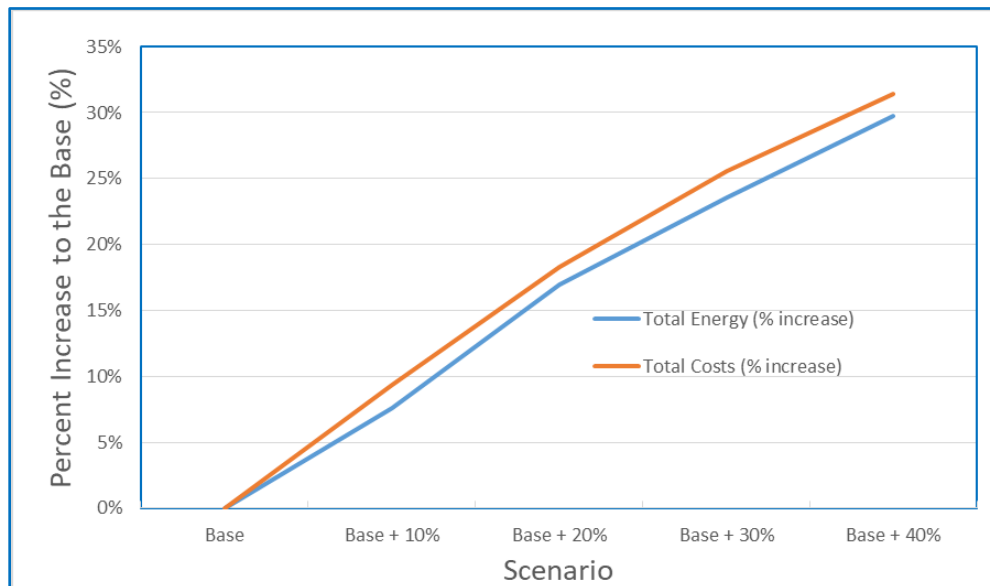


Figure 26 Network 1 energy consumption and cost increase ("Base" = year of analysis)

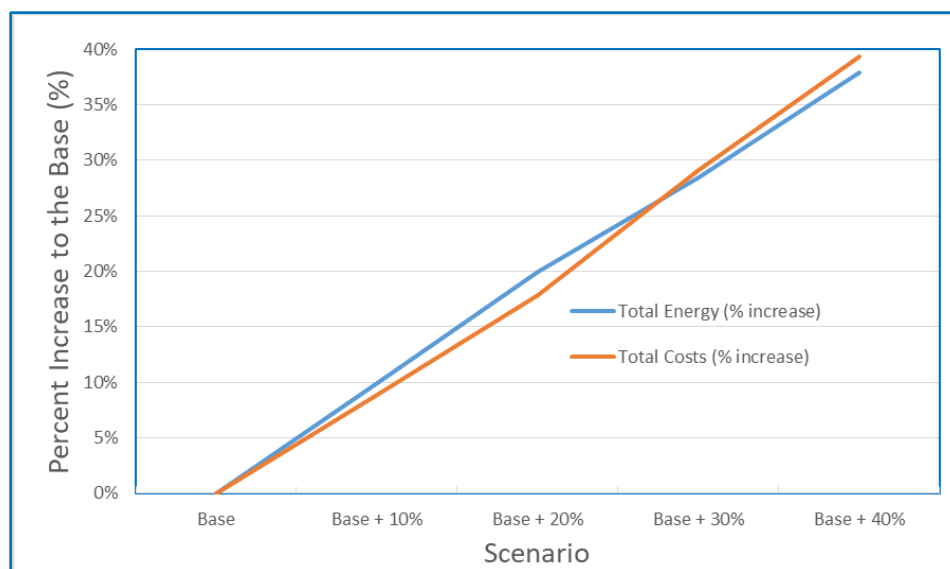


Figure 27 Network 3 energy consumption and cost increase ("Base" = year of analysis)

Results are illustrated in Figure 26 and Figure 27. They show near linear energy consumption increase, corresponding to (assumed) linear increase in demand. The rate of increase in energy consumption is slightly lower than the rate of demand increase. The likely explanation for this is that in both case studies the predominant driver for the observed higher energy demand is the pumping of more water rather than increase in pressure losses. Pressure head was generally lower in most of the demand nodes during peak and near peak demand due to increase in headloss in pipes but minimum acceptable pressure was preserved in all nodes throughout the analysis period.

In both case studies the total cost of energy follows the energy consumption, however, in the first case study the total energy cost increase is consistently higher than (i.e., by 2% to 3%) the increase in the total energy consumption relative to the base scenario. This could be attributed to the utilization rate of pumps. In the first case study, pumps are utilized about 73% of the times (average of all scenarios) compared to 64% in the case study number 3. This means that Case 1 has less time-redundancy to maneuver pump operation so as to benefit from reduced rate periods.

5.3 Concluding comments

- Networks with higher pump utilization rate will experience higher increase in their energy bill which is due to the diurnal electricity pricing scheme and the fact that pumps have to be utilized in periods of the day when electricity rates are high. These systems have to consider optimizing their pumping schedule and reservoir capacity during the day. Utilizing pumps with higher efficiency and filling larger reservoirs during off peak hours could lead to reduction in their electricity bills.

- Preparing an Extended Period Simulation (EPS) model is a key in estimating energy consumption and it could provide valuable information in other areas as well. Therefore, development we strongly recommend developing such models.
- We used a consumer electricity tariff model to estimate the energy costs in the case studies, however, pump stations often have to pay an extra high peak capacity tariff to their electricity provider. To simplify the problem, this extra cost was not accounted for, however, the cost associated with the high peak capacity could also be impacted by higher demands. It is recommended to apply this cost if it is part of your electricity pricing scheme.
- The estimation of future energy consumption assumes steady state societal behaviour and does not consider possible modifications to demand patterns due to policy changes, demand elasticity, educational campaigns, etc.
- The actual dollar value of the increased energy consumption is highly dependent on local policy decisions, such as rate structure, and may therefore undergo many significant variations during the analysis period.
- Networks with many transmission water mains already near hydraulic capacity are likely to see large (nonlinear) increases in their energy use unless they incorporate pipe replacement/reinforcement (which would require the segmentation of the analysis period into two or more sub-periods).

6 Impacts on Chlorine Residuals

Disinfection residuals in drinking water protect water quality and public health by limiting microbial growth (due to possible breakthrough from treatment plant with subsequent regrowth, potential intrusion due to compromised pipes, failure to disinfect after pipe repair, etc.) in distribution systems. Changes in air temperature could result in changing water temperature (Section 0), which in turn could reduce the disinfectant residual concentration, thereby increasing vulnerability to microbial growth. In cases where monochloramine is used for secondary disinfection, this could potentially increase nitrate concentration. Both represent increased risk to public health and water purveyors have to take additional steps to increase disinfectant residuals by adding chlorine/chloramine and flushing stale water. A good example of current practices of adding disinfectant with higher air temperature could be seen in Network 3 case study (Figure 28), where the water treatment plant managers add approximately 0.02 PPM to the concentration of Hypochlorite per 1 degree increase in the air temperature to make sure that residual disinfectant stays at acceptable levels. Temperature increase expected due to climate change could exacerbate this process and the correct quantification of this phenomenon could help with proper planning and preparation.

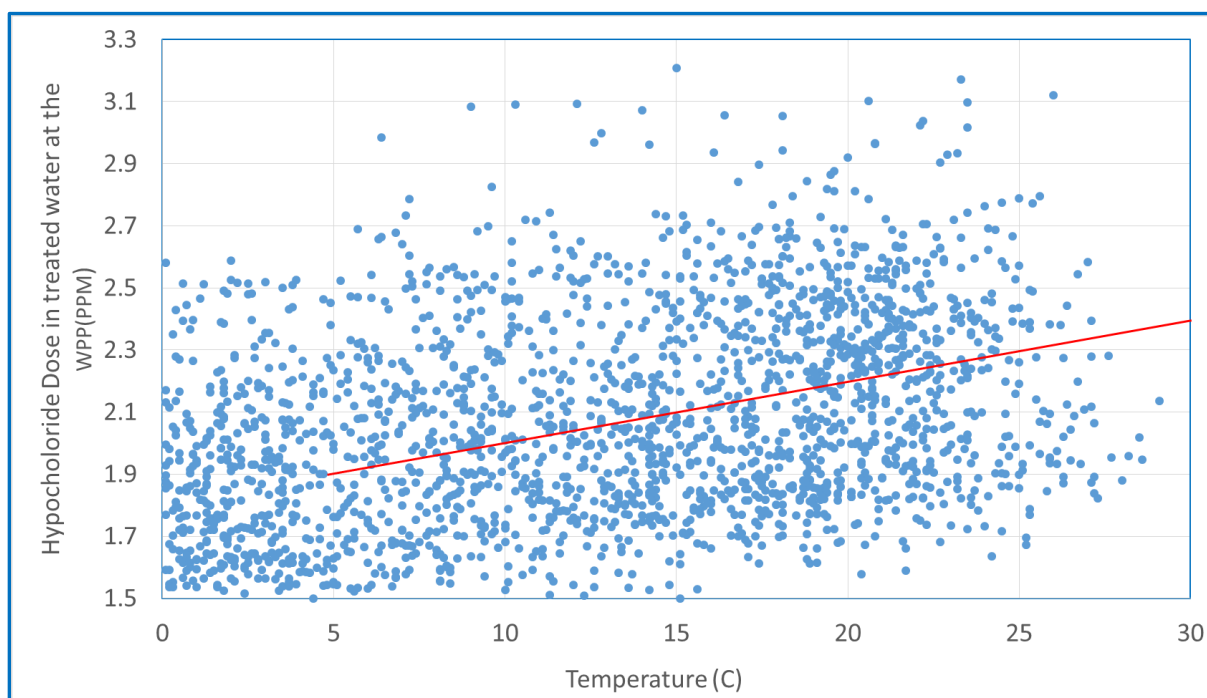


Figure 28 Daily concentration of Hypochlorite in Network 3 water distribution systems correlated with air temperature from 2011 to 2021.

The literature contains a few publications on the impact of temperature on chlorine residuals and those are based mainly on field and experimental works. (Casas-Monroy, et al., 2018) investigated the effect of temperature on chlorine treatment for the elimination of freshwater phytoplankton in ballast water, in laboratory setup under cold and warm water temperatures (2°C to 22°C) across winter and summer seasons. They exposed their samples to seven

chlorine treatments from 0.02 to 5.0 ppm while measuring phytoplankton abundance and photosynthetic efficiency up to 48 hours. After 4 hours of treatment at concentrations less than 0.22 ppm, phytoplankton densities were reduced by more than 50%, without cell resurgence. Similar reduction was recorded immediately after exposure when chlorine concentrations were higher than 3.0 ppm. After 8 hours, free chlorine neared 0.0 ppm for initial chlorine concentrations below 1.2 ppm, irrespective of temperature regime. Winter phytoplankton exhibited slightly lower mortality to chlorine exposure regardless of the temperature, although they also exhibited lower photosynthetic efficiency. Their results indicated that higher doses of chlorine or longer exposure times may be required during winter to achieve full treatment effect. Their outcomes did not indicate a significant effect of temperature on the chlorine decay.

(Kimbrough, 2019) collected air temperature from 1985 to 2016 and compared those with water temperatures in four locations in the Pasadena distribution system. He showed that the median nighttime temperature of the period 2009-2016 was 1.6°C warmer than the period 1985-2000 and 0.5°C warmer than 2001-2008 period. He also indicated that median chloramine concentration fell significantly at three locations and nitrite concentrations increased significantly at all four locations. As air temperature in the study area increased, water temperatures also increased resulting in some loss of disinfectant residual and consequent increase in ammonia-oxidizing bacterial activities. It is worth noting that (Kimbrough, 2019) data was collected from a real world distribution system while (Casas-Monroy, et al., 2018) tested the chlorine effects on phytoplanktons in freshwater samples in laboratory setup.

A higher concentration of chlorine does not necessarily mean higher water quality. (Fish, Reeves-McLaren, Husband, & Boxall, 2020) used a full scale experimental facility to determine the physical, chemical and biological impacts of different free chlorine regimes on biofilm characteristics and water quality. Unexpectedly, their experiments indicated that higher free chlorine concentrations resulted in greater water quality degradation, observable as elevated inorganic loading and greater discolouration. Their results challenged the assumption that a measurable free chlorine residual necessarily assures drinking water safety.

It needs to be clearly stated here that despite the conclusions of Fish et al. (2020), and absent alternative methods to quantitatively express the quality of the water in distribution systems, residual chlorine level is employed as a surrogate for water quality in this study.

The impact of climate change on chlorine residuals could also be quantified through numerical modeling. The literature that looks into integrating water temperature into chlorine decay modeling is discussed in Section 6.2.

6.1 Correlation between air and water temperature

Changes in air temperature would likely result in changing water temperature in distribution systems that draw their water from surface water source as well as (but likely to a lesser extent) system that are fed groundwater. These changes are mostly seasonal.

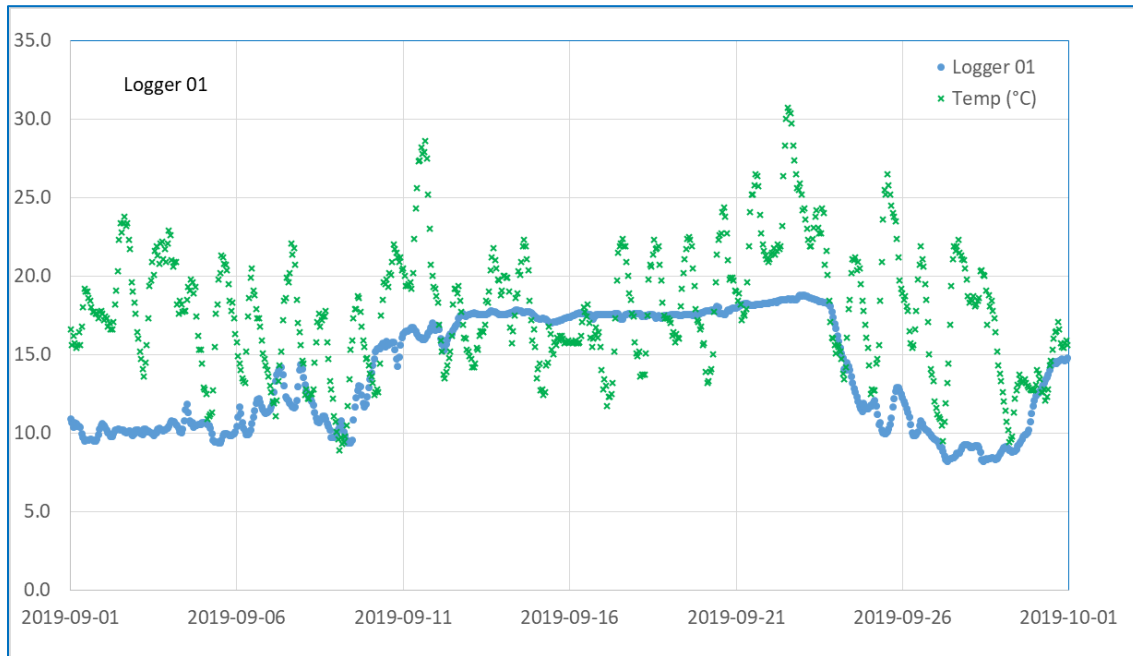


Figure 29 Hourly air and water temperature variation during September in Logger 1.

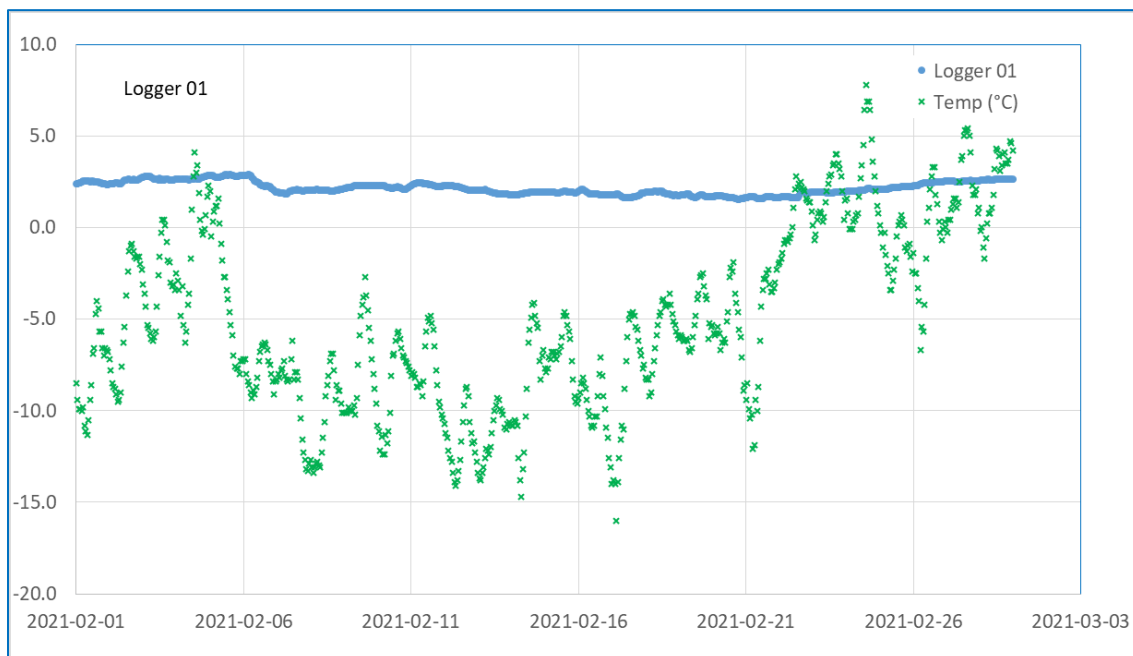


Figure 30 Hourly air and water temperature variation during February in Logger 1.

Network 1 case study was instrumented with 12 sensor clusters that included water temperature sensors. The location of these sensor clusters in the network are illustrated in Figure 31 and water and air temperature readings for the period 2019 to 2021 are provided in Figure 32 to Figure 34. These data indicate that the seasonal peak water temperature happens in late August or early September and lags four to eight weeks behind ambient peak temperature, which typically occurs in July. Minimum water temperature occurs in late February in each of the monitored years. The logger closest to the water purification plants (i.e., Logger 04 – at the south side of the network) recorded the lowest minimum temperatures just above zero (i.e., 0.25 °C). Loggers 2 and 11, located farthest from the purification plant, recorded the highest minimum temperature of 2.5 °C.

It is worth noting that, daily (even weakly) air temperature fluctuation does not seem to have significant impact on the water temperature fluctuations. This is shown in Figure 29 and Figure 30, where the hourly water and air temperature were recorded by Logger 1 during September (peak water temperature month) and February (minimum water temperature month). This corresponds to the observation that in general water temperature changes in the distribution system appear to follow air temperature fluctuations with a time gap of 4-6 weeks, depending on the distance from the water source (see Figure 32 through Figure 34).

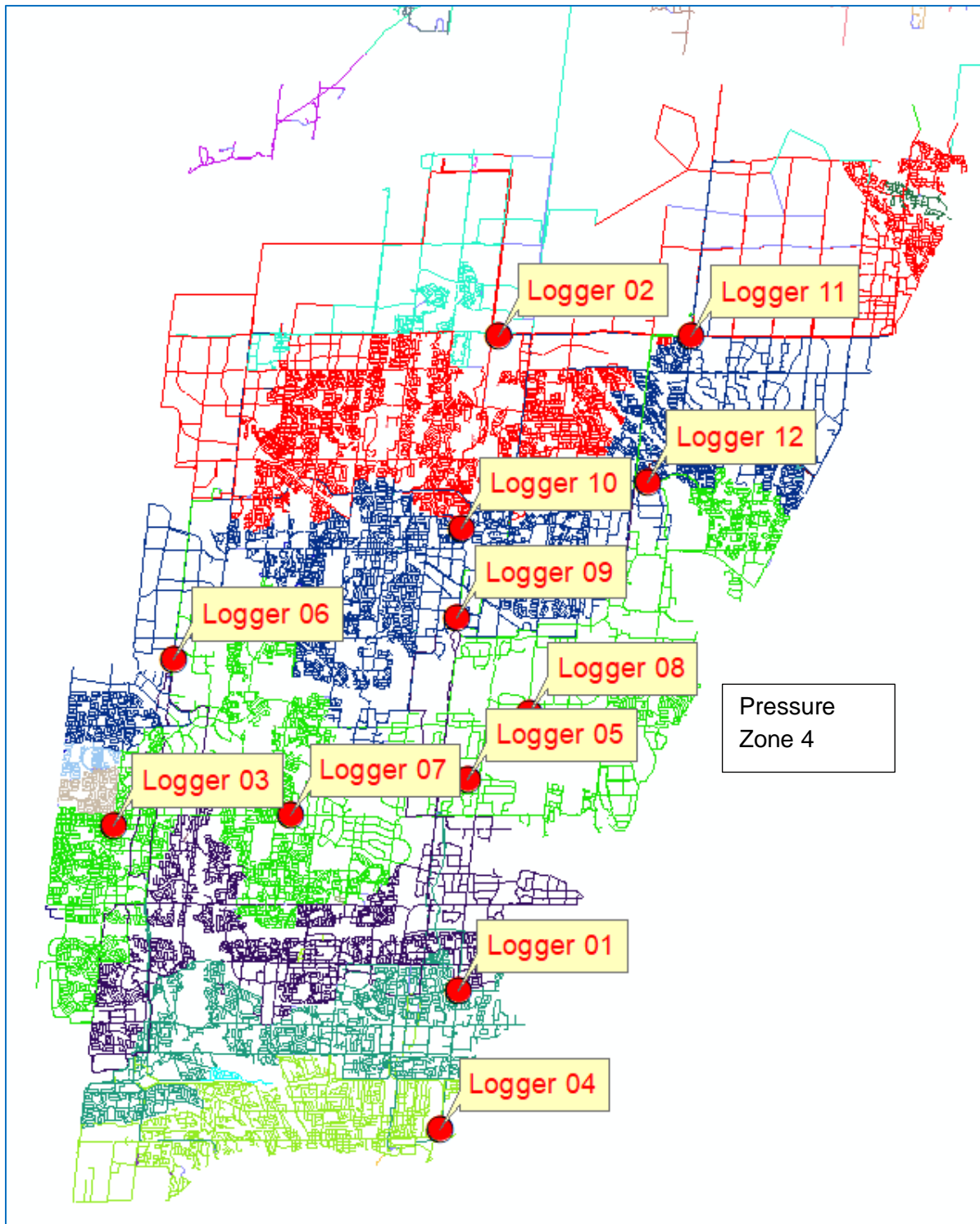


Figure 31 Logger locations and distribution across Network 1 Case Study.

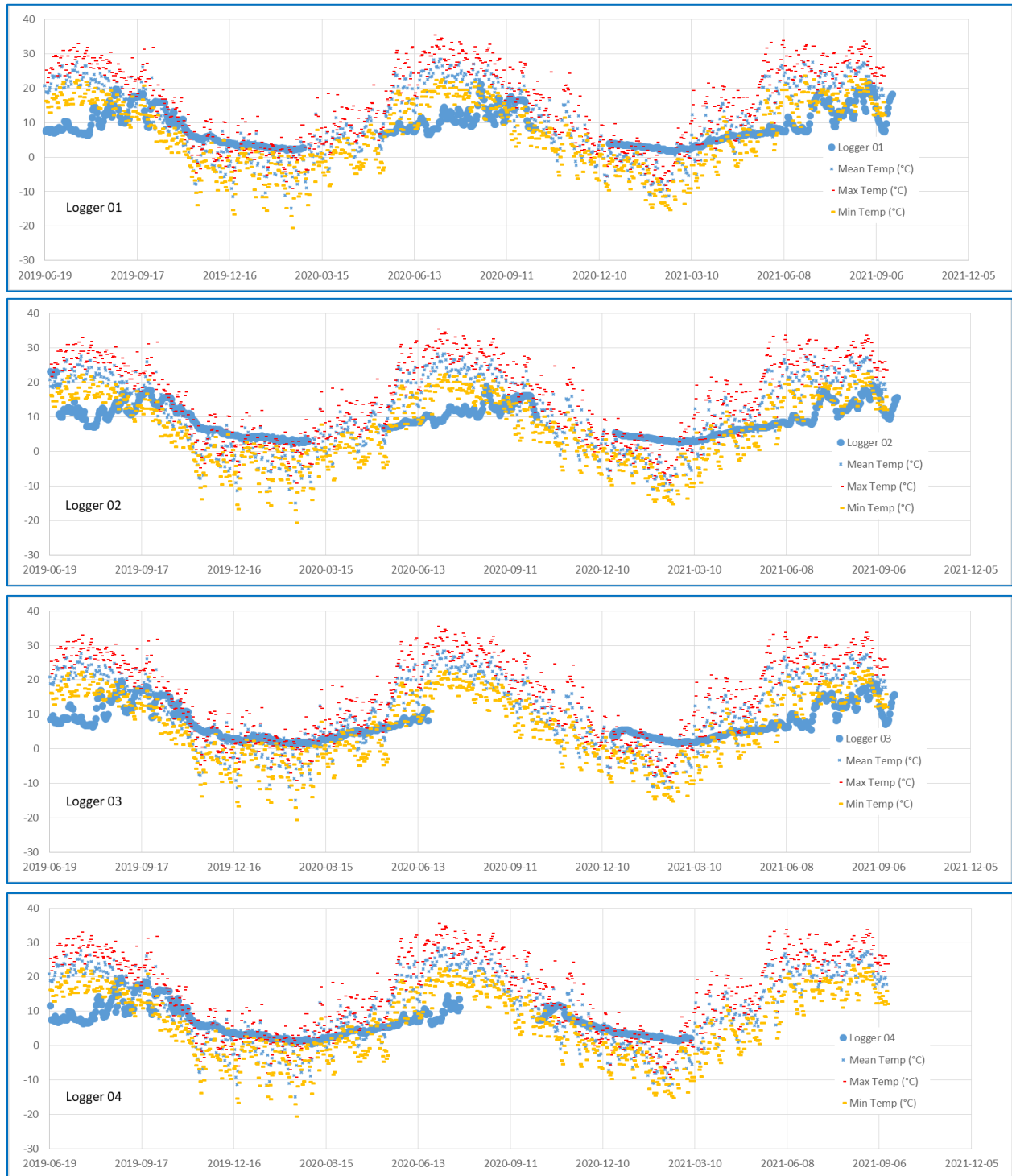


Figure 32 Daily minimum, mean, and maximum temperature in Network 1, and water temperature inside watermains in Logger 1 to 4 (gaps in logger data due to malfunction or battery power depletion).

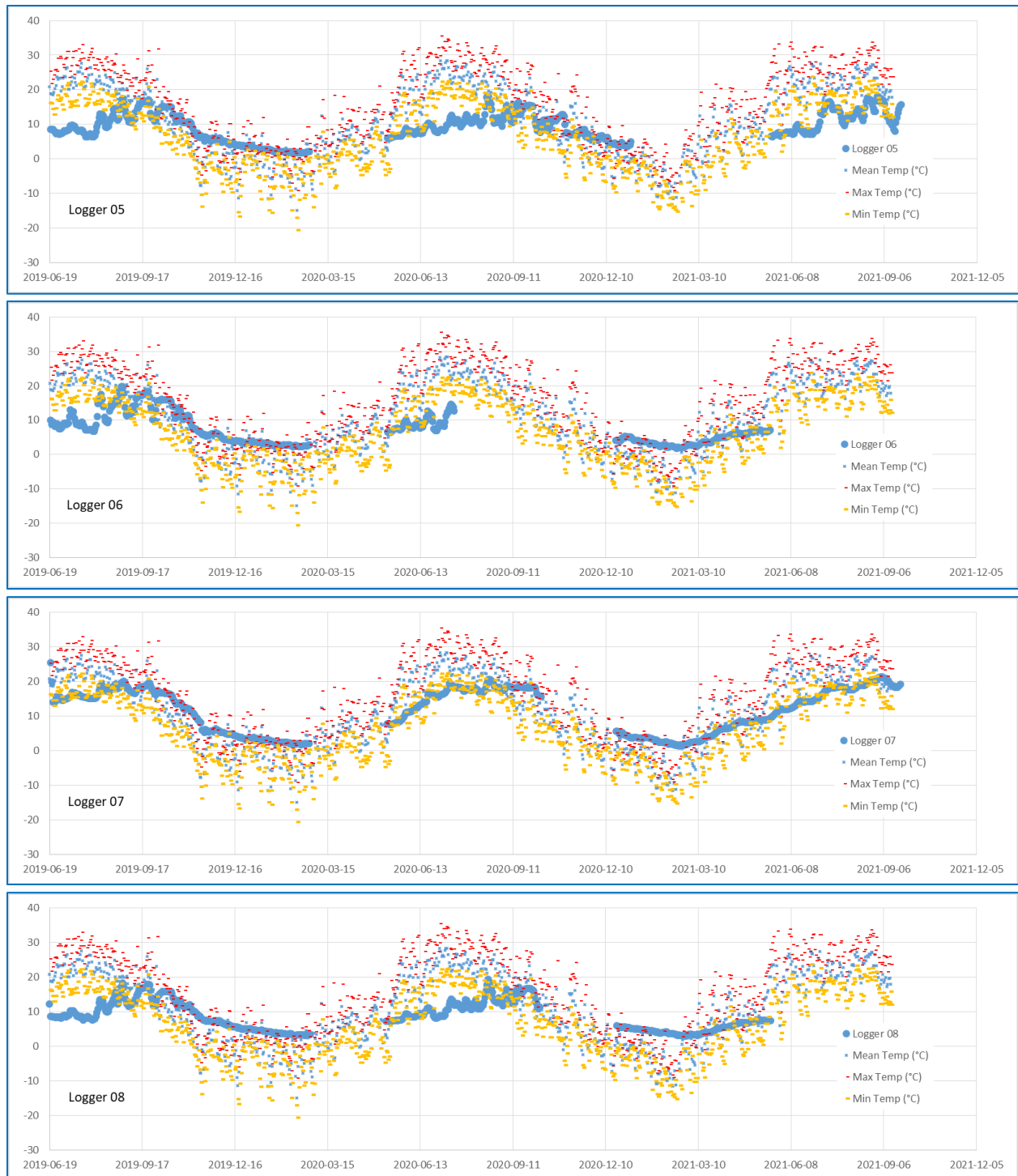


Figure 33 Daily minimum, mean, and maximum temperature in Network 1, and water temperature inside watermains in Logger 5 to 8 (gaps in logger data due to malfunction or battery power depletion).

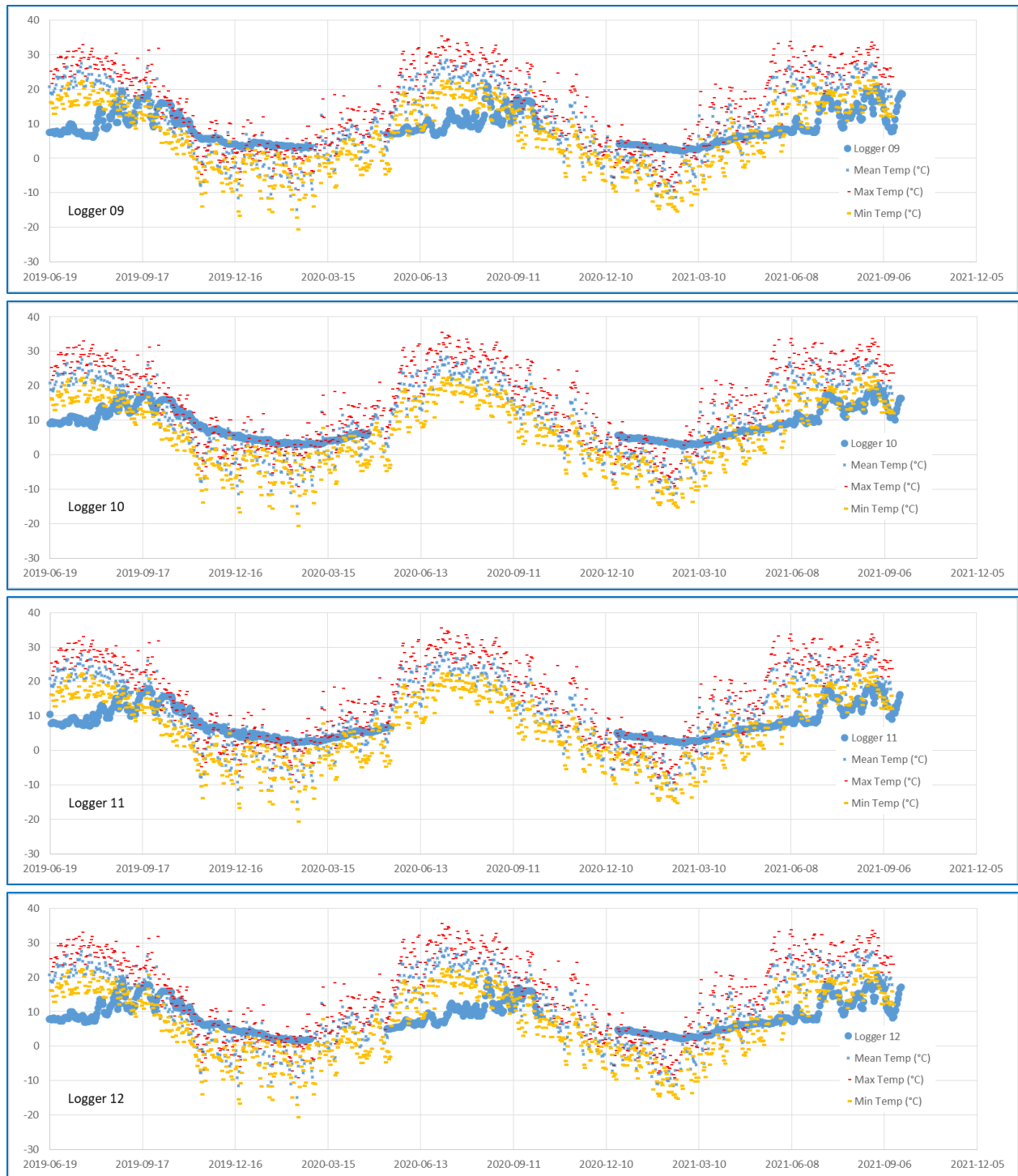


Figure 34 Daily minimum, mean, and maximum temperature in Network 1, and water temperature inside watermains in Logger 9 to 12 (gaps in logger data due to malfunction or battery power depletion).

6.2 Integrating water temperature in chlorine decay modeling in WDSs⁴

Simulations of water quality in water distribution systems (WDSs) have been a research topic for a few decades. Although chlorine decay is influenced by the water temperature and that the water temperature in the WDS may change significantly throughout the network, limited work has been done in this aspect of the chlorine decay process. This section summarizes the published work in this field and proposes a conceptual model with the aim of developing a method and tool for integrating water temperature in chlorine decay modeling in WDSs. Then, the developed model is applied to one of the pressure zone of the Network 1 water distribution network (Figure 18 and Figure 21).

Modelling Chlorine decay in the WDS is usually given by:

$$\frac{dC}{dt} = k_b C + \frac{4}{d} k_w \quad (1)$$

where: C is free Chlorine concentration (mg/l), t is the time, k_b is the first-order bulk decay coefficient (1/day), k_w is the zero-order wall reaction decay coefficient (mg/m²/day) and d is the pipe diameter (mm). k_b is a function of the temperature T_{water} and may be estimated by the following empirical relation:

$$k_b^{T_{water}} = k_b^{20} 1.1^{(T_{water}-20)} \quad (2)$$

where k_b^{20} is the decay rate coefficient at 20°C which should be obtained for the specific network source. k_w is more difficult to estimate and needs further investigation. One of its components, k_f the mass transfer coefficient, may be estimated by the Reynolds and Sherwood numbers which are also functions of the temperature.

Modelling temperature in the water distribution network is possible with the EPANET-MSX extension (EPA, 2018). For pipes, the change in water temperature is given in Eq. (3).

⁴ Sections 6.26.2 to 6.3 were written by Elad Salomons of Optiwater, Haifa, Israel, who also developed the model, coded it and helped to test and validate it. These sections detail various modeling considerations for simulating the impact of temperature on chlorine residual decay in a water distribution system, numerical model development, and application of the developed model to a real world case study. Readers that are not interested into these technical discussions could skip these sections and continue from Section 6.4.

$$\frac{dT_{water}}{dt} = \frac{\alpha_{water}}{r^2 \left(\lambda_w + \frac{1}{Nu} \right)} (T_{soil} - T_{water}) \quad (3)$$

where α_{water} , λ_w , Nu are parameters of the water and pipe which change with temperature and T_{soil} is the soil temperature which is assumed to be a short term constant at the pipe's depth. For tanks, the change of water temperature is modelled according to the surrounding environment temperature, T_s , and the cooling rate of water, k_c .

$$\frac{dT_{water}}{dt} = k_c (T_s - T_{water}) \quad (4)$$

When utilizing this temperature and Chlorine decay model on the Case study's water distribution network, it is clear that lower levels of Chlorine are observed as the source water and ground temperature rises. This change is up to 5% over the range of 5 to 25 degrees Celsius.

6.2.1 Modeling Chlorine decay in the drinking water distribution system

(Rossman, Clark, & Grayman, 1994) states that based on previous work (Wable, et al., 1991), it appears reasonable to assume that the disappearance of chlorine flowing through a pipe is governed by first-order kinetics. They assume that this disappearance is due to reactions both within the bulk flow and at sites along the pipe wall.

$$\frac{\partial C}{\partial t} = -u \frac{\partial C}{\partial X} - K_b C - \frac{K_f}{r_h} (C - C_w) \quad (5)$$

where C is the chlorine concentration in the bulk flow; t is the time; u is the flow velocity in pipe; x is the distance along pipe; K_b is the decay rate constant in the bulk flow; K_f is the mass-transfer coefficient; r_h is the hydraulic radius of pipe (one half the pipe radius); and C_w is the chlorine concentration at the pipe wall.

The term on the left side of the equation represents the rate of change of chlorine concentration within a differential section of pipe. The first term on the right side of the equation accounts for the advective flux of chlorine through the section (dispersive flux is assumed to be negligible under typical operating conditions). The second term represents chlorine decay within the bulk flow, and the third term accounts for transport of chlorine from the bulk flow to the pipe wall and subsequent reaction. The inverse of the hydraulic radius represents the specific surface area (i.e., the pipe-wall area per unit of pipe volume) available for reaction.

The above model was adopted within the EPANET software (Rossman L. , 2000):

$$\frac{\partial C_i}{\partial t} = -u \frac{\partial C_i}{\partial x} + r(C_i) \quad (6)$$

where C_i is the concentration (mass/volume) in pipe i as a function of distance x and time t , u_i is the flow velocity (length/time) in pipe i , and r is the rate of reaction (mass/volume/time) as a function of concentration - that is both for bulk and wall. The term on the right is a set of functions, which represent all chlorine reactions, both in the bulk flow and near the wall.

6.2.2 Bulk Flow Reactions

EPANET models reactions occurring in the bulk flow with n -th order kinetics, where the instantaneous rate of reaction (R in mass/volume/time) is assumed to be concentration-dependent according to:

$$R = K_b C^n \quad (7)$$

Here K_b is a bulk reaction rate coefficient, C is the reactant concentration (mass/volume), and n is the reaction order. K_b has units of concentration raised to the $(1-n)$ power divided by time. It is positive for growth reactions and negative for decay reactions such as the decay of Chlorine.

Table 10: Results of first-order bulk decay tests (Boulos, Vasconcelos, Rossman, Clark, & Grayman, 1997)

Finished Water Source	pH	Temperature °C	TOC mg/ L	Free Chlorine mg/ L	Bulk Decay Coefficient 1/ d
Bellingham Watcom Water Treatment Plant	8.05	17.4	0.84	0.72	0.833
Fairfield Waterman Treatment Plant	8.15	17.9	1.87	1.73	1.16
Harrisburg Oberlin Pump Station	7.52	16.4	1.73	0.98	0.232
North Marin Russian River Aqueduct	7.42	22.2	0.56	0.31	1.32
North Marin Stafford Lake Treatment Plant	8.85	21.9	3.55	0.49	17.7
North Marin 50/50 blend of Aqueduct and Stafford Lake water	7.92	22.1		0.40	10.8
North Penn Keystone tie-in		16.2	0.79	1.65*	0.082
North Penn Forest Park Treatment Plant		13.2	1.64	1.30*	0.767
North Penn 50/50 blend of Keystone and Forest Park water		14.7	1.23	1.38*	0.264
North Penn Well W17		14.8	1.06	0.50*	0.355
North Penn Well W12		18.3	0.52	0.85*	0.102
* Total chlorine					

The K_b for first-order reactions can be estimated by placing a sample of water in a series of non-reacting glass bottles and analyzing the contents of each bottle at different points in time. If the reaction is first order, then plotting the natural log (C_t/C_0) against time should result in a straight line, where C_t is concentration at time t and C_0 is concentration at time zero. K_b would then be estimated as the slope of this line. A default value used in EPANET is $K_b = -1(1/\text{day})$.

As a reference, some values of the bulk flow decay coefficient are given in *Table 10* (Boulos, Vasconcelos, Rossman, Clark, & Grayman, 1997).

6.2.3 Bulk reaction rate coefficient changes with temperature

(Rossman L. , 2000) states that the bulk reaction coefficients usually increase with increasing temperature. Running multiple bottle tests at different temperatures will provide more accurate assessment of how the rate coefficient varies with temperature. The relationship between the bulk rate constant seen at one temperature (T_1) to that at another temperature (T_2) is often expressed using a van't Hoff – Arrhenius equation of the form (Metcalf & Eddy, 2003):

$$K_{b2} = K_{b1} \theta^{T_2 - T_1} \quad (8)$$

where θ is a constant. In one investigation for chlorine, θ was estimated to be 1.1 (Table 11) when T_1 was 20 deg. C (Koechling, 1998) so Eq. (8) becomes:

$$K_T = K_{20} 1.1^{(T - 20)} \quad (9)$$

Table 11: calculation of θ by (Koechling, 1998)

Table 8.9: Effect of temperature on α_1 and k_2							
FuNOM			BRW			SJR	
Temp.	α_1 *		Temp.	α_1		α_1	
11	-3.82		5	-5.04		-11.8	
20	-3.77		20	-5.00		-11.8	
34	-3.71		35	-5.10		-12.2	
Temp.	$k_2 \cdot 100^+$	θ	Temp.	$k_2 \cdot 100$	θ	$k_2 \cdot 100$	θ
11	-0.098	1.08	5	-0.21	1.10	-0.67	1.11
20	-0.201		20	-0.87		-3.37	
34	-0.858	1.11	35	-4.16	1.11	-15.5	1.11

* α_1 in mg/L; + k_2 in m³mg²/L²/hr

Returning to the Arrhenius equation (Missen et al. 1999, page 44): A rate of reaction usually depends more strongly on temperature than on concentration. Thus, in a first order ($n = 1$) reaction, the rate doubles if the concentration is doubled. However, a rate may double if the temperature is raised by only 10 K, in the range, say, from 290 to 300 K that is 16.8C to 26.8C (300K – 273.15 = 26.85°C). It should be noted that with Eq. (9), the rate doubles with a change of 7.3°C as this is an approximation with relative good accuracy as shown below.

Influenced by the form of the van't Hoff equation, Arrhenius (1889) proposed an expression for the rate constant K (here K_A):

$$K_A = A \exp(-E / RT) \quad (10)$$

Where T is the temperature, E is a characteristic (molar) energy, called the energy of activation, R is the ideal gas constant and A is a constant referred to as the pre-exponential factor. Together, E and A are called the Arrhenius parameters which are independent of T and may be calculated experimentally for a given reaction.

In (Ki  n  , Lu, & L  vi, 1998), the influence of Total Organic Carbon (TOC) and temperature on the chlorine decay rate in the aqueous phase has been studied. For this purpose, the kinetics of chlorine decay has been established. Experimental results showed a rapid chlorine depletion during a first phase of about 1 or 2 hours. This phase corresponds to reactions with easily oxidizable compounds and is usually completed during the disinfection step at the treatment plant. Therefore, this phase should not be observed within the distribution network. During a second phase, chlorine decayed more slowly and it was always possible to describe this phase with a first order kinetic rate with respect to chlorine. All the experimental results have been expressed by the value of the first order kinetic constant k , related to the long-term chlorine consumption. The study of 21 water samples with temperatures between 5 and 25  C, and TOC concentrations between 1 and 3 mg/l, made it possible to establish the following empirical relationship:

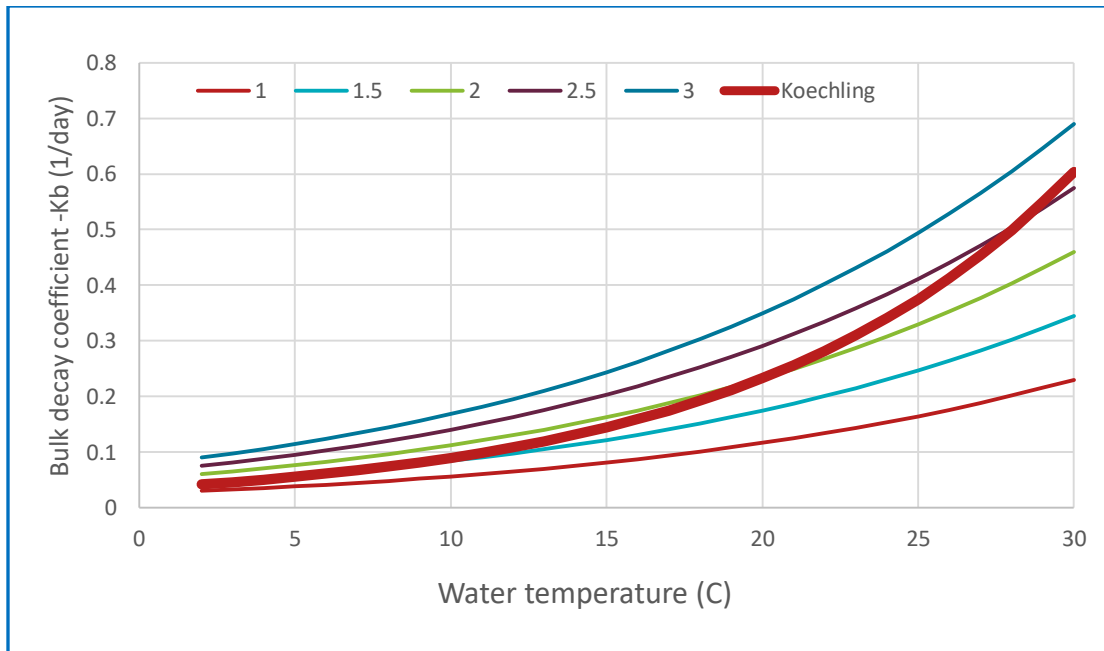


Figure 35: Relationship between bulk decay coefficient and water temperature for different TOC levels using (Ki  n  , Lu, & L  vi, 1998) and (Koechling, 1998)

$$k_b = 1.8 \cdot 10^6 [TOC] \exp\left(-\frac{6080}{T}\right) \quad (11)$$

Where T is the temperature in Kelvin and TOC is the Total Organic Carbon in mg / L . When comparing the results of (Ki  n  , Lu, & L  vi, 1998) and (Koechling, 1998), Figure 35, it can be seen that Koechling Eq. (9) averagely fits the results by Ki  n   in Eq. (11).

(Eck, Saito, & McKenna, 2016) used the above Ki  n   equation to model disinfection by-products (DBPs) with changing temperature: The bulk decay coefficient k_b (1/min) is modeled as a function of the temperature and total organic carbon concentration TOC according to the relation of (Ki  n  , Lu, & L  vi, 1998). (Eck, Saito, & McKenna, 2016) used EPANET-MSX to model DBPs and temperature. The temperature model used is based on (Mirjam Blokker & Pieterse-Quirijns, 2013), which is described below. It should be noted that the Ki  n   equation is like Arrhenius's equation with $E/R=6080K$ and $A=1.8 \times 10^6 [TOC]$. One major downside of using the Ki  n   equation and the TOC is that the TOC must also be tracked in the network, something not done by (Eck, Saito, & McKenna, 2016).

(Nagatani, et al., 2006) reported the relationship between K_b and water temperature by analyzing the results of bottle tests that were conducted on treated water at Niwakubo purification plant in Japan based on (Tomohiro & Katsuhiko, 2003):

$$k_b = -0.0398 \exp(0.0742T) \quad (12)$$

K_b in 1/day and T in C. However, this is only one sampled source.

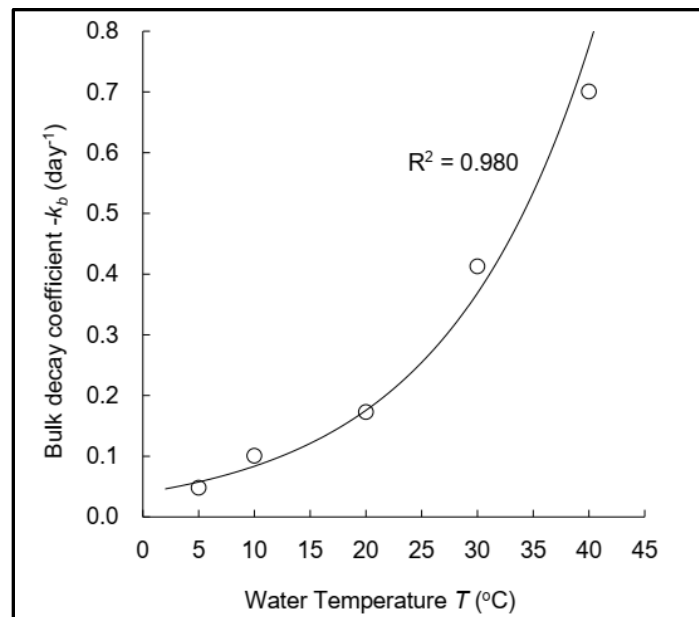


Figure 36: bulk decay coefficient as a function of temperature (Nagatani, et al., 2006)

Again, comparing Nagatani results to (Koechling, 1998), Eq. (12) to Eq. (9), yields similar results.

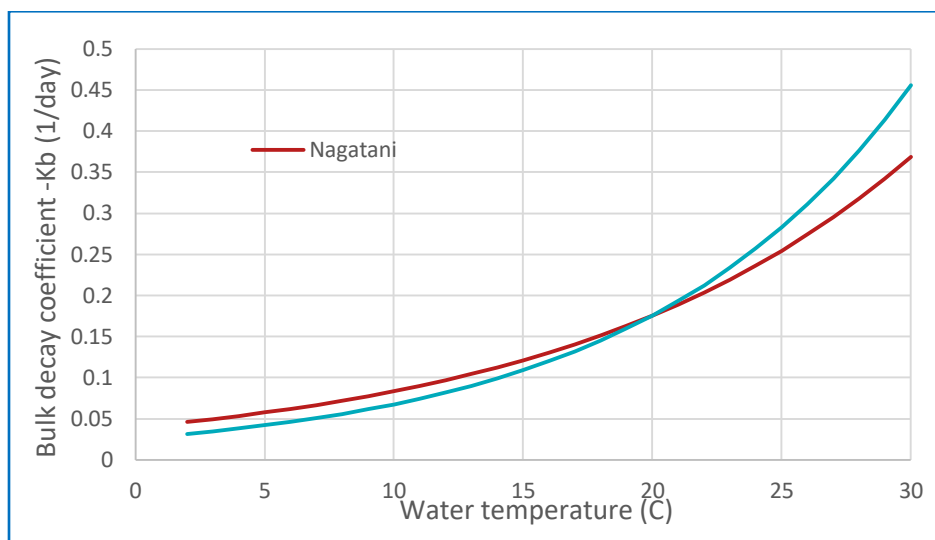


Figure 37: Relationship between bulk decay coefficient and water temperature using (Nagatani, et al., 2006) and (Koechling, 1998)

TOC is one of the measures of Natural Organic Matter (NOM). (Monteiro, Menaia, & Covas, 2012) stated that in addition to water NOM contents and reactivity, K_b is mainly affected by the water temperature (Powell, Hallam, West, Forster, & Simms, 2000). (Powell, Hallam, West, Forster, & Simms, 2000) found that 10°C raises in water temperature may lead to 2.5-fold increases in K_b values (which is consistent with Eq. (9)). However, increments as small as 5°C may double the rates of bulk chlorine decay (Kastl, Fisher, & Jegatheesan, 1999). Such a phenomenon is particularly important in continental climates where the water temperature spans from near-freezing to very high. Ongoing climate changes, including global warming and higher frequency and severity of extremes, such as heat and cold waves, are likely to aggravate such conditions and to extend them to other areas, including the Mediterranean regions like Algarve (Portugal). There the distribution systems water temperature may range from 13°C in winter to 21°C in summer (Pina, et al., 2010). In this study, experiments were made to calculate E and A, the Arrhenius equation constants, for raw and treated waters from two locations in Portugal.

(Fisher, Kastl, & Sathasivan, 2011) reported on a two reactant (2R) second order model as "the most simple and generally suitable model for simulating chlorine concentration profiles in distribution system networks". The model assumes that chlorine reacts with two groups of water compounds, one reacting rapidly and the other reacting slowly:

$$\frac{dC}{dt} = \frac{dC_f}{dt} + \frac{dC_s}{dt} = -k_f C C_f - k_s C C_s \quad (13)$$

where C_f and C_s are, respectively, the concentrations of fast and slow reducing agents in the water that react with chlorine (as mg Cl-equivalent/L) and k_f and k_s are decay rate coefficients

for fast and slow reactions (L/mg Cl/h). The model requires the estimation of four parameters, namely the reaction rate coefficients and initial concentrations of C_f and C_s , which can be inferred from extensive laboratory decay tests data.

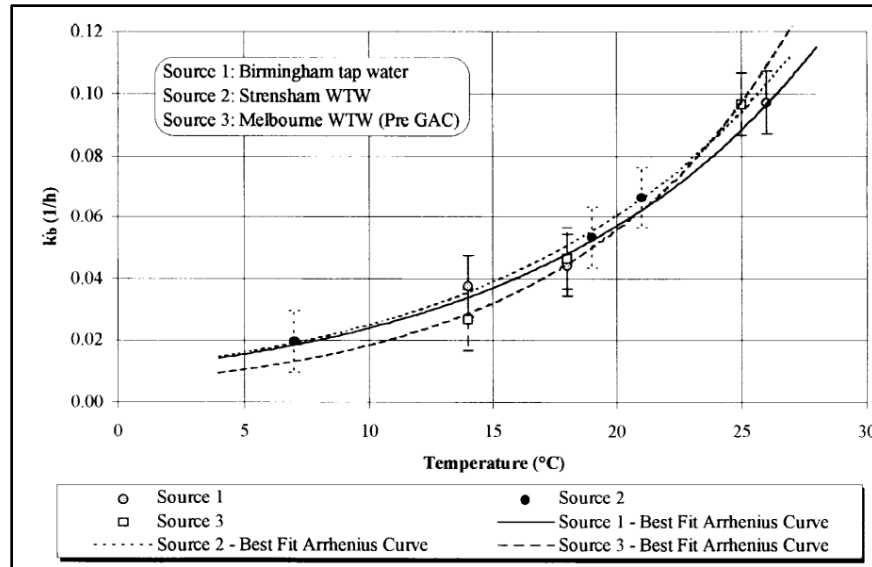


Figure 38: bulk decay coefficient as a function of temperature (Powell, Hallam, West, Forster, & Simms, 2000)

Once again, (Powell, Hallam, West, Forster, & Simms, 2000) results are compared to (Koechling, 1998), and yields similar results.

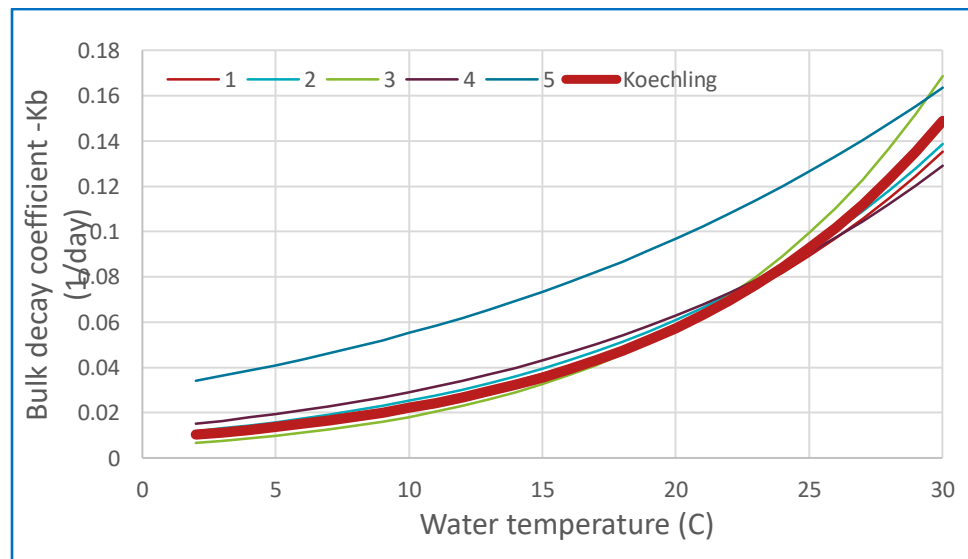


Figure 39: Relationship between bulk decay coefficient and water temperature using (Powell, Hallam, West, Forster, & Simms, 2000) and (Koechling, 1998)

(Powell, Hallam, West, Forster, & Simms, 2000) tested three types of waters (both in the lab and in the field) and evaluated the Arrhenius equation constants A and E :

6.2.4 Summary for the bulk decay coefficient

- Not many researchers have done extensive laboratory studies regarding the effect of change in temperature on the Chlorine bulk decay rate.
- All use some form of the Arrhenius equation.
- Different tests show different Arrhenius constants.
- However, deviations from the (Koechling, 1998) equation, Eq. (9), are not large (see above figures).

$$K_{bT} = K_{b20} 1.1^{(T-20)} \quad (14)$$

- The advantage of the Koechling equation is its simplicity. However, the bulk decay rate at 20 degrees C must be known (which is the normal assumption for "regular" Chlorine decay simulations).

6.2.5 Wall Reactions

In subject of wall reactions and wall decay coefficients, we found limited practical work. In many cases (Boulos, Vasconcelos, Rossman, Clark, & Grayman, 1997), (Hallam, West, Forster, Powell, & Spencer, 2002), (Monteiro, et al., 2013), (Monteiro, Figueiredo, Covas, & Menaia, 2017), (Rossman, Clark, & Grayman, 1994) the way the wall decay coefficients were estimated is by first estimating the bulk decay coefficients and then calibrating the wall decay coefficients accordingly. Fisher et al. (2011) stated that: "It is seldom sufficiently emphasized that bulk-decay needs to be accurately modelled first, as it is a characteristic only of the transported water, independent of the system. In contrast, the wall decay (chlorine loss) can only be quantified as differences between in-system measurements of chlorine and values calculated from a bulk-decay (only) model at corresponding points and times in the network model."

The rate of water quality reactions occurring at or near the pipe wall can be considered to be dependent on the concentration in the bulk flow by using an expression of the form:

$$R = (A/V) K_w C^n \quad (15)$$

where K_w = a wall reaction rate coefficient and (A/V) = the surface area per unit volume within a pipe (equal to 4 divided by the pipe diameter). The latter term converts the mass reacting per unit of wall area to a per unit volume basis. EPANET limits the choice of wall reaction order to either 0 or 1, so that the units of K_w are either mass/area/time or length/time, respectively. As with K_b , K_w must be supplied to the program by the modeller. First-order K_w values can range anywhere from 0 to as much as 5 ft/day. K_w should be adjusted to account for any mass transfer limitations in moving reactants and products between the bulk flow and the wall. EPANET does

this automatically, basing the adjustment on the molecular diffusivity of the substance being modeled and on the flow's Reynolds number.

The wall reaction coefficient can depend on temperature and can also be correlated to pipe age and material. It is well known that as metal pipes age their roughness tends to increase due to encrustation and tuberculation of corrosion products on the pipe walls. This increase in roughness produces a lower Hazen-Williams C-factor or a higher Darcy-Weisbach roughness coefficient, resulting in greater frictional head loss in flow through the pipe.

There is some evidence to suggest that the same processes that increase a pipe's roughness with age also tend to increase the reactivity of its wall with some chemical species, particularly chlorine and other disinfectants. EPANET can make each pipe's K_w be a function of the coefficient used to describe its roughness. A different function applies depending on the formula used to compute headloss through the pipe:

Headloss Formula	Wall Reaction Formula
Hazen-Williams	$K_w = F / C$
Darcy-Weisbach	$K_w = -F \log(e/d)$
Chezy-Manning	$K_w = F_n$

where C = Hazen-Williams C-factor, e = Darcy-Weisbach roughness, d = pipe diameter, n = Manning roughness coefficient, and F = wall reaction - pipe roughness coefficient. The coefficient F must be developed from site-specific field measurements and will have a different meaning depending on which head loss equation is used. The advantage of using this approach is that it requires only a single parameter, F , to allow wall reaction coefficients to vary throughout the network in a physically meaningful way.

While flowing through pipes, dissolved substances can be transported to the pipe wall and react with material such as corrosion products or biofilm that are on or close to the wall. The amount of wall area available for reaction and the rate of mass transfer between the bulk fluid and the wall will also influence the overall rate of this reaction. The surface area per unit volume, which for a pipe equals 2 divided by the radius, determines the former factor. The latter factor can be represented by a mass transfer coefficient whose value depends on the molecular diffusivity of the reactive species and on the Reynolds number of the flow (Rossman, Clark, & Grayman, 1994). For first-order kinetics, the rate of a pipe wall reaction can be expressed as:

$$r = \frac{2k_w k_f C}{R(k_w + k_f)} \quad (16)$$

where k_w = wall reaction rate constant (length/time), k_f = mass transfer coefficient (length/time), and R = pipe radius. For zero-order kinetics the reaction rate cannot be any higher than the rate of mass transfer, so:

$$r = \min(k_w, k_f C)(2 / R) \quad (17)$$

where k_w now has units of mass/area/time. Mass transfer coefficients are usually expressed in terms of a dimensionless Sherwood number (Sh):

$$k_f = Sh \frac{Dif}{d} \quad (18)$$

in which Dif is the molecular diffusivity of chlorine in water (length²/time) and d = pipe diameter. In fully developed laminar flow, the average Sherwood number along the length of a pipe can be expressed as:

$$Sh = 3.65 + \frac{0.0668(d / L) Re \cdot Sc}{1 + 0.04[(d / L) Re \cdot Sc]^{2/3}} \quad (19)$$

in which Re = Reynolds number and Sc = Schmidt number (kinematic viscosity of water divided by the diffusivity of the chemical). For turbulent flow the empirical correlation of Notter and Sleicher (1971) can be used:

$$Sh = 0.0149 Re^{0.88} Sc^{1/3} \quad (20)$$

The Reynolds number is given by:

$$Re = \frac{u \cdot d}{\nu} \quad (21)$$

where u is the water velocity in the pipe, d is the pipe diameter and ν is the kinematic viscosity of water which changes with temperature (Engineers Edge, 2021).

6.2.6 Wall reaction rate coefficient change with temperature

K_f is depended on the molecular diffusivity of chlorine in water and the kinematic viscosity of water which both change with temperature as shown in Figure 40 and Figure 41.

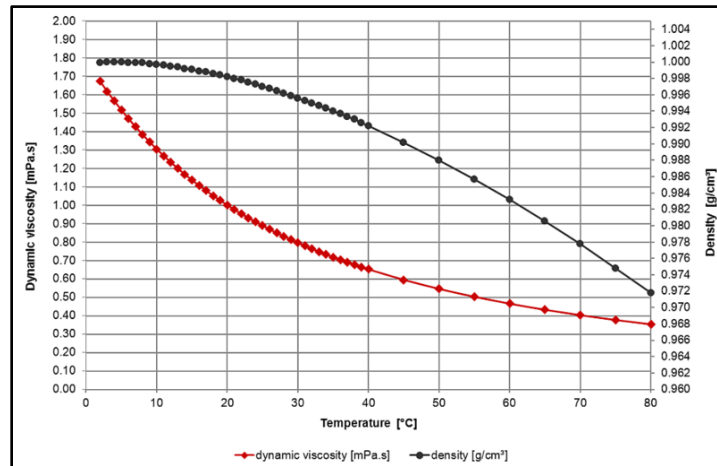


Figure 40: Viscosity of Water as a function of Temperature (<https://wiki.anton-paar.com/en/water/>)

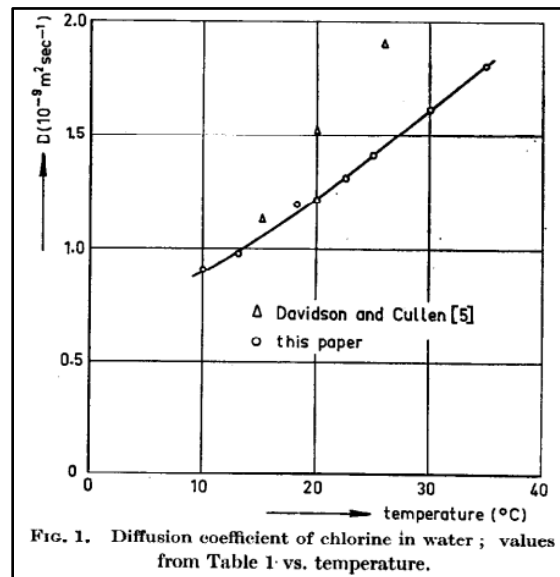


Figure 41: Diffusion coefficient of chlorine in water, Kramers et al. (1959)

The change of the diffusion coefficient of chlorine in water with temperature can be linearized to be (in m^2 / s):

$$Dif = (0.0365T + 0.5176) \cdot 10^{-9} \quad (22)$$

Schmidt number (Sc) is the kinematic viscosity of water divided by the diffusivity of the Chlorine which both change with temperature are seen above:

$$Sc = \frac{\nu}{D} \quad (23)$$

6.2.7 Summary for the wall decay coefficient

- The magnitude of the effect of the wall decay is not totally clear. Not many studies on this subject.
- Most studies calibrate the wall decay coefficient according to the bulk decay coefficient.
- The mass transfer coefficient k_f may be estimated with the change of temperature according to Eqs. (18), (19), (20) and (21)
- The wall reaction rate constant k_w still needs to be investigated.

6.2.8 Modeling temperature in the drinking water distribution system

There are only a few studies on modeling temperature in water distribution systems. The main contribution in this field is the work by (Mirjam Blokker & Pieterse-Quirijns, 2013) with some printing corrections made later (Mirjam Blokker & Pieterse-Quirijns, 2018). They considered "complicated" soil temperature model but "the temperature of the soil is hardly influenced by the temperature of the drinking water because the mass of the soil is so much larger than the mass of the water-filled pipe. This means that the soil temperature at the pipe wall is assumed to be a boundary condition for the heat transfer from soil to drinking water". Soil temperature studies have showed that "the earth temperature beyond a depth of 1 meter is usually insensitive to the diurnal cycle of air temperature and solar radiation" (Florides & Kalogirou, 2001) as presented in Table 12.

Table 12: depth of penetration of diurnal and annual temperature cycles (Florides & Kalogirou, 2001)

Table I: Depth of Penetration of Diurnal and Annual Temperature Cycles.

Types of Ground	Thermal diffusivity of the ground (soil) $\alpha = k/c_v$ (cm ² /sec)	Penetration Depth of Cycle	
		Diurnal (m)	Annual (m)
Rock	0.020	1.10	20.5
Dry sand	0.001	0.30	4.5
Wet sand	0.010	0.80	14.5
Dry clay	0.002	0.40	6.5
Wet clay	0.015	0.95	18.0

This can also be seen in (Goodrich, 1982) "The influence of snow cover on the ground thermal regime" (NRC research), Figure 42, where the change of ground level temperature and snow coverage have no diurnal influence on the soil temperature under a depth of 1-2 meters.

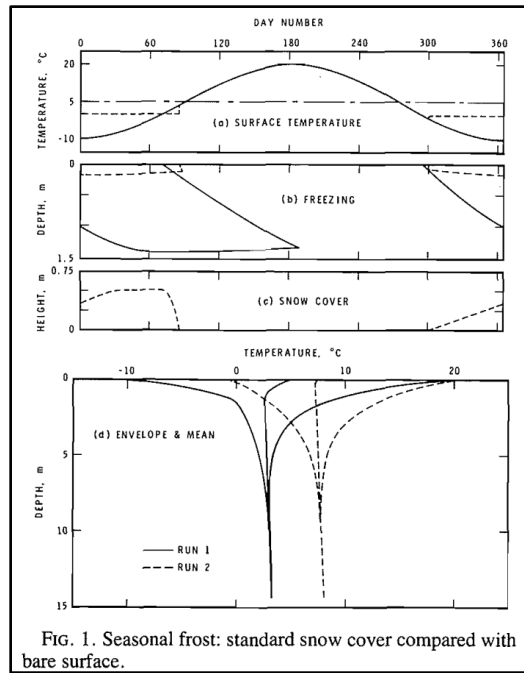


FIG. 1. Seasonal frost: standard snow cover compared with bare surface.

Figure 42: seasonal frost effects on soil temperatures (Goodrich 1982)

6.2.9 Temperature modelling in pipes

(Mirjam Blokker & Pieterse-Quirijns, 2013) indicated that “the soil surrounding the water main determines the temperature changes of the drinking water. ... The energy-transfer rate from the soil to the inner pipe wall is determined by the conductivity of the pipe material ($\lambda_{pipe-wall}$) and the thickness of the pipe wall ($d_{pipe-wall}$). Subsequently, the energy is transferred from the inner wall to the flowing water. In flowing liquids, heat is transferred by convection. However, first the energy needs to be transferred through a stagnant liquid film layer between the wall and the flowing water (Earle, 1983). The convective heat transfer coefficient (α) combines the total set of heat transfer processes in the drinking water, both in the stagnant layer and the flowing liquid, and is a complex function of the flow rate, liquid properties, dimensions of the pipe, and its roughness. The temperature of the flowing water after a certain time can be described as (Çengel, 1998)”:

$$\frac{dT_{water}}{dt} = \frac{2k}{\rho_{water} r C_{p,water}} (T_{soil} - T_{water}) \quad (24)$$

in which T_{water} is the bulk water temperature (K), T_{soil} is the temperature of the outer wall (K) that equals the temperature of the surrounding soil, r is the pipe radius (m), $C_{p,water}$ is the specific heat capacity of water and k is the overall heat transfer coefficient ($W/m^2 K$). This model considers an average bulk temperature of the drinking water. The overall heat transfer

coefficient is determined by conduction through the pipe wall and convective processes in drinking water:

$$k = \frac{1}{\frac{d_{\text{pipe-wall}}}{\lambda_{\text{pipe-wall}}} + \frac{1}{\alpha}} \quad (25)$$

in which the convective heat transfer coefficient is described by the dimensionless Nusselt number (Nu):

$$Nu = \frac{\alpha \cdot l}{\lambda_{\text{water}}} \quad (26)$$

in which l is the characteristic length (m), for a cylinder this is the diameter d , and λ_{water} is the thermal conductivity of water. And:

$$\alpha_{\text{water}} = \frac{\lambda_{\text{water}}}{\rho_{\text{water}} C_{p,\text{water}}} \quad (27)$$

$$\lambda_* = \frac{\lambda_{\text{water}}}{10\lambda_{\text{pipe-wall}}} \quad (28)$$

Then from Eq. (24) we get the following with some assumption on the pipe thickness $d_{\text{pipe-wall}}$:

$$\frac{dT_{\text{water}}}{dt} = \frac{\alpha_{\text{water}}}{r^2 \left(\lambda_* + \frac{1}{Nu} \right)} (T_{\text{soil}} - T_{\text{water}}) \quad (29)$$

Nu is a function of the Reynolds number (Re) and the Prandtl number (Pr). Empirical correlation for Nu number is available from (Çengel, 1998) which was also used by Mirjam Blokker and Pieterse-Quirijns (2013) and shown in Table 13.

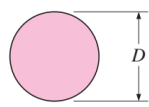
Empirical correlations for the average Nusselt number for forced convection over circular and noncircular cylinders in cross flow (from Zukauskas, Ref. 14, and Jakob, Ref. 6)			
Cross-section of the cylinder	Fluid	Range of Re	Nusselt number
	Gas or liquid	0.4–4	$Nu = 0.989Re^{0.330} Pr^{1/3}$
		4–40	$Nu = 0.911Re^{0.385} Pr^{1/3}$
		40–4000	$Nu = 0.683Re^{0.466} Pr^{1/3}$
		4000–40,000	$Nu = 0.193Re^{0.618} Pr^{1/3}$
		40,000–400,000	$Nu = 0.027Re^{0.805} Pr^{1/3}$

Table 13: Empirical correlations for the average Nusselt number (Çengel, 1998)

The Reynolds number changes with temperature as noted above and the Prandtl changes as well according to Table 14:

Table 14: change of Prandtl number with temperature⁵

State	Temperature		Prandtl number	Temperature		Prandtl number
	[K]	[°C]	[-]	[K]	[°F]	[-]
Liquid	273	0	13.6	273	32	13.6
	278	5	11.2	278	40	11.5
	283	10	9.46	283	50	9.46
	293	20	6.99	297	75	6.31
	298	25	6.13	311	100	4.56
	303	30	5.43	325	125	3.45
	323	50	3.56	339	150	2.74
	348	75	2.39	353	175	2.25
	373	100	1.76	366	200	1.88

Some typical values of heat transfer–related parameters for air, water, soil and pipe materials are given in Table 15.

6.2.10 Temperature modelling in tanks

Isaac Newton⁶ studied cooling of bodies. Experiments showed that the cooling rate approximately proportional to the difference of temperatures between the heated body and the environment. This relationship may be written as a differential equation:

$$\frac{dQ}{dt} = hA(T_s - T) \quad (30)$$

where Q is the heat, t is the time, A is the surface area of the body through which the heat is transferred, T is the temperature of the body, T_s is the temperature of the surrounding environment, h is the heat transfer coefficient depending on the geometry of the body, state of the surface, heat transfer mode, and other factors. As $Q = CT$ where C is the heat capacity of the body, we can write:

$$\frac{dT_{water}}{dt} = \frac{hA}{C_h}(T_s - T_{water}) = k_c(T_s - T_{water}) \quad (31)$$

where k is the cooling rate of the body which is a function of body material, water in our case, and the surface area of the heat transfer. C , the heat capacity of water changes with temperature, Figure 43. However, for temperatures up to 30°C, the heat capacity of water is almost constant.

⁵ https://www.engineeringtoolbox.com/water-steam-Prandtl-number-d_2059.html

⁶ <https://www.math24.net/newtons-law-cooling/>

Table 15: typical values of heat transfer-related parameters (Mirjam Blokker & Pieterse-Quirijns, Modeling temperature in the drinking water distribution system, 2013)

TABLE 1 Some typical values of heat transfer-related parameters for air, water, soil (van der Molen et al, 2008; Arya, 2001), and DWDS pipe materials (Rafferty, 1998; Janssen & Warmoeskerken, 1991).					
Material	Condition	Density	Heat Capacity	Thermal Conductivity	Thermal Diffusion Coefficient
		ρ — $\text{kg/m}^3 \times 10^3$	C_p — $\text{J/kg K} \times 10^3$	λ — W/m K	$\alpha = \lambda / \rho C_p$ — $\text{m}^2/\text{s} \times 10^{-6}$
Air	20°C, still	0.0012	1.01	0.025	20.50
Water	20°C, still	1.00	4.19	0.57	0.14
Sand	New		0.80	0.30	0.24
	Dry	1.60	0.8–1.0	0.3–1.6	1.2
	Wet		1.2–1.8	1.7–5.0	1.0
	Very dry ($x < 0.04$ — kg/kg^{-1})				0.26
	Dry ($x = 0.04$ — kg/kg^{-1})				0.98
Clay	Wet ($x > 0.04$ — kg/kg^{-1})				0.58
	Dry	1.60	0.89	0.25	0.18
	Dry		0.6–1.3	0.4–1.0	0.3
Peat	Wet		1.0–2.1	0.9–2.3	0.4
	Dry	0.30	1.92	0.06	0.10
Rock	Wet	1.12	2.68	0.40	0.13
	Hard	2.70	0.75	2.90	1.43
CI		7.30	0.50	60	16.44
AC	Water	2.00	1.00	0.43	0.22
PVC	main	1.38	1.00	0.16	0.12
Copper		8.96	0.39	403	0.11
α —convective heat transfer coefficient, AC—asbestos cement, CI—cast iron, DWDS—drinking water distribution system, λ —thermal conductivity, ρ —density of air, PVC—polyvinyl chloride					

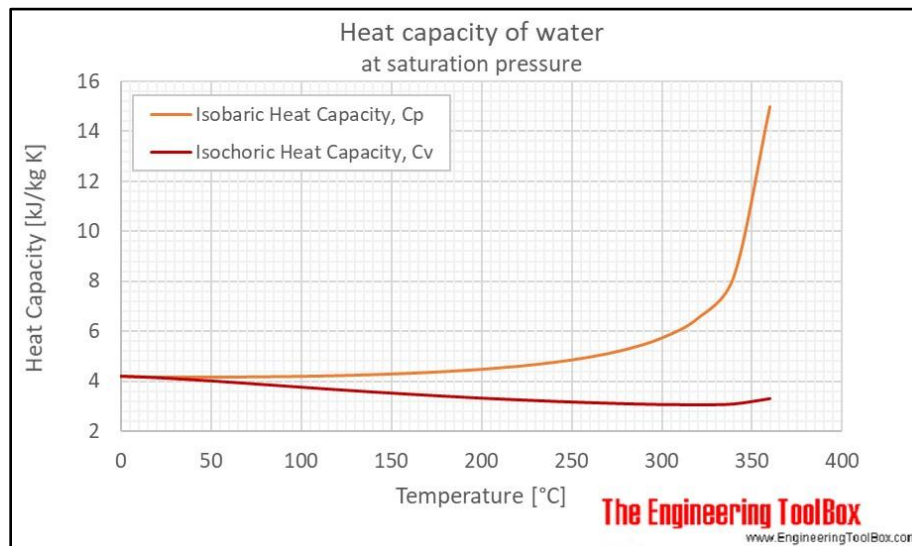


Figure 43: heat capacity of water change with temperature⁷

Typical values of convection heat transfer coefficient, h , for free convection of liquids: 10–1000 W/(m²·°C) (Multiply by 0.176 to convert to Btu/h · ft² · °F), (Çengel, 1998). Heat capacity value of water, C , is 0.00116 kWh/(Kg·°C).

EPANET-MSX allows to set specific parameters for different tanks via the [PARAMETERS] section so a different temperature change rate may be assigned to the tanks. However, EPANET-MSX will allow the use of dynamic parameters in the tanks section thus a constant change rate must be assigned for each tank.

6.2.11 Summary of temperature modelling in WDN

Modelling temperature in the water distribution network is possible with the EPANET-MSX extension. For pipes, the change in water temperature is given in Eq. (3) and repeated here:

$$\frac{dT_{water}}{dt} = \frac{\alpha_{water}}{r^2 \left(\lambda_w + \frac{1}{Nu} \right)} (T_{soil} - T_{water}) \quad (32)$$

⁷ https://www.engineeringtoolbox.com/specific-heat-capacity-water-d_660.html

where α_{water} , λ_* , Nu are parameters of the water and pipe which some change with temperature and T_{soil} is the soil temperature which assumed to be short term constant in the pipe's depth. For tanks the change of water temperature is modelled according to the surrounding environment temperature, T_s , and the cooling rate of water, k_c .

$$\frac{dT_{water}}{dt} = k_c (T_s - T_{water}) \quad (33)$$

6.3 Conceptual model development for modeling temperature and chlorine decay

The conceptual model is divided into two sections. First, the temperature in the network is calculated, and in the second stage, the chlorine decay and its concentration in the network are evaluated.

6.3.1 Temperature modelling

The temperature in the network is modelled according to Eq. (34) (which is copied here from Eq. (29) for clarity):

$$\frac{dT_{water}}{dt} = \frac{\alpha_{water}}{r^2 \left(\lambda_* + \frac{1}{Nu} \right)} (T_{soil} - T_{water}) \quad (34)$$

where the Thermal diffusivity coefficient, $\alpha_{water} = 1.4 \cdot 10^{-6} (m^2 / s)$, r is the pipe radius, T_{soil} is the constant soil temperature and λ_* is given by Eq. (35):

$$\lambda_* = \frac{\lambda_{water}}{10\lambda_{pipe-wall}} \quad (35)$$

where, according to Table 15, the thermal conduction coefficient of water, $\lambda_{water} = 0.57 (W / mC)$ and the thermal conduction coefficient of pipe wall, $\lambda_{pipe-wall}$ depends on the pipe material (60 for Cast Iron without lining, 0.43 for Asbestos Cement and 0.16 for PVC as shown in Table 15).

The Nusselt number in Eq. (34) is calculated according to the Reynolds number ranges as given in Table 13. The Nusselt number is a function of both the Reynolds number and the Prandtl number which both change with temperature. According to Eq. (21), the Reynolds number is a function of the flow velocity, which is calculated by EPANET, the pipes diameter and the

Kinematic Viscosity of the water. The Kinematic Viscosity changes with temperature as shown in Figure 44 and Eq. (36)

$$\nu = 0.000550T^2 - 0.049432T + 1.766968 \quad (36)$$

where T is the temperature in Celsius.

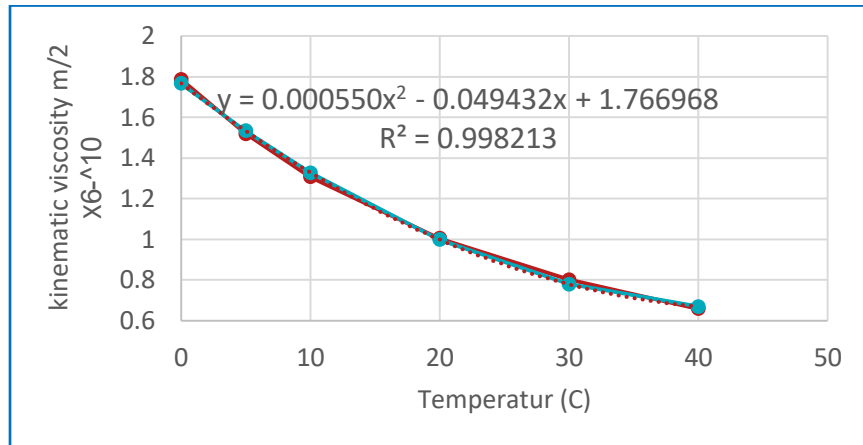


Figure 44: Kinematic Viscosity change with temperature

The Prandtl number changes with temperature as shown in Figure 45 and Eq.

$$Pr = -0.000090T^3 + 0.010654T^2 - 0.508159T + 13.559672 \quad (37)$$

where T is the temperature in Celsius.

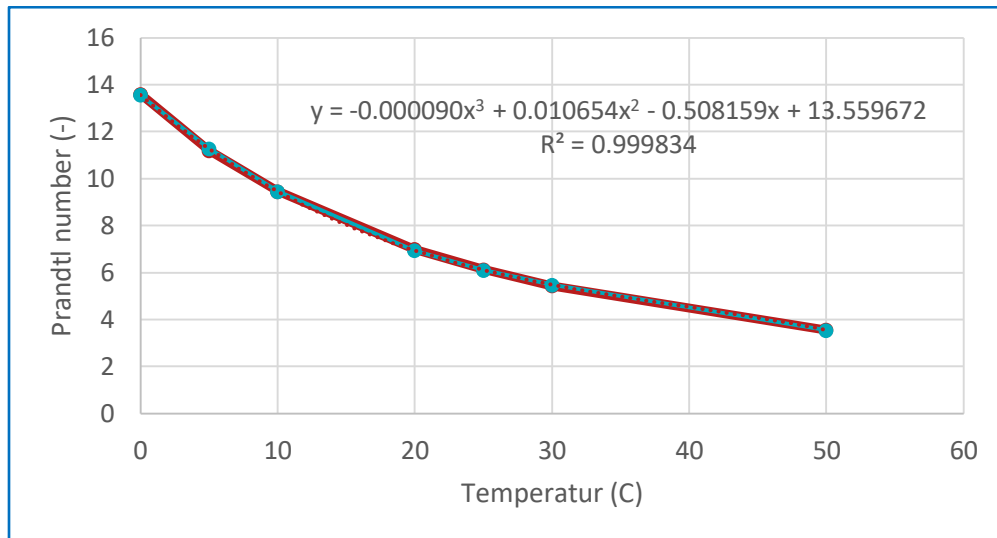


Figure 45: Prandtl number change by temperature

Temperature change in tanks will be modelled according to Eq. (31):

$$\frac{dT}{dt} = k_{\text{tank}} (T_{\text{out}} - T) \quad (38)$$

where k_{tank} is the cooling rate of a tank and T_{out} is outer temperature.

6.3.2 Chlorine decay modelling

Bulk Chlorine decay in the water system will be modelled using the (Koechling, 1998) equation, (Eq. (39) is a copy of Eq. (9)) where only the "regular" decay coefficient at 20°C, K_{b20} , needs to be estimated.

$$K_{bT} = K_{b20} 1.1^{(T-20)} \quad (39)$$

Effects of temperature on the wall decay of Chlorine is more complex and, as described in section 3.2, the literature is totally clear on how it should be modelled. However, efforts will be made to model it according to Eq. (18) which will include the calculations of Reynolds and Schmidt numbers as well as the diffusion coefficient of chlorine in water as presented in Eq. (22).

6.3.3 Proof of Concept

Two tests as proof of concept (PoC) were conducted. The first is for the simulation of water temperature in a long pipe and a second combines the simulation of both temperature and Chlorine in a small and simple network (Net1 of the EPANET example networks).

6.3.4 Temperature model in a long pipe

A simple proof of concept for temperature modelling was done with a simple 70Km long pipe (cut into six sections, Figure 46). The source is a reservoir with a constant water temperature of 10°C and so is the initial water temperature in the pipe. The soil temperature is held constant at 25°C. The network is modelled for 48 hours.

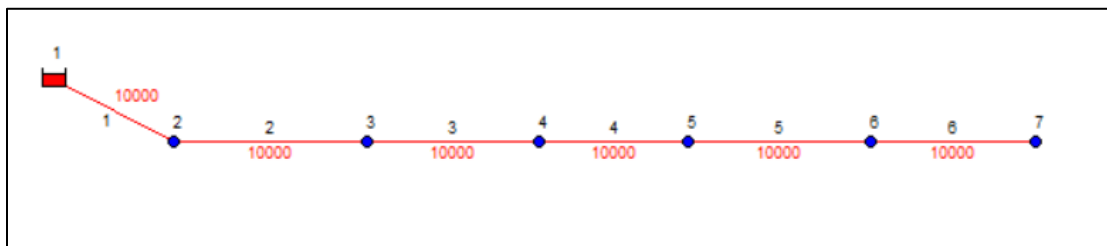


Figure 46: simple network for temperature modelling

The following data was used:

Table 16: data for temperature modelling proof of concept

Parameter	Value	Remark
Soil temperature	25°C	
Prandtl number		Table 14
Water thermal diffusivity coefficient	1.4e-7	Table 15
Water temperature conduction coefficient	0.57	Table 15
Pipe wall temperature conduction coefficient	0.16	For PVC Table 15
Nusselt number		Table 13
Reynolds number		Eq. (21)

Figure 47 shows the temperature change at the nodes of the network over the 48 hours period. For the source, the temperature remains constant over time at 10°C. The rest of the nodes start at their initial temperature of 10°C and increases over time. Each node's temperature reaches a different maximum and constant value at the time the water from the source reaches it. The furthest node, #7, reaches a final temperature of 24.6°C which is close to the soil's constant temperature of 25°C.

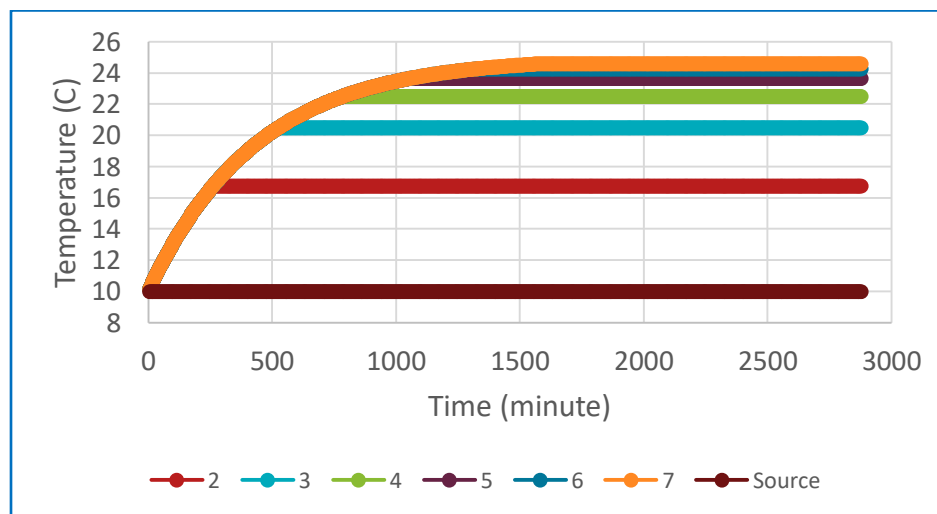


Figure 47: temperature change at nodes over time for the single pipe example

6.3.5 Temperature and Chlorine model in a small network

A small network, NET1 EPANET first example network, was used to demonstrate temperature and Chlorine simulations. The network consists of one source, one pump, one tank and eight demand junctions, Figure 48.

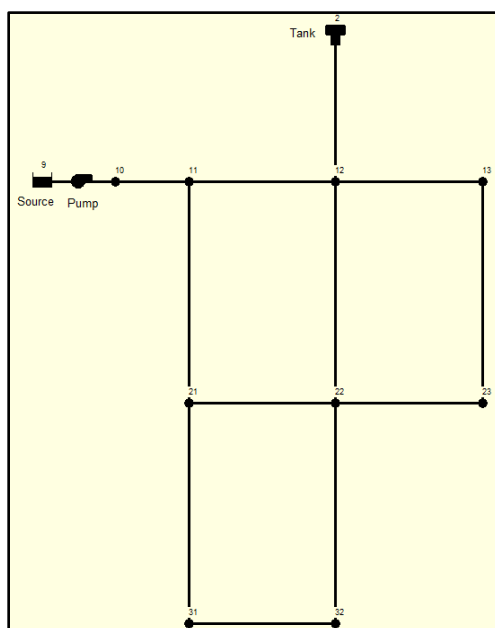


Figure 48: EPANET NET1 example network

Some basic and demo coefficients are used:

[COEFFICIENTS]

CONSTANT	Tsoil	25	;Temperature at wall / ground = 25 C
CONSTANT	Tout	5	;Tank outside temperature
CONSTANT	alpha	1.4e-7	;Thermal diffusivity coefficient, water 20C (m2/s)
CONSTANT	lambda_water	0.57	;Thermal conduction coefficient of water (W/m.C)
CONSTANT	lambda_pipe	0.16	;Thermal conduction coefficient of pipe wall (W/m.C)
PARAMETER	Ktank	0	;Global temperature change rate in tanks
CONSTANT	Kb20	-5.555E-6	;Global bulk Chlorine decay coefficient at 20C = -0.5/day
CONSTANT	Kw	-5.878E-6	;Global wall Chlorine decay coefficient = -1m/d

[PARAMETERS]

TANK	2	Ktank	0.00001	;Per tank temperature change rate
------	---	-------	---------	-----------------------------------

And the terms outlined in the previous sections are used:

[TERMS]

Pran	-0.00009*Twater*Twater*Twater+0.010654*Twater*Twater-0.508159*Twater+13.559672	;Prandtl number
Viss	(0.00055*Twater*Twater-0.049432*Twater+1.766968)*0.00001	;Kinematic viscosity of water
Reyn	U*D/Viss	;Reynolds number
Nu	(0.027*Pran^0.333)*(Reyn^0.805)	;Nusselt number for Re > 40,000
lambda_ratio	lambda_water / (10*lambda_pipe)	;Lambda ratio
Nu_spec	1/(lambda_ratio+1/Nu)	
k	4*alpha*Nu_spec/(D^2)	;constant in Twater rate equation
Kb	Kb20*(1.1^Twater)/6.72749994933 ; 1.1^20=6.72749994933	;Bulk decay rate
KKw	(4/D)*Kw	;Wall decay rate
Sc	Viss/D	;Schmidt number
Sh	0.0149*Reyn^0.88*Sc^(1/3)	;Sherwood number
Dif	(0.0365*Twater + 0.5176)*10^-9	;Molecular diffusivity of chlorine in water
Kf	-(Sh*Dif/D);*(4/D)	;Wall mass transfer coefficient

Once the above coefficients and terms are set, the temperature and Chlorine rates may be computed and used by EPANET-MSX:

```
[PIPES]
RATE  Twater  k*(Tsoil - Twater)  ;Temperature of water
RATE  CL2     (Kb+KKw)*CL2      ;Chlorine

[TANKS]
RATE  Twater  Ktank*(Tout - Twater)
RATE  CL2     Kb*CL2
```

With these settings we obtain the results for temperature and Chlorine decay. Figure 49 shows the temperature at selected nodes in the network (all start with the initial condition of 10°C). Node 11 is the demand junction which is closest to the source which has a constant 10°C . The higher temperature values are for the cases where the pump is not operating and water is supplied from the network (and some from the tank). Node 2 is the tank with outer temperature of 5°C so the temperature is approaching this value. Node 32 is the farthest junction in the network and mainly effected by the ground temperature of 25°C .

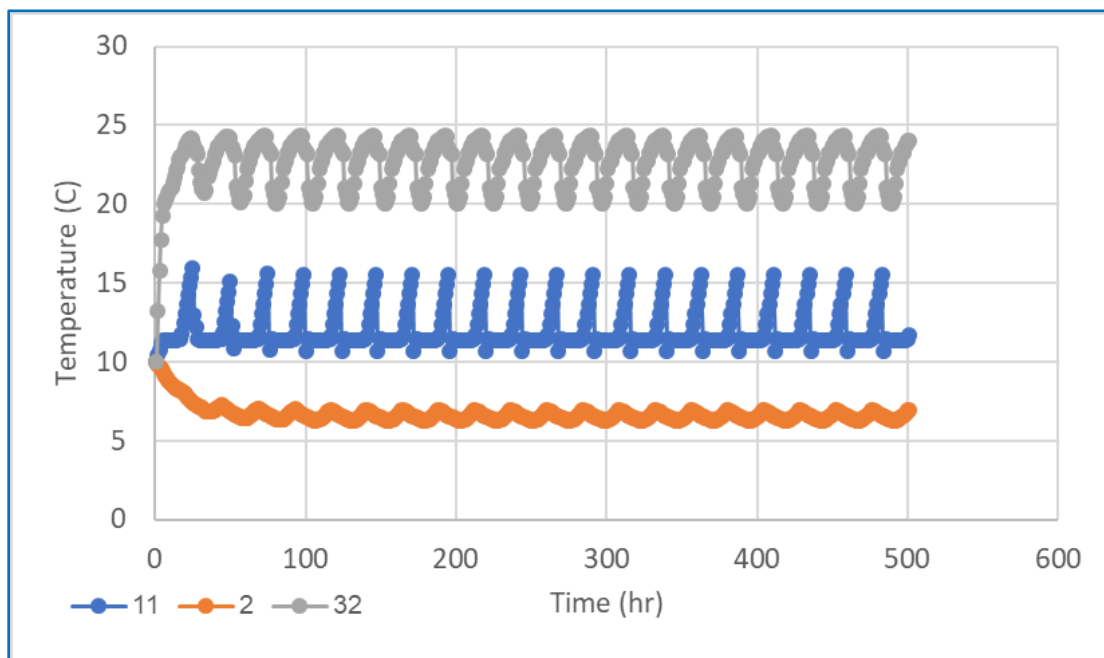


Figure 49: temperature simulation for Net1

Figure 50 shows the Chlorine values at the same nodes (all start with the initial condition of 0.4mg/l apart for the source with a value of 1mg/l). Again, junction 11 is mainly effected by the source, the tank has some middle value and the farthest junction has a very low Chlorine concentration.

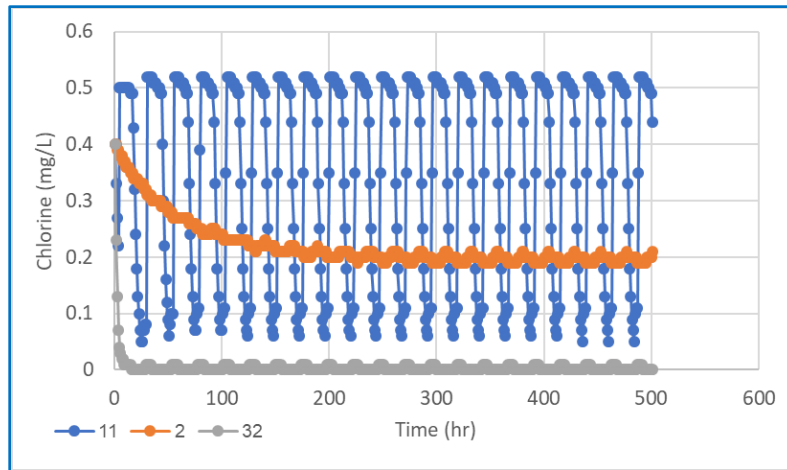


Figure 50: Chlorine simulation for Net1

Running a similar Chlorine simulation in the "traditional" way, using EPANET without temperature considerations, shown in Figure 51, results in similar behavior but with some shifts for the maximum and minimum values. For example, considering the temperature, node 2 stabilize at around 0.2mg/L while in the "traditional" simulation the value is around 0.07mg/L. It may be argued that these extreme values are the important ones since they might result in some Chloritization actions.

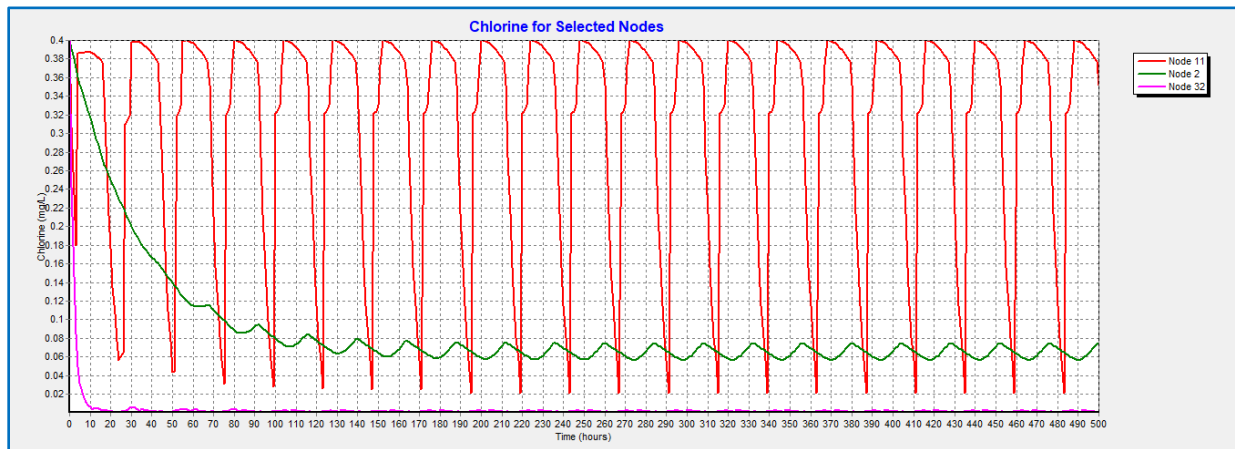


Figure 51: Chlorine simulation using EPANET

Checking the results for different pipe materials is done by adjusting the thermal conduction coefficient of the pipe wall (λ_{pipe} in the sample MSX data above). Ranging from a value of 0.16W/mC for a PVC pipe, up to a value of 10W/mC for a Cast Iron pipe with a cement lining shows a change of about 10% in the Chlorine concentration (Figure 52). Compared to the "traditional" Chlorine simulation, inclusion of temperature changes yields values by up to 40% larger.

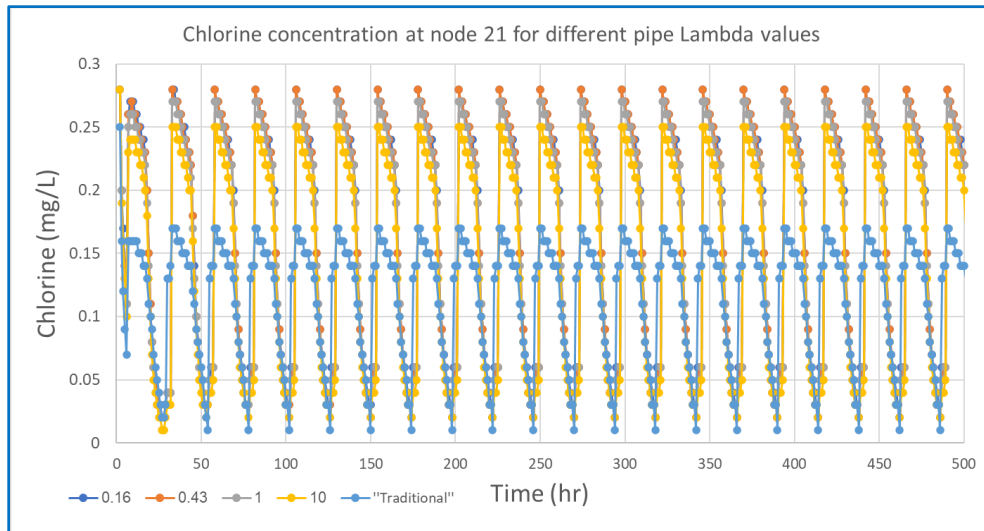


Figure 52: Chlorine concentration at node 21 for different pipe Lambda values

Figure 53 shows the temperature profile at node 11 (the node close to the network source), for two cases: a fixed temperature source and a variable temperature source. The variable temperature source is modeled in EPANET-MSX using the [SOURCES] and [PATTERNS] sections.

[SOURCES]

CONCEN 9 Twater 1 pat9 ;source

[PATTERNS]

pat9	10.0	11.2	12.4	13.6	14.4	15.2
pat9	15.0	14.8	13.6	12.4	11.6	10.8

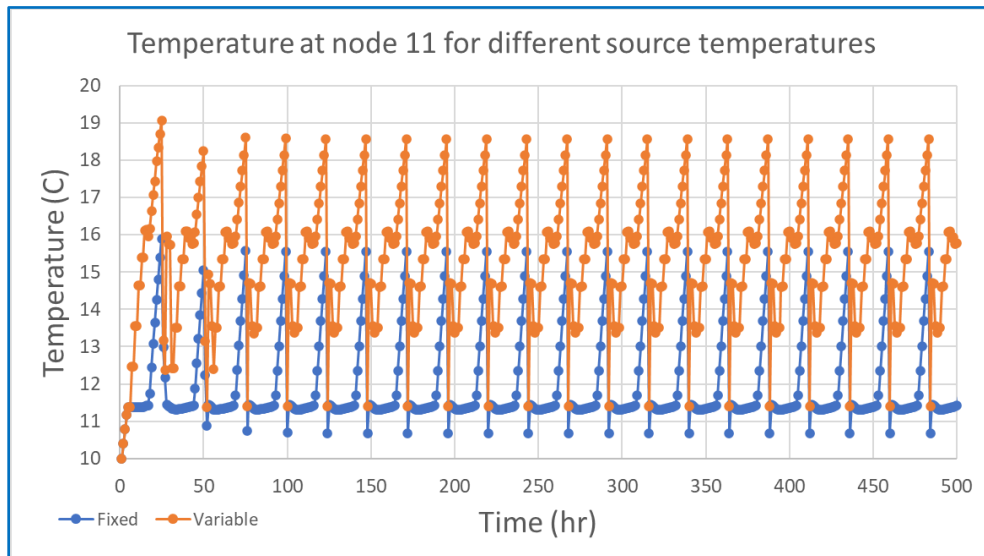


Figure 53: Temperature at node 11 for different source temperatures

6.3.6 Network 1 water distribution network

The developed model was applied to the Network 1 water distribution system, illustrated in Figure 18, Figure 21 and Figure 31. The utility maintains a hydraulic model of the water network based on the InfoWater software. The hydraulic model was built and calibrated about five years ago. However, no information was received regarding the calibration process or the related calibration of the Supervisory Control and Data Acquisition (SCADA) data. The full model consists of about 32,000 junctions, 38,000 pipes, 20 tanks, and 162 pumps. The InfoWater model was exported to an EPANET INP input file format and all further work was done with EPANET. In addition, SCADA data was provided, which included about 450 tags for the time frame of mid-June 2019 to mid-November 2019. Also, time series data for 12 temperature data loggers within the network were available for the locations shown in Figure 31. The temperature profiles are shown in Figure 54. It can be seen that almost all the stations follow a similar pattern, each with a variation of about 5 degrees Celsius.

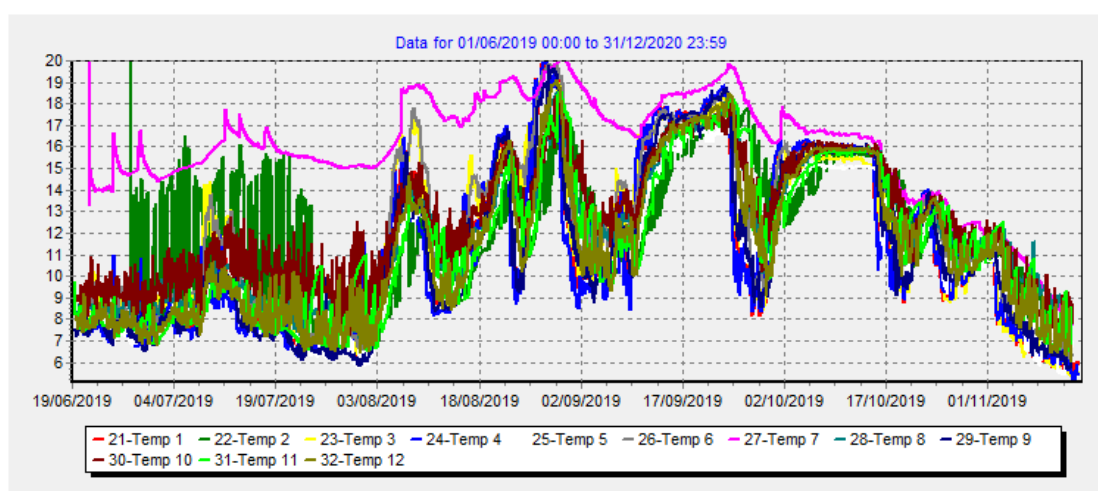


Figure 54: Temperature profiles at logger's locations

We initially intended to update the provided hydraulic model with the recent SCADA data to create an updated model. However, it was clear that such a task is infeasible due to inconsistencies in the data, specifically the lack of demand data and its spatial distribution across the network. That is, the provided model included customer demand data for a given time but no updated demand information was available for the time period overlapping the SCADA data. Furthermore, the SCADA data did not include the required information for mass balance calculations even at the zone level. Consequently, there was no way to calculate the demands in the different zones using the inlet and outlet flows, and storage datastreams. Therefore, an alternative option was considered to focus on modeling pressure zone 4 in the system.

6.3.6.1 The Zone 4 hydraulic model specifications

Zone 4 of Network 1 is located at the southern end of the network. All the pipes in Zone 4 are shown in light green Figure 31. Its connectivity schema is shown in Figure 55. The zone is fed from five pumping stations (PS 1 to PS5) and feeds zones 5 and 6 via pumping stations PS 6,

PS 7 and PS 8. There are three storage facilities within the zone (Res 1, Res 2, and Res 3) and the overall head of the zone is about 230 meters.

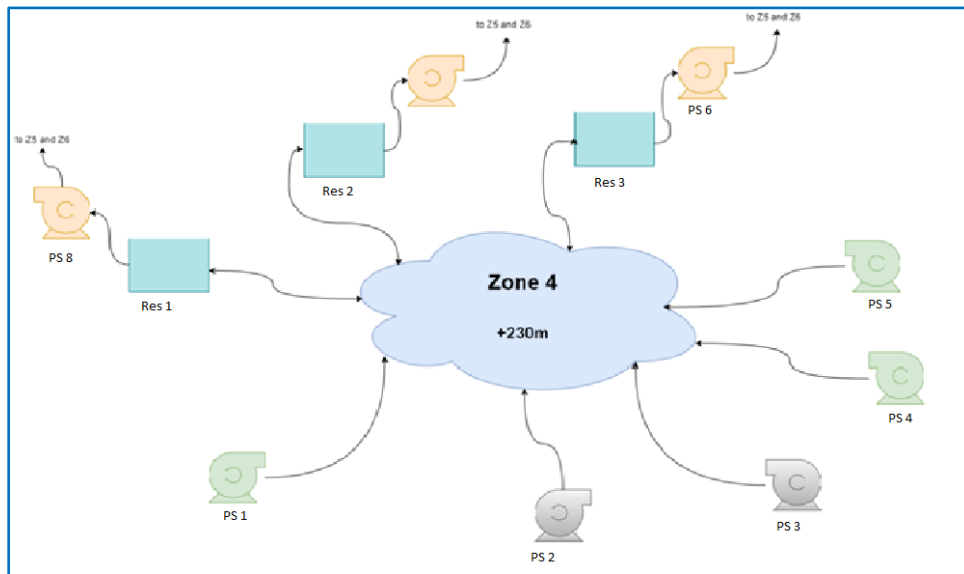


Figure 55: Zone 4 connectivity schema

For the purpose of model testing and validation, the Zone 4 network was treated as a standalone system (isolated from the rest of the water distribution network), comprising about 10,000 junctions, 11,500 pipes, 26 pumps (in 3 pumping stations) and 3 reservoirs. Due to unavailability of some pertinent data (e.g., not all the flow out of PS 4 pumping station could be identified, nor the flow into Res 1), it was impossible to update demands and demand profiles by mass balance was impossible. Consequently, available demand pattern was used in conjunction with constant multipliers to facilitate demand calibration. Whenever possible actual SCADA flow values were used (e.g., at pumping stations as illustrated in Figure 56 through Figure 62).

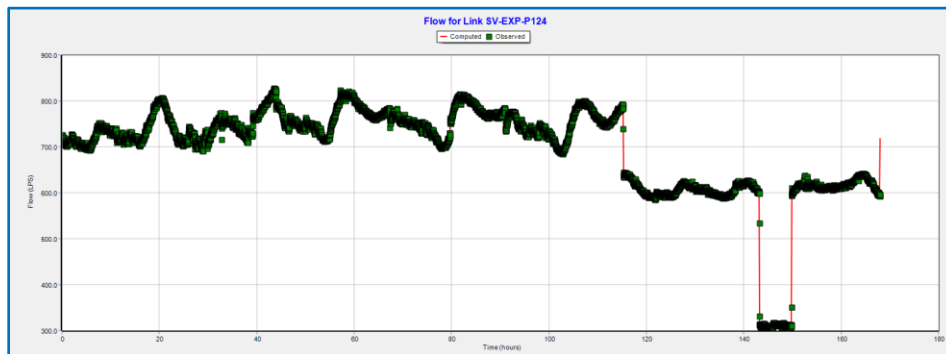


Figure 56: PS 2 pumping station outflow

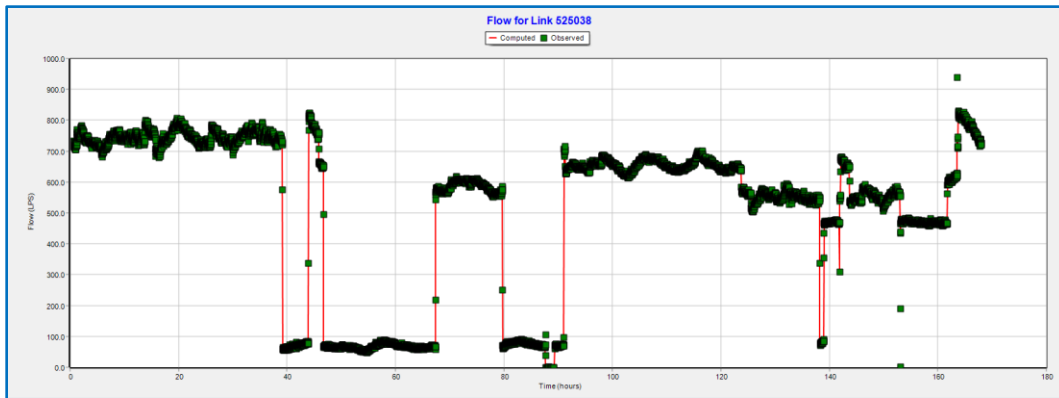


Figure 57: PS 2 pumping station outflow

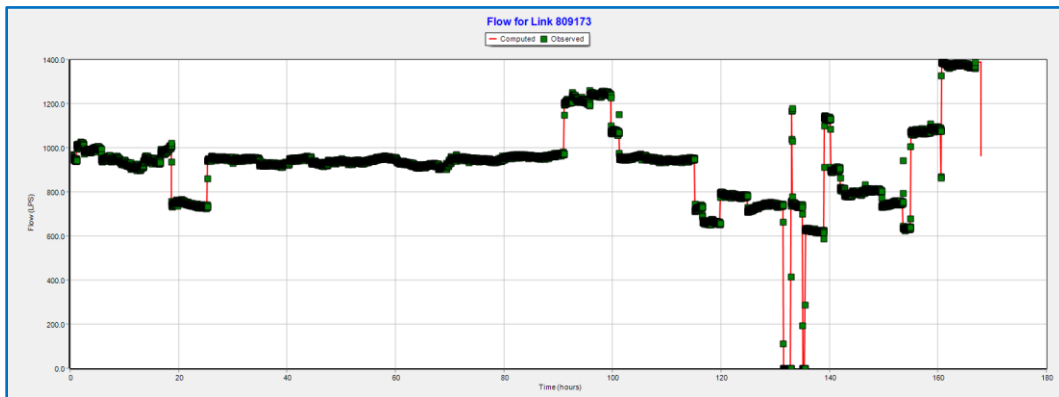


Figure 58: PS 5 pumping station outflow

At PS 1 pumping station the flow measurements are split into two directions and reverse flow may be possible, which is not indicated in the SCADA data (Figure 59 and Figure 60).

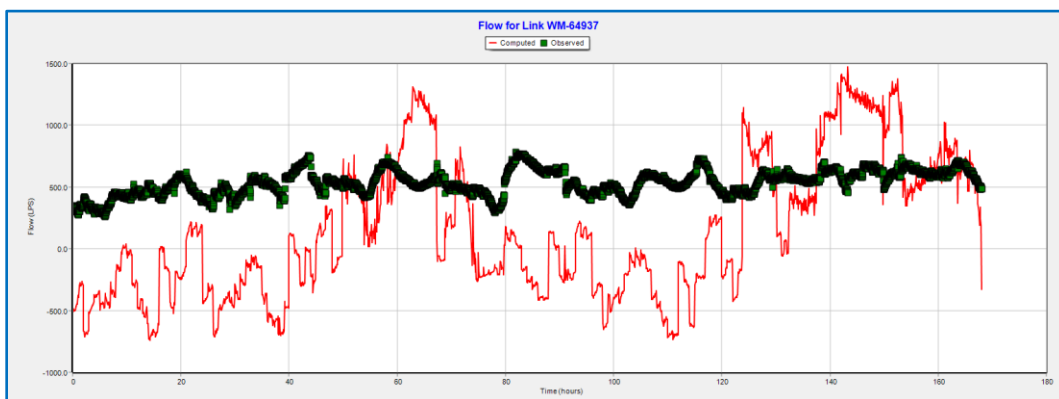


Figure 59: PS 1 pumping station outflow 1

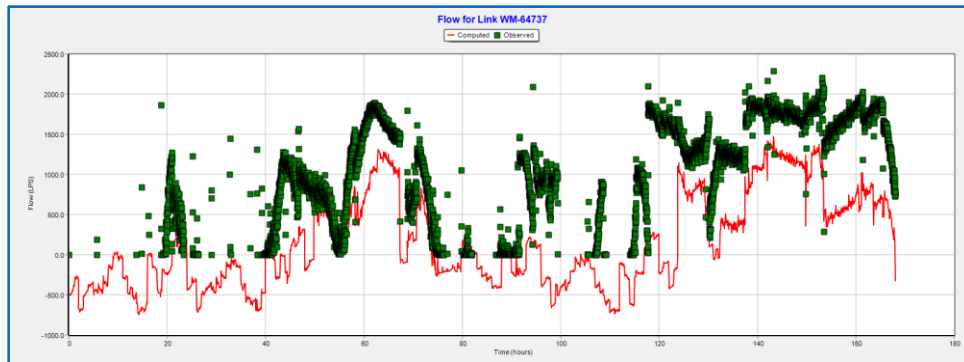


Figure 60: PS 1 pumping station outflow 2

At PS 4 pumping station, the flow meter does not measure the entire outflow of the station (Figure 61).

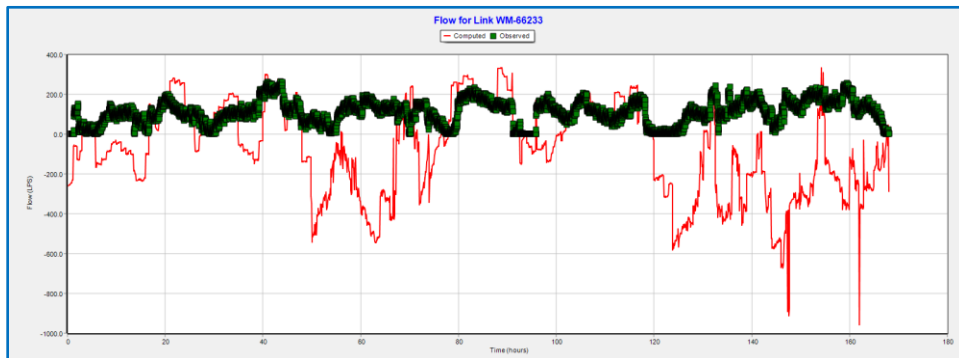


Figure 61: PS 4 pumping station outflow 1

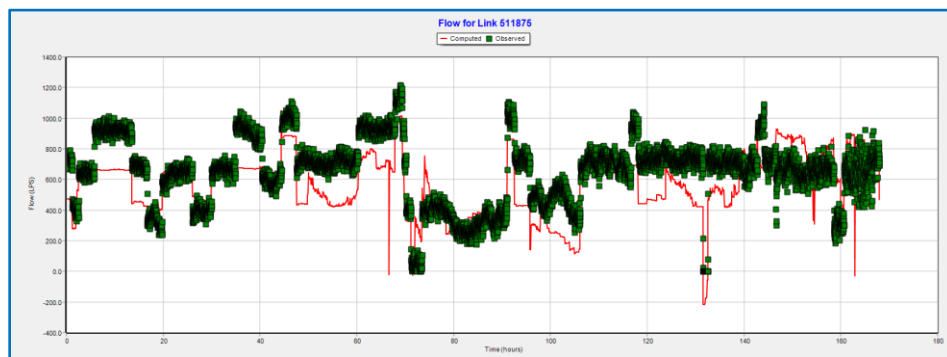


Figure 62: PS 4 pumping station outflow 2

The simulation is not perfectly calibrated as can be seen in water flows and levels for the reservoirs (Figure 63-Figure 67), this is to be expected, however, the simulation does run for a

full week with acceptable results for the purpose of temperature simulation as the explicit values are less important than the change in them for different scenarios.

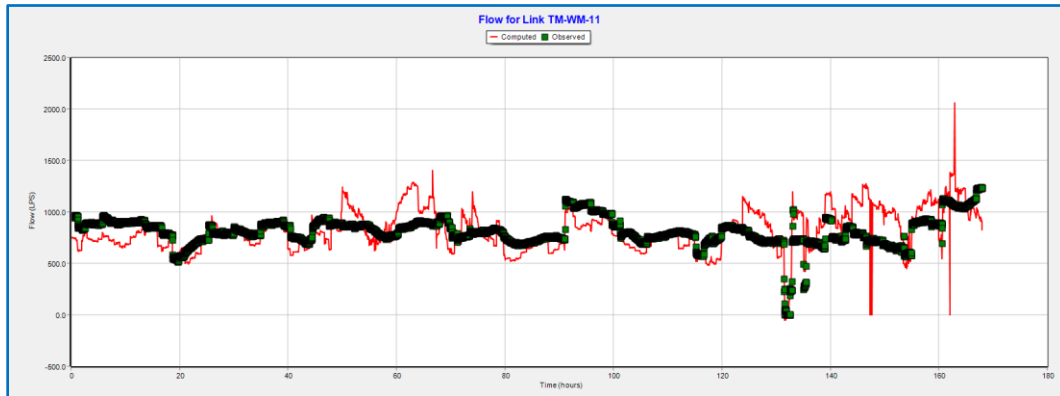


Figure 63: Res 3 inflow

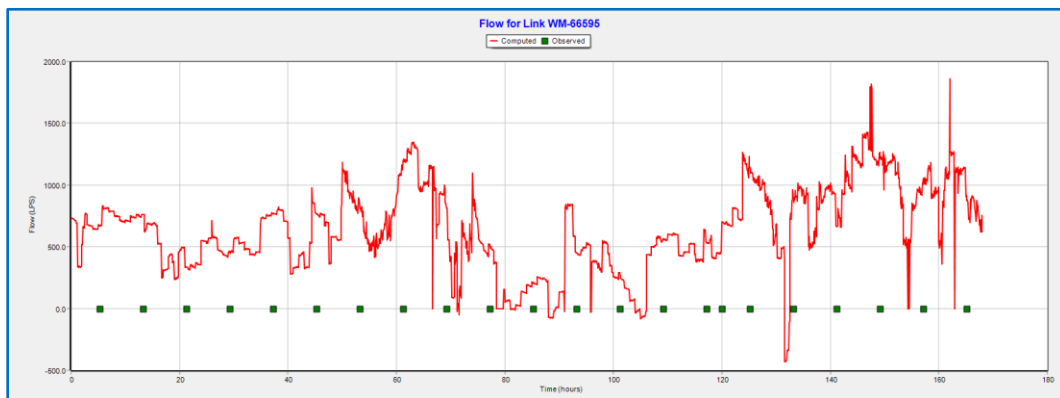


Figure 64: Res 2 Reservoir inflow

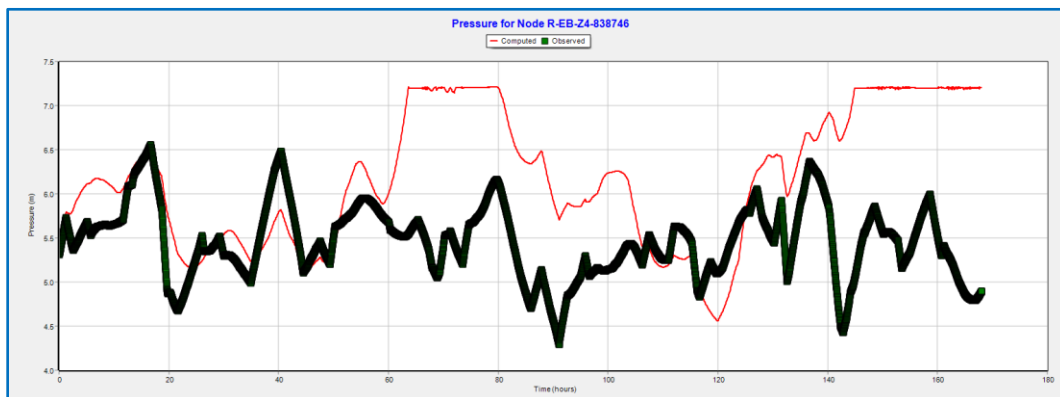


Figure 65: Res 2 Reservoir level

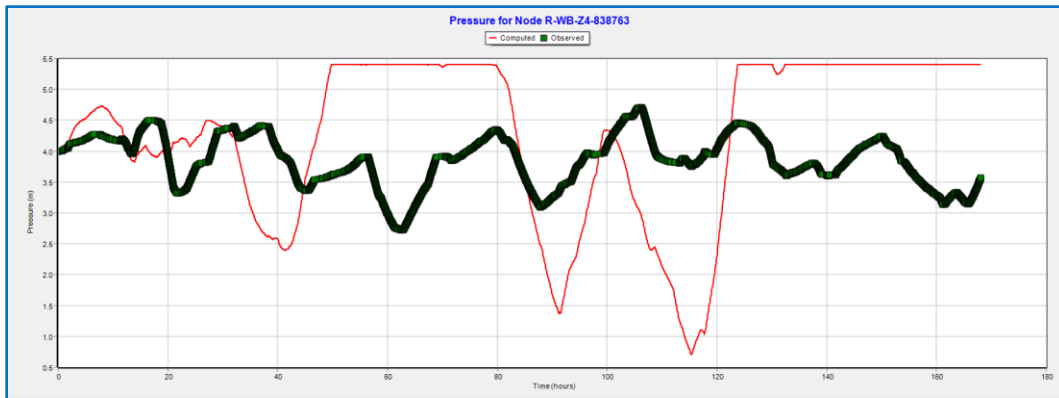


Figure 66: Res1 Reservoir level

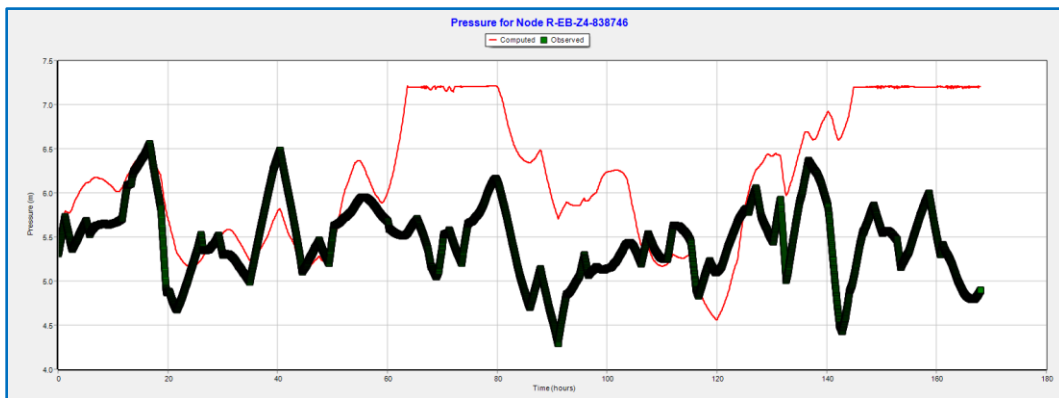


Figure 67: Res 3 level

6.3.6.2 Temperature and Chlorine MSX model⁸

The temperature and Chlorine MSX model used herein is based on the model presented earlier in Section 6.3.5. As a first trial, for the input temperatures at the sources to Zone 4, the closest temperature data loggers were used. Once the model was running, a series of simulations were carried out, in which the source water and ground temperatures were changed in a wide range of 5 to 25 degrees Celsius. This range was selected based on ground level temperatures measured by NRC staff (Figure 68) in the same location. This approach was deemed suitable since the hydraulic and water quality models are not very well calibrated and the main interest is not the absolute temperature and water quality results, but rather the relative values that depend on the

⁸ Limitation of using EpaNET MSX model is described in Appendix A1.

source temperature. In other words, how might chlorine level in the distribution pipes change with the change in the ambient temperature.

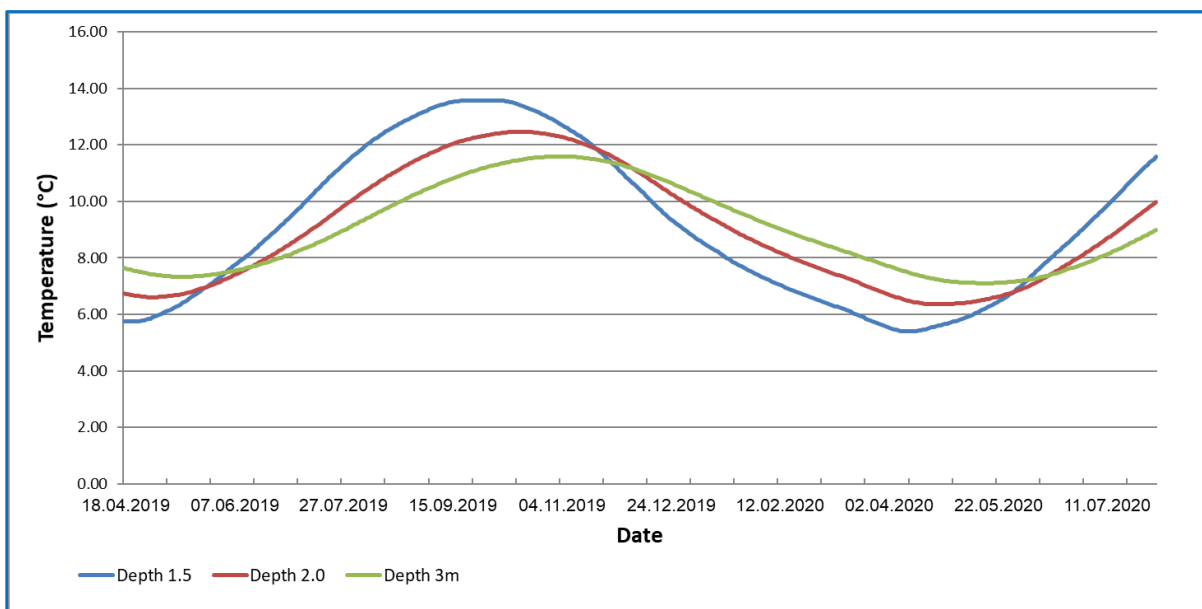


Figure 68: Daily Ground Temperature, NRC(°C)

6.3.6.3 Results

Simulations with different source and ground temperatures were made for 5, 10, 12, 15, 18, 20 and 25 degrees Celsius, for a time period of one week (168 hours). Although each run took relatively long time (1-2 hours), this period was selected to minimise the impact of initial conditions on the results. Then, for each demand junction (i.e., junctions with demands greater than zero), the Chlorine level was recorded, and the average Chlorine levels was calculated in each time step of the simulation. The results are shown in Figure 69.

As a general observation, and as expected, it is clear that for lower source water and ground temperatures the Chlorine levels are higher than for those of the higher temperatures. In Figure 69, the Chlorine levels that correspond to the minimum (5°C) and maximum (25°C) temperatures are marked with thick green and yellow lines respectively. As a rough estimate, residual chlorine levels at 5°C tend to be about 4-5% higher than those at 25°C (possibly more like 4% at steady state, as it appear towards the end of the simulation) .

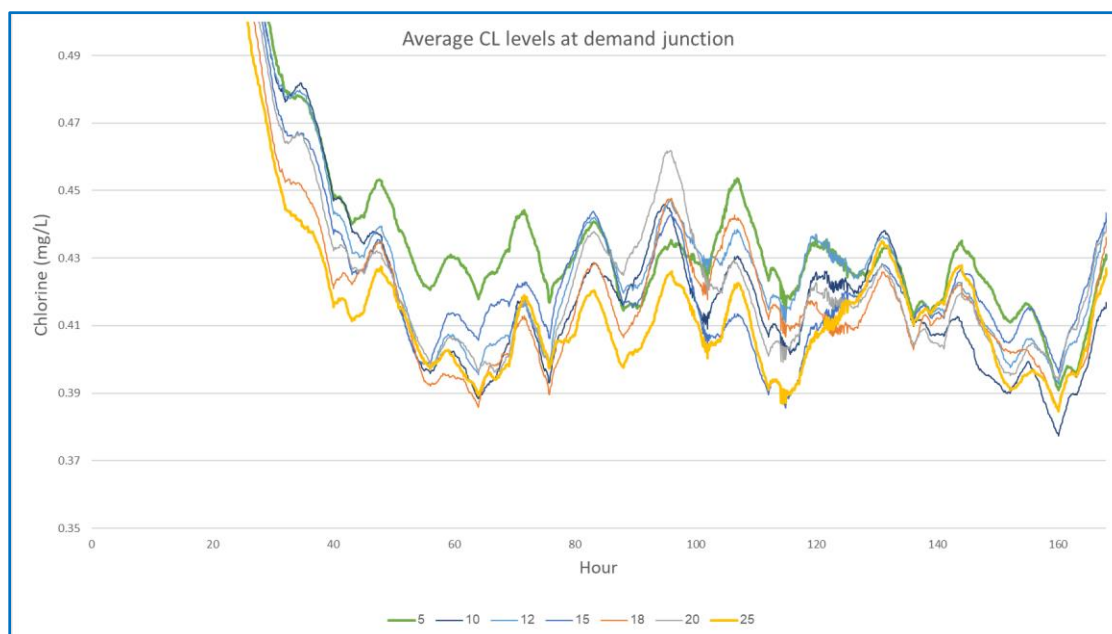


Figure 69: Average Chlorine levels at demand junction

6.4 Conclusions

Notwithstanding deficiencies in model calibration due to limited data availability, the model provides a general idea of what might be expected regarding water quality in distribution systems under warming climate. It can generally be assumed that as mean ambient temperature increase, so will source water temperatures, especially surface water sources. Moreover, soil temperature at relevant depths (1.5 to 2.5 m) is also expected to rise proportionally towards a new air/soil temperature equilibrium. Consequently, the mean temperatures of water in the buried water mains are expected to rise as well. In the long term, an increase of 1°C in the mean air temperature is likely to result in an increase of 1°C in mean water temperature as well as soil temperature in the relevant depths. Of course, the high heat capacity of both water and soil will introduce substantial time gaps as well as significantly small temperature fluctuations but the tendencies of the respective long-term means will like be similar.

There are two aspects to the issue of elevated depletion of residual chlorine due to rising temperatures:

1. As mean temperatures rise chlorine doses will have to rise too in order to keep minimum thresholds. Taking Figure 69 as an approximate estimate, an increase of 1°C in water temperature will result in a decrease of about 0.2% in residual chlorine. This in turn will require a corresponding increase in chlorine doses.
2. As climate change is expected to introduce more extreme temperatures, the operational aspects of chlorination may experience some impact due to short –duration temperature

peaks that may cause chlorine residual depletion that significantly compromise the safety of the drinking water. The quantification of such phenomena requires significant computational resources to perform extended period simulations and are beyond the scope of this research.

With regard to the simulation effort described above, quantifying the impact of climate change on Chlorine residual depends on reliable hydraulic model, water temperature and quality models. This means, any uncertainties associated with these models will be manifested in the results. Therefore, if numerical modeling were the preferred approach to quantify these impacts in your system, we would recommend evaluating the range of temperature as described in Section 6.3.6.3.

A simpler approach to quantify the impact of temperature rise on chlorine residuals could be based on the correlations between daily temperature and disinfectant concentration levels at water treatment plants, similar to what is shown in Figure 28. This approach benefits from the data that is often collected in SCADA systems and requires minimal knowledge and no numerical modeling.

7 Summary and Conclusions

The potential impact of climate change on water distribution systems is multifaceted and complex, where issues like anticipated changes in water demand have implications for the hydraulic capacity of the network, its energy footprint, the structural integrity of its pipes through their vulnerability to breaks, and water quality. This study considered multiple aspects of these potential impacts, while providing quantitative analysis to assist in identifying trends and vulnerabilities. While most studies focus on the numerous real risks, there may be some unexpected benefits, such as a reduction in the number of pipe breaks as air and water temperatures warm. Both negative impacts and potentially unforeseen advantages need to be better characterized to improve infrastructure planning and operation.

Accordingly, this report aims to inform practitioners on such potential impacts and provide them with simple, yet well-established and inexpensive approaches to quantitatively estimate these impacts. These approaches would empower practitioners to perform the analyses in-house. The described approaches in this report were supported with real world case studies.

Sections 2.1 and 2.2 addressed the issue of anticipated changes in water demand. A literature scan was undertaken, although not all entries are relevant to a cold country like Canada. A few simplified, both linear and nonlinear, approaches are presented to estimate future water demands based on available historical demand and climate data and on model-based climate forecasts. Advantages and limitations of these approaches are described. The salient points of these sections:

- In Canada (cold climate) climate-related demand fluctuations exist predominantly in the summer, likely due to summer activities such as landscape irrigation and swimming pools.
- The data and analysis of the described case study confirm the intuitive understanding that higher temperature and lower precipitation cause increases in water demand, likely due to the aforementioned summer activities.
- Both linear and nonlinear models can capture trends in demand response to temperature change but have a limited in ability to account for extreme values. This is likely because fluctuations in water demand are only partially “explained” by climate and there are other, non-climate factors at play.
- An increase of 1°C in the average summer temperature was associated with an increase of about 1.5% in water demand in the summer. An increase of 1 mm of summer rain was associated with about 0.35% reduction in summer water demand. These values should be treated as orders of magnitude rather than precise estimates, as they may be location-specific.

Section 3 addressed the issue of hydraulic capacity. Climate change is not expected to directly affect hydraulic capacity of water mains, but rather indirectly through the expected increase in water demand, which in turn affects flow rates in the network, especially peak flow rates. The section introduces a stochastic approach to estimate future nodal supply pressure and flow

velocity in water mains, given potential scenarios of climate change. Subsequently, supply pressure shortfall and/or exceedingly high flow velocities in pipes determine the need for investment in hydraulic capacity augmentation through pipe renewal/replacement.

Section 4 addresses the potential impact of climate change on future water main breaks. In a cold country like Canada, the main mechanism through which climate can have such impact is through frost penetration during winter and to a lesser extent through soil moisture depletion in summer where water mains are laid in clayey expansive soils. Cold temperature impact on pipe breakage can be largely mitigated through deep burial of pipes (which is the practice in many Canadian water utilities). An approach is described in which an established model is used (in this case the nonhomogeneous Poisson model realised using the I-WARP software) to discern the impact of multiple factors, including climatic factors, on the breakage rate of the water mains, based on historical data. Once the magnitude of these impacts is established, climate change models are used to forecast climate scenarios for a desired planning horizon and the pipe breakage model is applied to future conditions and resulting future breakage rates are obtained.

In the case-study used to demonstrate the approach, it was found that only PVC pipes were influenced by temperature in a statistically significant manner. This does not necessarily reflect a general phenomenon and could be just location-specific. Further, the case study reflected a situation that is both intuitively understood and widely observed in the literature, whereby in cold locations higher mean temperatures will result in lower rates of water main breaks due to the diminished impact of frost penetration.

Section 5 addressed the issue of climate change's potential impact on the energy usage in water supply systems. Similar to hydraulic capacity, climate impact on energy use is not direct but rather indirect and related to the larger amount of energy required to satisfy the anticipated higher water demand. A simple, extended period simulation with projected future demands, which account for changing climate is demonstrated. Publicly available network simulators, such as the EPANET can be used to determine future energy needs. The demonstration case-study highlighted some salient observations:

- Networks that already operate with a high utilisation rate (i.e., pump idle time is minimal) can expect to have higher energy bills because the extra demand, coupled with little redundancy, will likely limit the capability of the operators to maneuver operation timing so as to benefit from low rates associated with diurnal electricity pricing scheme.
- Networks where many water mains already operate near hydraulic capacity are likely to see a more significant increase in their energy use (or alternatively a drop in supply pressure) unless they incorporate pipe replacement/reinforcement.

Section 6 addressed the issue of potential climate change impact on water quality in the distribution network. A literature scan reflected surprising little research carried out on this topic and a complete absence of a software tool capable of considering any thermal effects on the water in a distribution system. Consequently, a water quality model was developed which is

capable of accounting for water temperature covariations in the distribution network that result from ambient temperature variations in the air and in the soil. This model was realised as an add-in module in EPANET software.

Since water quality, a multi-variable consideration, is difficult to monitor and model in a WDS, surrogate parameters like water age and, especially, chlorine residual, are used. This surrogate approach is an accepted practice in the industry. The model therefore could account for the concentration of residual chlorine in the system, while also considering the factors impacting this concentration, including water temperature. The model was applied to a real world case study, resulting in a few salient observations:

- Since chlorine decay rate increases in higher temperature, as future mean temperatures rise, chlorine doses for disinfection will have to increase in order to keep minimum thresholds. In the case study, an increase of 1°C in water temperature resulted in a decrease of about 0.2% in residual chlorine. More research would be required to ascertain whether this ratio is generally true or is case-specific.
- As climate change is expected to introduce more extreme temperatures, the operational aspects of chlorination may need to undergo modification due to short –duration temperature peaks that may cause chlorine residual depletion. The quantification of such phenomena (that are also subject to uncertain time gaps) would require significant computational resources to perform extended time simulations.
- A reliable hydraulic model of the network, coupled with good temperature data, would be required to obtain accurate values of residual chlorine. In the absence of these, a simpler approach could be taken based on the correlations between daily temperature and disinfectant concentration levels at various points in the system. This approach benefits from SCADA-generated data and requires minimal knowledge and no numerical modeling.

While this report endeavoured to be comprehensive it is by no means exhaustive. Issues that could benefit from additional research include:

- 1- How climate change is likely to affect system design and rehabilitation planning?
- 2- Are there other climate variables that could affect water main breaks and what might those be?
- 3- How might pump scheduling and reservoir management compensate for the changing climate impacts on energy consumption?
- 4- How might demand reduction policies/incentives and climate induced demand increases influence the system capacity?

Acknowledgments

The authors team would like to express their sincere thanks to Infrastructure Canada and Chad Nelson for their financial support of this project. This research could not have been done without significant support from various water utilities across Canada, which had to remain anonymous for security reasons. In particular, we would like to thank Martin Pendlebury, Agnes Klimowski, Casimo Caringi, Hiran Sandanayake and the CWWA team, Ahmad Shohan, Maxime Lafrance, Marianne Armstrong, Sarah Gagné, Lewis Rossman and many other individuals who provided data and advice as well as generously shared their knowledge and experience in support of this project.

References

- Akuoko-Asibey, A., Nkemdirim, L., & Draper, D. (2013). The impacts of climatic variables on seasonal water consumption in Calgary, Alberta. *Can. Water Resour. J.*, 107–116.
- Ansell, J., & Phillips, M. (1994). *Practical methods for reliability data analysis*. Oxford, UK: Oxford University Press.
- Basupi, I., & Kapelan, Z. (2015). Flexible Water Distribution System Design under Future Demand Uncertainty. *Journal of Water Resources Planning and Management*.
- Boulos, P. F., Vasconcelos, J. J., Rossman, L. A., Clark, R. M., & Grayman, W. M. (1997). Kinetics of chlorine decay. *Journal - American Water Works Association*.
- Bush, E. (2019). *Canada's Changing Climate Report*. Ottawa: ECCC.
- Casas-Monroy, O., Byllaardt, J. V., Bradie, J., Sneekes, A., Kaag, K., & Bailey, S. A. (2018). Effect of temperature on chlorine treatment for elimination of freshwater phytoplankton in ballast water: bench-scale test. *Canadian Journal of Fisheries and Aquatic Sciences*.
- Çengel, Y. A. (1998). *HEAT TRANSFER - A Practical Approach*. New York: McGraw-Hill.
- Clark, C. M. (1970). EXPANSIVE-SOIL EFFECT ON BURIED PIPE. *American Water Works Association, ISSN: 0003-150X, Volume: 63,, 424-427*.
- Colombo, A., Etkin, D., & Karney, B. (1999). Climatic variability and the frequency of extreme temperature events for nine sites across Canada: Implications for power usage. *Journal of Climate*, 2490-2502.
- Constantine, A. G., & Darroch, J. N. (1993). Pipeline reliability: stochastic models in engineering technology and management. *World Scientific Publishing Co*.
- Constantine, A. G., Darroch, J. N., & Miller, R. (1996). Predicting Underground Pipe Failure. *Australian Water Works Association*.
- Dandy, G., Bogdanowicz, A., Craven, J., Maywald, A., & Liu, P. (2008). Optimizing the Sustainability of Water Distribution Systems. *Water Distribution System Analysis (WDSA)*. South Africa.
- Dandy, G., Roberts, A., Hewitson, C., & Chrystie, P. (2006). Sustainability objectives for the optimization of water distribution networks. *8th Annual Water Distribution Systems Analysis Symposium*. Cincinnati, Ohio, USA.
- Dimkić, D. (2020). Temperature Impact on Drinking Water Consumption. *Environmental Sciences Proceedings* (p. 12). MDPI.

- Downing, T., Butterfield, R., Edmonds, B., J.W.Knox, S.Moss, Piper, B., . . . team, t. C. (2003). *Climate change and the demand for water*. Oxford: Stockholm Environment Institute, Oxford Office.
- Eck, B. J., Saito, H., & McKenna, S. A. (2016). Temperature dynamics and water quality in distribution systems. *IBM Journal of Research and Development*, 60(5/6), 7:1-7:8.
- Economou, T., Kapelan, Z., & Bailey, T. (2008). A Zero-Inflated Bayesian Model for the Prediction of Water Pipe Bursts. *Proc. 10th International Water Distribution System Analysis Conference, CD-ROM edition*. Kruger National Park, South Africa.
- Engineers Edge. (2021, 09 20). *Water Density Viscosity Specific Weight*. Retrieved from engineersedge.com:
https://www.engineersedge.com/physics/water__density_viscosity_specific_weight_13146.htm
- EPA. (2018). *EPANET | Water Research | US EPA*. <https://www.epa.gov/water-research/epanet>.
- EPRI. (2002). *U.S. Electricity Consumption for Water Supply and Treatment: The Next Half Century. Vol. 4*. Palo Alto: Electric Power Research Institute.
- Fish, K. E., Reeves-McLaren, N., Husband, S., & Boxall, J. (2020). Uncharted waters: the unintended impacts of residual chlorine on water quality and biofilms. *npj Biofilms and Microbiomes*.
- Fisher, I., Kastl, G., & Sathasivan, A. (2011). Evaluation of suitable chlorine bulk-decay models for water distribution systems. *Water Research*, 45(16), 4896–4908.
- Florides, G., & Kalogirou, S. (2001). Measurements of Ground Temperature at Various Depths. *3rd International Conference on Sustainable Energy Technologies*, (pp. 1–6).
- Goodrich, L. E. (1982). The influence of snow cover on the ground thermal regime. *Canadian Geotechnical Journal*, 19(4), 421–432.
- Habibian, A. (1994). Effect of temperature changes on water-main breaks. *Journal of Water Resources Planning & Management*, ASCE 120(2), 312–321.
- Hallam, N. B., West, J. R., Forster, C. F., Powell, J. C., & Spencer, I. (2002). The decay of chlorine associated with the pipe wall in water distribution systems. *Water Research*, 36(14), 3479–3488.
- Hu, Y., & Hubble, D. W. (2007). Factors contributing to the failure of asbestos cement water mains. *Canadian Journal of Civil Engineering* 34(5), 608–621.
- Jarrett, R., Hussain, O., & Van der Touw, J. (2003). Reliability assessment of water pipelines using limited data. *OzWater, Perth, Australia*.

- Kastl, G. J., Fisher, I. H., & Jegatheesan, V. (1999). Evaluation of chlorine decay kinetics expressions for drinking water distribution systems modelling. *Journal of Water Supply: Research and Technology - AQUA*.
- Kiéné, L., Lu, W., & Lévi, Y. (1998). Relative importance of the phenomena responsible for chlorine decay in drinking water distribution systems. *Water Science and Technology*, 219–227.
- Kimbrough, D. E. (2019). Impact of local climate change on drinking water quality in a distribution system. *Water Quality Research Journal*, 179-192.
- Kleiner, Y., & Rajani, B. (2002). Forecasting variations and trends in water-main breaks. *Journal of Infrastructure Systems* 8(4), 122–131.
- Kleiner, Y., & Rajani, B. (2004). Quantifying effectiveness of cathodic protection in water mains: theory. *Journal of Infrastructure Systems, ASCE*, 43-51.
- Kleiner, Y., & Rajani, B. (2010). *Dynamic influences on the deterioration rates of individual water manis (I-WARP)*. Denver USA. : Water Research Foundation research report.
- Kleiner, Y., & Rajani, B. (2010). I-warp: Individual water main renewal planner. *Drink. Water Eng. Sci.* 3(1), 71–77.
- Kleiner, Y., & Rajani, B. (2012). Comparison of four models to rank failure likelihood of individual pipes. *Journal of Hydroinformatics* (2012) 14 (3), 659–681.
- Koechling, M. T. (1998). Assessment and modeling of chlorine reactions with natural organic matter: impact of source water quality and reaction conditions.
- Lambert, D. (1992). Zero-Inflated Poisson regression, with an application to defects in manufacturing. *Technometrics*, Vol. 34, No. 1, 1-14.
- Laucelli, D., Rajani, B., Kleiner, Y., & Giustolisi, O. (2014). Study on relationships between climate-related covariates and pipe bursts using evolutionary-based modelling. *Journal of Hydroinformatics* 16(4), 743–757.
- Lochbaum, B. S. (1993). PSE&G develops models to predict main breaks. *Pipeline and Gas J.*, 20(9), 20-27.
- M.L. Parry, O. C. (2007). *Contribution of Working Group II to the Fourth Assessment Report of the Intergovernmental Panel on Climate Change*. Cambridge: Cambridge University Press.
- Maidment, D. R., & Miaou, S.-P. (1986). Daily Water Use in Nine Cities. *Water Resources Research*, 845-851.

- Metcalf, & Eddy. (2003). *Metcalf and Eddy Wastewater engineering: treatment, disposal and reuse, 4th edn. McGraw-Hill, New York. Wastewater Engineering: Treatment and Reuse.* New York, NY.: McGraw Hill.
- Mirjam Blokker, E. J., & Pieterse-Quirijns, E. J. (2013). Modeling temperature in the drinking water distribution system. *Journal - American Water Works Association.*
- Mirjam Blokker, E. J., & Pieterse-Quirijns, E. J. (2018). Errata: Modeling temperature in the drinking water distribution system. *Journal - American Water Works Association.*
- Monteiro, L., Figueiredo, D., Covas, D., & Menaia, J. (2017). Integrating water temperature in chlorine decay modelling: a case study. *Urban Water Journal*, 14(10), 1097–1101.
- Monteiro, L., Figueiredo, D., Dias, S., Freitas, R., Covas, D., Menaia, J., & Coelho, S. T. (2013). Modeling of chlorine decay in drinking water supply systems using EPANET MSX. *Procedia Engineering*, 1192–1200.
- Monteiro, L., Menaia, J., & Covas, D. (2012). The influence of temperature on chlorine bulk-decay rates in drinking water. *IWA World Congress on Water Climate and Energy.*
- Mote, P., Canning, D., Fluharty, D., Francis, R., Franklin, J., Hamlet, A., . . . Snover, A. (1999). *Impacts of Climate Variability and Change, Pacific Northwest.* Seattle, Washington: National Atmospheric and Oceanic Administration, Office of Global Programs, and JISAO/SMAClimate Impacts Group.
- Nagatani, T., Yasuhara, K., Murata, K., Takeda, M., Nakamura, T., Fuchigami, T., & Terashima, K. (2006). Residual Chlorine Decay Simulation in Water Distribution System. *The 7th International Symposium on Water Supply Technology.*
- Neale, T., Carmichael, J., & Cohen, S. (2007). Urban Water Futures: A Multivariate Analysis of Population Growth and Climate Change Impacts on Urban Water Demand in the Okanagan Basin, BC. *Canadian Water Resources Journal*, 315-330.
- Newport, R. (1981). Factors influencing the occurrence of bursts in iron water mains. *Water Supply and Management*, 274–278.
- Pachauri, R., & Meyer, L. (2015). *IPCC: Climate Change 2014: Synthesis Report. Contribution of Working Groups I, II and III to the Fifth Assessment Report of the Intergovernmental Panel on Climate Change.* Geneva, Switzerland: IPCC.
- Pintér, J. D. (2005). *LGO: A Model Development and Solver System for Continuous Global Optimization.* Halifax, NS, Canada.: Pintér Consulting Services, Inc.
- Powell, J. C., Hallam, N. B., West, J. R., Forster, C. F., & Simms, J. (2000). Factors which control bulk chlorine decay rates. *Water Research.*

- Praskievicz, S., & Chang, H. (2009). Identifying the Relationships Between Urban Water Consumption and Weather Variables in Seoul, Korea. *Physical Geography*, 324-337.
- Protopapas, A. L., Katchamart, S., & Platonova, A. (2000). Weather Effects on Daily Water Use in New York City. *Journal of Hydrologic Engineering*, 332-338.
- Rajani, B. B., & Kleiner, Y. (2001). *Comprehensive review of structural deterioration of water mains: physical based models*. Ottawa: NRC Publications.
- Rajani, B., Kleiner, Y., & Sink, J.-E. (2012). Exploration of the relationship between water main breaks and temperature covariates. *Urban Water Journal*, 67-84.
- Rasifaghihi, N., Li, S. S., & Haghighat, F. (2020). Forecast of urban water consumption under the impact of climate change. *Sustainable Cities and Society*.
- Roshani, E. (2014). *HydraCAL User's Manual*. Ottawa, Ontario: DataAb Inc.
- Roshani, E., & Fillion, Y. (2013). Water Distribution System Rehabilitation Under Climate Change Mitigation Scenarios in Canada. *Journal of Water Resources Planning and Management*.
- Roshani, E., & Fillion, Y. (2014). The Effects of Future Water Demand Reduction on WDS Rehabilitation Planning. *16th Water Distribution System Analysis Conference*. Bari, Italy.
- Roshani, E., MacLeod, S., & Fillion, Y. (2012). Evaluating the Impact of Climate Change Mitigation Strategies on the Optimal Design and Expansion of the Amherstview, Ontario Water Network: A Canadian Case Study. *Journal of Water Resources Planning and Management, ASCE, Vol 138, Issue 2*, 100-110.
- Rossman, L. (2000). *EPANET2 User's Manual*. Washington, D.C.: US EPA.
- Rossman, L. A., Clark, R. M., & Grayman, W. M. (1994). Modeling Chlorine Residuals in Drinking-Water Distribution Systems. *Journal of Environmental Engineering*, 120(4), 803–820.
- Rossman, L. A., Clark, R. M., & Grayman, W. M. (1994). Modeling Chlorine Residuals in Drinking-Water Distribution Systems. *Journal of Environmental Engineering*, 20(4), 803–820.
- Røstum, J. (2000). *Statistical modelling of pipe failures in water networks*. Trondheim, Norway.: PhD thesis, Norwegian University of Science and Technology.
- Sadiq, & Karney. (2004). Modeling Water Demand Considering Impact of Climate Change – a Toronto Case Study. *Journal of Water Management Modeling*.
- Staats, M. (2018, 04 24). *Chapman Creek Water System, Water Availability and Climate Change*. Retrieved from ubc.ca: <http://blogs.ubc.ca/mstaats8/>

- Tomohiro, F., & Katsuhiko, T. (2003). Behavior of Residual Free Chlorine in Tap Water Treated by the Advanced Water Treatment and the Management in Municipal Water Distribution System. *JOURNAL JWWA*, 72(6), 12–24.
- UKWIR. (2012). *Impact of climate change on asset management planning, Technical Report 12/CL/01/16*. UKWIR.
- Wable, Dumoutier, Duguet, Jarrige, Gelas, & Depierre. (1991). Modeling chlorine concentrations in a network and applications to Paris distribution network. *Water Quality Modeling in Distribution Systems Conf.*
- Wols, B. A., & Van Thienen, P. (2014). Impact of weather conditions on pipe failure: A statistical analysis. *Journal of Water Supply: Research and Technology - AQUA* 63(3), 212–223.
- Wols, B. A., & Van Thienen, P. (2016). Impact of climate on pipe failure: predictions of failures for drinking water distribution systems. *EJTIR Issue 16(1)*, 240 □ 253.
- Wu, W., Maier, H., & Simpson, A. (2010). Single-Objective versus Multi-Objective Optimization of Water Distribution Systems Accounting for Greenhouse Gas Emissions by Carbon Pricing. *Journal of Water Resources Planning and Management*, 136(5), 555-565.
- Wu, W., Simpson, A., & Maier, H. (2010). Accounting for Greenhouse Gas Emissions in Multiobjective Genetic Algorithm Optimization of Water Distribution Systems. *Journal of Water Resources Planning and Management*, 136(2), 146-155.
- Wu, W., Simpson, A., & Maier, H. (2012). Sensitivity of Optimal Tradeoffs between Cost and Greenhouse Gas Emissions for Water Distribution Systems to Electricity Tariff and Generation. *Journal of Water Resources Planning Management*, 138(2), 182–186.
- Wu, W., Simpson, A., Maier, H., & Marchi, A. (2012). Incorporation of Variable-Speed Pumping in Multiobjective Genetic Algorithm Optimization of the Design of Water Transmission Systems. *Journal of Water Resources Planning Management*, 138(5), 543–552.

Appendix A -

A.1 Limitations and issues with EPANET-MSX

EPANET-MSX (EPA, 2018) was developed by the USEPA. The latest official version was released in December 2011 with no updates and bug fixes since. The Open Water Analytics initiative, with some cooperation with the USEPA, is aiming to continue the development and maintenance of the MSX extension (Open Water Analytics, 2017). During the implementation of the Temperature-Chlorine model for the Network 1 case study in EPANET-MSX, several issues had to be addressed, as detailed below.

1. A mismatch between the original USEPA source code and the latest available code on OWA's repository was observed which prevented the correct parsing of exponents.
2. In EPANET-MSX input file, the user outlines the chemical reactions terms between the different species. These terms are parsed and evaluated by the extension, which is a time consuming task. To reduce running time, "EPANET-MSX has the option to compile the chemical reaction equations that a user specifies within their MSX input file using a C compiler that already resides on the user's system. This can speed up execution time by a factor of 2 to 5, depending on the nature of the reaction system and the choice of integration method". However, EPANET-MSX was written with VC 6 in mind but since then Microsoft changed the location of the VC compiler and the paths needed to run it. Therefore, the use of the compiler option with EPANET-MSX stopped working. To overcome this issue, a fix was provided by Lew Rossman, which included the following code to be placed in a batch file ("runvc.bat"):

```
@echo off

set curdir=%cd%

cd "%ProgramFiles(x86)%\Microsoft Visual Studio\Installer\"

for /F "tokens=* USEBACKQ" %%F in (`vswhere.exe -latest -
property installationPath`) do (set VSDIR=%%F)

call "%VSDIR%\Common7\Tools\VsDevCmd.bat" > nul

cd %curdir%

CL /O2 /LD /nologo %1%
```

Then, this batch file should be called from the "msxcompiler.c" source code:

```
#ifdef WINDOWS

    if ( MSX.Compiler == VC )
    {
        sprintf(cmd, "runvc.bat %s", srcFile);
        err = MSXfuncs_run(cmd);
    }

#endif
```

Following this fix the EPANET-MSX source code was compiled.

3. For an unclear reason, EPANET-MSX failed to run in some cases where parallel pipes were connected directly to a tank. For such cases, the pipes were combined which had no impact on the hydraulics of the network.